Advanced Materials Research Vols. 204-210, Part 1

Advanced Research on Industry, Information System and Material Engineering

Part 1

Edited by
Helen Zhang, Gang Shen and David Jin

TRANS TECH PUBLICATIONS

Advanced Research on Industry, Information System and Material Engineering

Edited by
Helen Zhang
Gang Shen
David Jin

Advanced Research on Industry, Information System and Material Engineering

Selected, peer reviewed papers from the
2011 International Conference on
Industry, Information System and Material Engineering
(IISME2011),
April 16-17, 2011, Guangzhou, China

Edited by

Helen Zhang, Gang Shen and David Jin

Trans Tech Publications Ltd
Laubisrutistr. 24
CH-8712 Stafa-Zurich
Switzerland
http://www.ttp.net

Volumes 204-210 of 7-vol.-set
Advanced Materials Research
ISSN 1022-6680

Full text available online at *http://www.scientific.net*

***Distributed** worldwide by*

Trans Tech Publications Ltd
Laubisrutistr. 24
CH-8712 Stafa-Zurich
Switzerland

Fax: +41 (44) 922 10 33
e-mail: sales@ttp.net

and in the Americas by

Trans Tech Publications Inc.
PO Box 699, May Street
Enfield, NH 03748
USA

Phone: +1 (603) 632-7377
Fax: +1 (603) 632-5611
e-mail: sales-usa@ttp.net

Preface

International Science& Education Researcher Association（ISER) is an non-profit public organization made up of some educators, some education-researchers, some academic exchanging scholars and some project-researchers willingly around the world. The association puts her focus on studying and exchanging academic achievements of international teaching and scientific research, and she also promotes education reform in the world. In addition, she serves herself on academic discussion and communication too,which is beneficial for education and scientific research. Thus it will stimulate the research interests of all researchers to stir up academic resonance.

IISME2011 is a comprehensive conference,and it is an integrated conference concentrating its focus upon Industry, Information System and Material Engineering. In the proceeding, you can learn much more knowledge about Industry, Information System and Material Engineering of researchers all around the world. The main role of the proceeding is to be used as an exchange pillar for researchers who are working in the mentioned field. In order to meet high standard of *Advanced Materials Research*,the organization committee has made their efforts to do the following things. Firstly, poor quality paper has been refused after reviewing course by anonymous referee experts. Secondly, periodically review meetings have been held around the reviewers about five times for exchanging reviewing suggestions. Finally, the conference organization had several preliminary sessions before the conference. Through efforts of different people and departments, the conference will be successful and fruitful.

IISME2011 is co-sponsored by International Science & Education Researcher Association, Beijing Spon Research Institution, Beijing,China, Beijing Gireida Education Co.Ltd. The goal of the conference is to provide researchers from Industry, Information System and Material Engineering with a free exchanging forum to share the new ideas, new innovation and solutions with each other. In addition, the conference organizer will invite some famous keynote speaker to deliver their speech in the conference. All participants will have chance to discuss with the speakers face to face, which is very helpful for participants.

During the organization course, we have got help from different people, different departments, different institutions. Here, we would like to show our first sincere thanks to Mr. Thomas Wohlbier and Trans Tech Publications for their kind and enthusiastic help and support for our conference. Secondly, the authors should be thanked too for their enthusiastic writing attitudes toward their papers. Thirdly, all members of program chairs, reviewers and program committees should also be appreciated for their hard work.

In a word, it is the different team efforts that they make our conference be successful on April 16-17,2011,Guangzhou, China.We hope that all of participants can give us good suggestions to improve our working efficiency and service in the future. And we also hope to get your supporting all the way. Next year, In 2012, we look forward to seeing all of you at IISME2012.
January, 2011

IISME committee

Committee

Honor Chairs

Prof. Chen Bin, Beijing Normal University,China
Prof. G.Q. Chen, Peking University,China
Prof. Hu Chen, Peking University,China
Chunhua Tan, Beijing Normal University,China
Helen Zhang, University of Munich,China

Program Committee Chairs

Xiong Huang, International Science& Education Researcher Association,China
LiDing, International Science& Education Researcher Association,China
Zhihua Xu, International Science& Education Researcher Association,China

Organizing Chair

ZongMing Tu, Beijing Gireida Education Co.Ltd,China
Jijun Wang, Beijing Spon Technology Research Institution,China
Quanxiang, Beijing Prophet Science and Education Research Center,China

Publication Chair

Zhihua Xu, International Science& Education Researcher Association,China
Sally Wang, Beijing Normal University,China

International Committees

Sally Wang, Beijing normal university,China
LiLi, Dongguan University of Technology,China
BingXiao, Anhui university,China
Z. L. Wang, Wuhan university,China
Moon Seho,Hoseo University,Korea
Kongel Arearak,Suranaree University of Technology,Thailand
Zhihua Xu, International Science& Education Researcher Association,China
Xiangrong Jiang, Wuhan University of Technology,China
LiHu, Linguistic and Linguidtic Education Association,China
Moon Hyan,Sungkyunkwan University, Korea
Guangwen, South China University of Technology,China
Jack.H. Li, George Mason University, USA
Marry. Y. Feng, University of Technology Sydney, Australia
Li Hu, Wuhan University of Science and Technology, China,
ZhongYan, Wuhan University of Science and Technology, China
Haiquan Huang, Hubei University of Technology,China
Xiao Bing, WUhan University, China
Brown Wu, Sun Yat-Sen University, China

Co-sponsored by

International Science& Education Researcher Association, China
Beijing Spon Research Institution

Table of Contents

Chapter 2: Industry and Computer Application

Chapter 3: Industry, Network and Materials Engineering

Chapter 4: Intelligent Information and Industry Technology

Chapter 5: Information System, Industry and Materials

Chapter 6: Industry, Energy and Information Technology

Chapter 7: Intelligent Technology and Material Science

Chapter 8: Information Engineering and Management

Chapter 9: Information Services and Electronic Application

CHAPTER 1:

Industry and Information Technology

Advanced Materials Research Vols. 204-210 (2011) pp 1-4

doi:10.4028/www.scientific.net/AMR.204-210.1

Empirical Research on the Environmental Effect of Foreign Direct Investment: the Case of Jiangsu Province

MingQing Jia, JiaYu Yu

Binjiang College, Nanjing University of Information Science＆Technology, Nanjing 210044, China

School of Business, Soochow University, Suzhou 215021, China

mqjia67@126.com, yujiayu1988@sohu.com

Keywords: FDI, environment, Jiangsu Province, co-integration

Abstract: After opening its doors to the international business scene, foreign direct investment has made considerable contributions to the economic growth in Jiangsu Province. But as a coin has two sides, there is also a negative aspect that we are faced with the environmental degradation. The purpose of this paper is to analyze the environmental effect of FDI and provide some reference to the harmonious development of economy and environment in Jiangsu province. In this paper, we started with a research about a present situation of foreign direct investment and environment of Jiangsu Province, and then we made an empirical analysis on the environmental effect of foreign direct investment in Jiangsu Province, finally we put forward some policy proposals. The sustained growth of foreign direct investment is one of the important causes of environmental degradation in Jiangsu Province. We should improve environment supervision and management in developing FDI.

Introduction

In the tide of the economic globalization, foreign direct investment is playing an increasingly important role in the economic development, at the same time, environmental protection problems are rapidly evolving into a global issue with the development of FDI. More and more attention is being paid to how foreign direct investment affects the environmental quality in the host country. After opening its doors to the international business scene, sustainable development of economy has been witnessed in Jiangsu Province. Foreign direct investment has made considerable contributions to the economic growth. But as a coin has two sides, there is also a negative aspect that we are faced with the environmental degradation. One of the burning problems confronting us is to make the FDI and environment develop harmoniously. So it is necessary to combine theoretical methods and empirical methods together to analyze the FDI-environment issue.

The Present Situation of FDI and Environment in Jiangsu Province

The Characteristics of FDI in Jiangsu Province. Since reform and opening up to the outside world, the scale of FDI in Jiangsu Province had expanded, but the rate of fully funded was not high. The modes of FDI in Jiangsu Province had shown a trend of exclusive foreign-owned investments. The modes of cooperative venture and share-issuing enterprises took up a small proportion. The sources of FDI are around the world, Hong Kong takes the first place. The orientation of FDI is unbalanced, highly centralized to the secondary industry.

The Present Situation of Environment in Jiangsu Province. In recent years, environment protection in Jiangsu Province has scored significant achievement, but it is showed that the discharge of several kinds of environmental pollutants has been kept in increasing. (See Picture 1) If we ignore the environmental issues, chances are good that we will be put in danger. Industrial pollution is the main source of the environmental pollution in Jiangsu Province. With the economics growing fast in Jiangsu Province, it is essential that effective measures should be taken to control the environmental pollution.

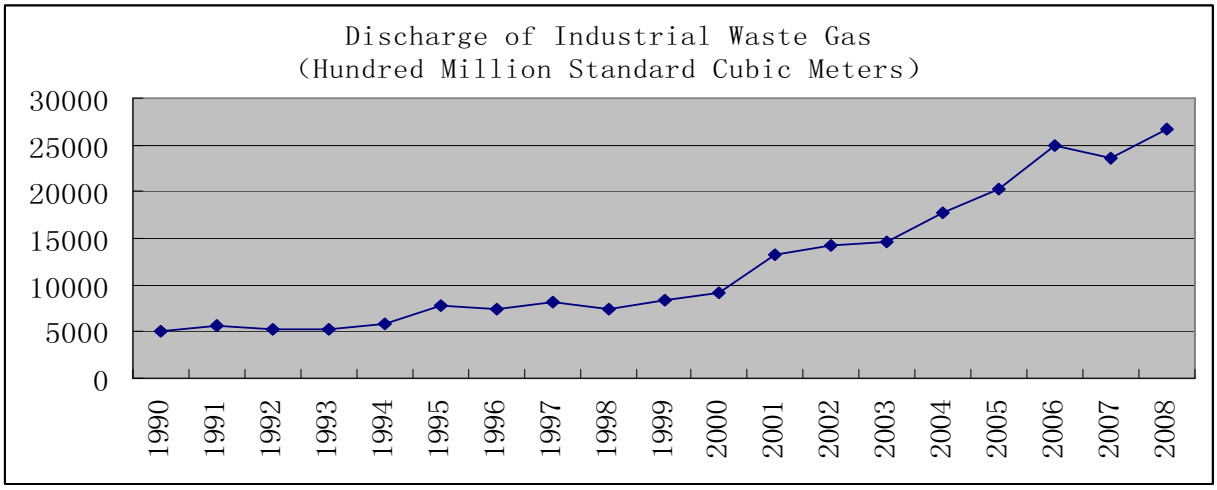

Picture 6. Discharge of Industrial Waste Gas in Jiangsu Province from 1990 to 2008

The Environmental Effect of Foreign Direct Investment——Empirical Research Based on Time Serial Data Stream

In this part, we select the time serial data streams about FDI and environment in Jiangsu Province during the period between 1991 and 2008. By setting up econometrics models and testing the cointegration relations, we find that FDI and environmental pollution have a steady equilibrium relationship in the long run. A spectrum of FDI-environment result has been achieved.

Research Methods and Models. Because the phenomenon of spurious regression may persist in nonstationary time series even if the sample is very large, we should do the unit root test at first. Augmented Dickey-Fuller (ADF) test is chosen here. Then we consider the method of Augmented Engle-Granger (AEG) test to test for cointegration, that is, the ADF unit root test on the residuals estimated from the cointegrating regression. If the residuals are stationary, we say that the two variables are cointegrated. The software package Eviews 5.0 is utilized in the empirical research.

Selecting appropriate environmental indicators is the key to setting up the econometrics model for the relationship between FDI and environmental quality. We use the indicators of the discharge amount of pollutants as the generous character of the environmental pollution degree and environmental quality. We also select the actual foreign direct investment capital utilized every year as the indicator of FDI. According to *Statistical Yearbook of Jiangsu Province* and *Environmental Statistics Bulletin of Jiangsu Province* of the past years, we select time series between 1990 and 2008 in Jiangsu Province, including the actual foreign direct investment capital, the discharge amount of industrial waste water, discharge amount of industrial waste gas and discharge amount of industrial solid waste.

We take the logarithm (base e) of these variables, denoted as Ln (FDI), Ln (solid), Ln (water) and Ln (gas). We also denoted their first differences of series as dLn (FDI), dLn (solid), dLn (water) and dLn (gas).

It is assumed that the discharge amount of some kind of environmental pollutants is Ei, we consider the following model:

$$\text{Ln}(Ei) = \alpha_i + \beta_i \text{Ln}(FDI) + \varepsilon_i \quad (1)$$

If β is significantly positive, it shows that the growth of foreign direct investment will lead to environmental degradation. And the opposite is also the case. As we select three kind of pollutants as the environmental indicators, we get three models as follow:

$$Ln(solid)=\alpha_1 + \beta_1 Ln(FDI)+\varepsilon_1 \quad (2)$$

$$Ln(water)=\alpha_2 + \beta_2 Ln(FDI)+\varepsilon_2 \quad (3)$$

$$Ln(gas)=\alpha_3 + \beta_3 Ln(FDI)+\varepsilon_3 \quad (4)$$

Empirical Research. When we do the unit root test on the series of Ln(FDI), Ln(solid), Ln(water) and Ln(gas), we find that the ADF test statistic are lager than even the 10 percent critical values, showing that the original time series are not stationary. In practice, most financial and economic time series are nonstationary. The solution here is to take the first differences of the original series. Then we do Augmented Dickey-Fuller test on the series of dLn (FDI), dLn (solid), dLn (water) and dLn (gas). The test result is shown as the following table.(See Table 1)

As can be seen in the table, the ADF test statistic of dLn (solid) is -2.458646, which is lager than even the 10 percent critical value of -2.673459.We can arrive at the conclusion that the dLn(solid) time series is not stationary. At the same time, the series of dLn (FDI), dLn (water) and dLn (gas) are stationary.

Table 1. ADF test result of the first differences of series

Variable	ADF Test Statistic	Critical Value(Level of Significance)	Result
dLn(FDI)	-3.927055	-3.081002 (5%)	stationary
dLn(solid)	-2.458646	-2.673459 (10%)	nonstationary
dLn(water)	-3.843663	-3.065585 (5%)	stationary
dLn(gas)	-4.551121	-3.920350 (1%)	stationary

In generally, if a nonstationary time series has to be differenced *d* times to make it stationary, that time series is said to be integrated of order *d*, denoted as I(*d*). Subjecting the time series of Ln (FDI), Ln (water) and Ln (gas) individually to unit root analysis, we find that they are both I(1);that is, they contain a unit root. It can also be concerned that the time series of Ln (solid) is not I (1), so Ln (solid) and Ln (FDI) can not be cointegrated; that is, we can eliminate the effect of FDI to the discharge of industrial solid waste.

When testing for cointegration, we consider the method of Augmented Engle-Granger (AEG) test. At first, we regress Ln (FDI) on Ln (FDI), Ln (water) and Ln (gas) individually, and obtained the following regression. (See Table 2, Table 3 and Table 4)

Table 2. Regression of Ln (FDI) and Ln (water)

Variable	Coefficient	Std. Error	t-Statistic	Prob.
C	2.863753	0.099221	28.86249	0.0000
export	0.071861	0.023148	3.104484	0.0068

Table 3. Regression of Ln (FDI) and Ln (gas)

Variable	Coefficient	Std. Error	t-Statistic	Prob.
C	7.665856	0.279497	27.42730	0.0000
export	0.399124	0.065205	6.121048	0.0000

Table 4. R-squared Value of the Two Models

Variable	Water	Gas
R-squared	0.375922	0.700751

Secondly, we performed a unit root test on residuals obtained from the regression above. The test result is shown as following. (See Table 5)

Table 5.The Result of ADF Test on residuals

Variable	ADF Test Statistic	Critical Value（Level of Significance）	Result
Water	-2.383481	-1.962813 (5%)	stationary
Gas	-2.197631	-1.962813 (5%)	stationary

From the test for cointegration, it is clear that β in the model is significantly positive; at 5% level of significance, the original hypothesis is rejected, they contain no unit root. We can come to the conclusion that Ln (FDI) and Ln (water), Ln (FDI) and Ln (gas) are cointegrated, they have a long-term, or equilibrium relationship.

According to the empirical research above, the foreign direct investment and discharge amount of industrial waste water, industrial waste gas are have a long-term, equilibrium relationship, and they are positive cointegrated. That means, with the development of foreign direct investment, the discharge amount of industrial waster water and industrial waster gas will also increase. The coefficient of the regression equation is the elasticity of FDI capital with respect to discharge amount of environmental pollutants; that is, the change in the discharge amount of environmental pollutants as an increase in the FDI by 1%. Taking into account all of the factors, we may reach the conclusion that the sustained growth of foreign direct investment is one of the important causes of environmental degradation in Jiangsu Province.

Summary

Foreign direct investment has contributed greatly to the economic growth in Jiangsu Province, but also leads to environmental degradation. The result of empirical research in this paper shows the sustained growth of foreign direct investment is one of the important causes of environmental degradation in Jiangsu Province. With the development of FDI, the environmental quality in Jiangsu Province may get worse and worse. It is essential that effective actions should be taken to correct the tendency. We should perfect the foreign direct investment policy and environmental protection laws. We should guide the orientation of FDI properly to optimize the industrial structure, utilize the foreign direct investment to develop the capital-and-technology-intensive high-tech industry. Improve environment supervision and management of the foreign investment enterprises and reduce pollution transfer. The environmental protection in FDI attraction brings both opportunities and challenges to us, However, opportunities outweigh challenges. We should grasp the opportunities to adjust the relation between them, and strive to play the role of environmental protection in promoting FDI growth. Only in this way can we keep foreign direct investment and environment develop harmoniously.

References

[1]Gujarati: Basic Econometrics(2004)

[2]Li JiangTao: Research on Attraction of FDI in Jiangsu Province (2007)

[3]Zhou JieQiong: Research on FDI and Environmental Problems in China (2008)

[4]Wang LiNa: The Environmental Effect of FDI in Hunan Province (2008)

[5] Zhang Ying: Research on Mutual Development of FDI and Environment. Shandong Textile Economy,2008(6),p16-18

Advanced Materials Research Vols. 204-210 (2011) pp 5-10

doi:10.4028/www.scientific.net/AMR.204-210.5

A study of language in functional cortex of audiphone deaf signers Used fMRI

Qiang Li [1, a], Shuang Xia [2,b] Fei Zhao[3,c]

[1] Engineering College for the Deaf，Tianjin University of Technoloy，Tianjin，China

[2] First Central Hospital of Tianjin Medical University，Tianjin Medical University，Tianjin, China

[3] Centre for Hearing and Balance Studies，University of Bristol，UK

[a]liqianglr@sina.com.cn, [b]lqlr2002@163.com, [c]Fei.Zhao@bristol.ac.uk

Keywords: audiphone; functional cortex; sign language; reorganization; fMRI

Abstract. Using functional magnetic resonance imaging (fMRI), to observe the changes of cerebral functional cortex in prelingual deaf singers for Chinese sign language(CSL). Results：During observing and imitating CSL, the activated areas in all groups include bilateral middle frontal gyrus, middle temporal gyrus, superior parietal lobule, cuneate lobe, fusiform gyrus and lingual gurus. The activation of bilateral inferior frontal gyrus were found in group Ⅰ, Ⅲ and Ⅳ, but no activation in group Ⅱ. The activation of bilateral superior temporal gyrus and inferior parietal lobule were found in group Ⅰ and Ⅲ, but no activation in others. The volumes of bilateral inferior frontal gyrus in group Ⅰ were greater than those in group Ⅲ and Ⅳ. The volumes of bilateral superior temporal gyrus in group Ⅰ were greater than those in group Ⅲ. Conclusion：The cortex in PDS had occurred reorganization, after losing their auditory and learning the CSL. The activation of linguistic cortex can be found during oberserving and imitating CSL in PDS. The secondary auditory cortex and association area turn to take part in processing visual language when no auditory afference, whereas the primary auditory cortex do not participate the reorganization. Additionally, the visual cortex of PDS is more sensitive than that of normal heaing individuals.

Introduction

Prelingual deafness occurs before spoken language is learned. Normal hearing people generally learn their first language before 5 years of age; hence, prelingual deaf signers (PDS) are either deaf at birth or became deaf prior to developing the grammatical basis of their native language, which is usually before the age of 5 years. In the view of psycholinguistics, there is positive correlation between the development of the brain and native language in children. The development of the brain restrict the linguistic capacity of the chilldren, while the linguistic capacity promote the mature of the brain. So what changes the functional cortex of the PDS occur, as the special people lacking of the normal native language, is worth to attention. Using the functional magnetic resonance imaging (fMRI), hearing non-signers (HnS), hearing native signers (HNS) and hearing late signers (HLS) were examined as subjects at the same time to find the activation of the lingual, auditory and visual cortex, so as to assure the reorganization model of PDS. Then then the effection of the lingual experience and hearing-loss to the reorganization of functional cortex of the PDS was discussed to assure the effection of the sign language to the education of the deaf signers.

Partcipant

14 PDS (group Ⅰ, aged 18-26 years, mean age = 21.9 years) were four males and ten females. 13 HnS（group Ⅱ, aged 19-25 years, mean age = 23.2 years) were five males and eight females. 11 HNS (group Ⅲ, aged 18-24 years, mean age = 22.9 years) consisted of five males and six females. 12 HLS (group Ⅳ, aged 20-26 years, mean age = 22.5 years) consisted of five males and seven females. The PDS are all severe or profoundly sensorineural hearing loss, who lost hearing before 2 years old. 12 PDS became deaf because of the drug toxicity, the rest were congenitally deaf from birth. HnS never

contacted with CSL. HNS were born to deaf parents and acquired both CSL and Chinese as native languages from birth. HLS acquired CSL after 18 years. The learning duration is 2-4 years (mean duration=2.5 years) . All of the subjects were strongly right-handed. All subjects were trained interpreters and gave their written informed consent. The subjects were asked recognition questions at the end of each run to ensure that their attention was focused on the stimuli.

Experiment Design

The block design consisted of 7 rest and 6 task periods, each of 20 seconds duration, with alternating rest and task periods. The tasks inclduded two contions: observing (3 periods) and imitating (3 periods) CSL, the CSL of each of task are same. During the 20-second task period, the subjects were instructed to observe or imitate four different CSL sentences presented by a male deaf signer in a picture every 5 seconds, which were projected onto a screen at the foot of the scanner bed and viewed through a mirror. During the 20-second rest period, the subjects fixed their eyes on the black "+".

Fig1 The stimulus modality diagram

Imaging Parameters

A 1.5T Marconi Eclipse syetem was used. The subjects lied on the back with head fixed in the standard quadrature head coil with bands and sponge mat. The EPI (echoplanar) sequence consisted of 130 runs. Each run consisted of 20 slices thinkness of 6.0 mm without gap, and included the entire cerebral and cerebellar cortex. The axial planes are parallel to the anterior-posterior commissural (AC-PC) line; TR (repetition time) = 2 000ms, TE (echo time) = 40 ms, FOV (field of view) = 240mm × 240mm. T1-weighted spin echo (SE) images were obtained from each subject using location variables that were identical to those of EPIs used for anatomical reference; TR = 500 ms, TE = 12 ms. Finally, 3D imagings were scanned using RF-FAST sequence; TR = 12 ms, TE = 4.47 ms, FOV = 240mm × 240mm, the filp angle was 20 degree, the matrix size was 192 × 256 pixels. There were 182 slices thinkness of 1.0 mm without gap.

Data Analysis

The software AFNI (analysis of functional neuroimaging) was applied to find area of activation, across subjects, via spatial normalization of each brain to the standardized Talairach stereotaxic space. The therschold of the activation was the volume >100 mm3, radius > 5mm ($P < 0.00005$). SPSS 12.0 was used for statistical analysis (ANVOA and matched t test).

Results

There were no statistical differences about the age and gender in these four groups (ANOVA and chi-square test for the age and gender respectively, $P>0.05$). The activated areas in all groups include bilateral middle frontal gyrus, middle temporal gyrus, superior parietal lobule, cuneate lobe, fusiform gyrus and lingual gurus during observing CSL. The activation of bilateral superior temporal gyrus and inferior parietal lobule were found in group Ⅰ and group Ⅲ in observing CSL, but no activation in others. The activation of bilateral inferior frontal gyrus were found in group Ⅰ, group Ⅲ and group Ⅳ, but no activation in group Ⅱ. During observing CSL, there were statistical differences (ANOVA, $p>0.05$) about the volumes of bilateral inferior frontal gyrus, superior temporal gyrus, superior parietal lobule, cuneate lobe and lingual gurus. The volumes of group Ⅰ (left: 194.73±19.27mm3, right: 189.82±9.72mm3) were greater than those of group Ⅲ (left: 175.22±8.06mm3, right: 176.56± 8.97mm3) and group Ⅳ (left: 168.22±10.20mm3, right: 169.22±8.61mm3) in bilateral inferior frontal gyrus. The volumes of group Ⅰ (left: 231.82 ± 33.38mm3, right: 240.55 ± 56.10mm3) were greater than those of group Ⅲ (left: 125.67 ± 13.58mm3, right: 124.67 ± 7.05mm3) in superior temporal gyrus. The volumes of group Ⅰ were greater than those of group Ⅱ, Ⅲ and Ⅳ in bilateral superior parietal lobule, cuneate lobe and lingual gurus (see Fig2). There were no statistical differences about the volumes in other activated areas (ANVOA, $p<0.05$). The activated

areas in all groups include bilateral middle frontal gyrus, middle temporal gyrus, superior parietal lobule, cuneate lobe, fusiform gyrus, lingual gurus, precentral gyrus, paracentral lobule,and cerebellar hemisphere during imitating CSL. The volumes of bilateral superior temporal gyrus and inferior parietal lobule were found in group Ⅰ and group Ⅲ, but no activation in others. The activation of bilateral inferior frontal gyrus were found in group Ⅰ, Ⅲ and Ⅳ, but no activation in group Ⅱ. There were statistical differences about the volumes of bilateral inferior frontal gyrus, superior temporal gyrus, superior parietal lobule, cuneate lobe and lingual gurus. The volumes of group Ⅰ (left: 285.82±10.78 mm3，right: 285.27±13.19mm3) were greater than those of group Ⅲ (left: 219.44±10.82mm3，right: 219.67±14.83mm3) and group Ⅳ (left: 183.78±5.49mm3，right: 178.22±8.69mm3) in bilateral inferior frontal gyrus. The volumes of group Ⅰ (left: 212.55±31.14mm3，right: 210.45±41.44mm3) were greater than those of group Ⅲ (left: 131.00±7.16mm3，right: 128.78±6.28mm3) in superior temporal gyrus. The volumes of group Ⅰ were greater than those of group Ⅱ, Ⅲ and Ⅳ in bilateral superior parietal lobule, cuneate lobe and lingual gurus. The volumes of group Ⅱ were greater than those of group Ⅲ and group Ⅳ in left cuneate lobule. There were no statistical differences about the volumes of other activated areas among all groups (ANVOA, $p<0.05$). There were no statistical differences about the volumes of the symmetrical functional cortex in all groups during both observing and imitating tasks (matched t test, $p>0.05$).

Fig2 The comparing of the volume of some activated areas during observing sign language among subjects. The volume of bilateral inferior frontal gyrus in group Ⅰ (left top) was greater than that in group Ⅲ(left lower) and Ⅳ(right lower). The volume of bilateral superior temporal gyrus in group Ⅰ was greater than that in group Ⅲ. The volume of bilateral superior parietal lobule, cuneate lobe and lingual gurus in group Ⅰ was greater than that in other groups.

Fig3 The comparing of the volume of some activated areas during observing(left) and imitating(right) sign language in group Ⅰ. The volume of bilateral inferior frontal gyrus, superior parietal lobule and left middle temporal gyrus in imitating task was greater than those in observing task. There was no difference about the volume of bilateral superior temporal gyrus during observing and imitating tasks.

Discussion

The blood oxygen level dependent (BOLD) is an approach to study the function of the brain with high spatial resolution and non-invasive which is applied in the field of cognitive science extensively. Many authors have studied the activation of brain to the sign language in the PDS, but most of them asked the subjects to observe the sign language passively and the sign languages in the experiments were long and complex sentences which may cause the activated areas extensively. Then it is difficult to link the activated areas and the function of processing sign language and identify the function of the activated areas. So the sign languages in our study were simple. At the same time, we asked the subjects to complete the tasks of observing and imitating CSL and analyzed the activated areas respectively in order to find the activated areas related to sign language more correctively. In addition, the HnS, HNS and HLS as the comparing groups were included in our experiment and we didn't find the comparing groups including all HnS, HNS and HLS simultaneously in the other studies.

A.The comparing of the activated areas among the PDS and normally hearing subjects

The Broca,s area (BA44,45), the posterior of left inferior gyrus, is usually considered to take responsibility of producing language in hearing subjects. The activation of bilateral inferior frontal gyrus was found in the subjects (DS, HNS and HLS) who have experience of sign language when they observed and imitated CSL, but there was no activation in HnS. HnS didn,t learn the sign language and there was no perception in their brain, so inferior frontal gyrus didn,t be activated to the sign language. The volumes of PDS were greater than those of HNS and HLS in bilateral inferior frontal gyrus. The DS express the phonetic and semantic with sign language, while the hearing subjects express with spoken language. Although the HNS are the bilingualism of spoken and sign language, they don,t use sign language in their daily life after adult.

B. Equations

Although the auditory cortex of PDS can be activated by the sign language, whether the primary auditory cortex (BA41) can be activated is still a controversy. In normally hearing subjects, the primary auditory cortex mainly receive the sound rather than translating the sound, while the secondary auditory cortex (BA42) and the association area (BA22) perform the advanced function, such as translating and understanding the sound.

Hickok etc found the primary auditory cortex didn,t be activated to the visual stimulus using fMRI and PET. Nishimura and Sadato etc indicated the cross-model reorganization only occurred in the secondary auditory cortex, while the primary auditory cortex had no plasticity. Some neurophysiological and magnetoencephalogram (MEG) studies indicated that the reorganization of the auditory cortex depended on the extent of hearing loss. Lambertz etc suggested the bilateral primary auditory cortex (mainly in the right) can be activated in the total deaf signers, while there was no activation in the residual deaf signers and the normally hearing subjects. They thought whether the auditory cortices can be activated depended on the extent of hearing loss. The PDS in our experiment were all severe or profoundly sensorineural hearing loss, some of who may have residual hearing. There were no activation of the primary auditory cortex in all PDS. So whether the primary auditory cortex can be activated by the visual language and the machine of the phenomenon will need to be further studied.

C. The comparing of the activated areas between observing and imitating CSL

The volumes of the Broca,s area during observing CSL were greater than that during imitating CSL in PDS, HNS and HLS subjects, which suggested the Broca,s area mainly take responsibility of producing sign language and the function to the sign language were the same as that to the oral language. There were no differences about the volumes of the Wernicke,s area between observing and imitating CSL, which suggested the Broca,s area mainly take responsibility of receptiving and understanding CSL. In addition, the bilateral precentral gyrus, paracentral lobule and cerebellar hemisphere were activated during imitating CSL, but no activity duiring observing CSL. This suggested those areas were related to the motion of the hands during imitating CSL rather than semantic of the CSL, which were the same as the results of Petitto.

Conclusion

The functional cortex in PDS had occurred crossing-model reorganization, after losing their auditory and learning the sign language. The language area activity can be found during oberserving and imitating sign language. It is bilateral-equilibrium and no linguistic hemisphere's predominance exits. The extent of activation in bilateral inferior frontal gyrus and superior parietal lobule are greater during imitating task may due to they produce sign language, whereas the volumes of bilateral superior temporal gyrus were similar between oberserving and imitating sign language, which may take responsibility of receptiving and understanding of sign language. During observing and imitating sign language, the secondary auditory cortex of PDS can be activated, illustrating that it turns to take part in the processing of vision when no auditory afference, whereas the primary cortex may not participate the reorganization. Additionally, the visual cortex of PDS may be more sensitive than that of heaing individuals. The reorganization of functional cortex in PDS may be related to the expericence of sign language, but was mainly caused by the effect of hearing loss. So the cochlea implant should be done earlier for PDS to avoid that the crossing-model reorganization produce the effect to the recovery of the oral language. For the patients who cann,t accept the cochlea implant, we should insist on the bilingualism teaching, use the various sensory channel, such as the tactile and visual sensation, and elevate their perception experience and cognition abilities.

Acknowledgment

This project was supported by a research grant from China Social Science (08CYY012) and China Social Science (10CYY016)

References

[1] Newman A., Bavelie, D, Corina D, Jezzard Pet al.: critical period for right hemisphere recruitment in american sign language processing. Nat. Neurosci.Vol. 5 (2002), p. 6–80.

[2] Petitto LA., Zatorre RJ, Gauna K, et al.: Speech-like cerebral activity in profoundly deaf people processing signed languages: implications for the neural basis of human language. Proc. Natl. Acad. Sci. Vol. 97(2000) , p. 3961–13966.

[3] Finney E, FineI., Dobkins K.: Visual stimuli activate auditory cortex in the deaf. Nat. Neurosci. Vol. 4(2001), p. 171–1173.

[4] Klinke, R., Kral, A., Heid, S., Tillein, J., Hartmann, R.: Recruitment of the auditory cortex in congenitally deaf cats by long-term cochlear electrostimulation. Science.Vol. 285(1999), p. 1729–1733.

[5] Kral A, Hartmann R, Tillein J,et al.: Congenital auditory deprivation reduces synaptic activity within the auditory cortex in a layer-specific manner. Cereb. Cortex .Vol. 10(2000), p. 714–726.

[6] Schneider P, Scherg M, Dosch H, et al.: Morphology of Heschl's gyrus reflects enhanced activation in the auditory cortex of musicians. Nat. Neurosci. Vol. 5(2002),p. 688–694.

[7] Penhune V B, Cismaru R，Dorsaint-Pierre R，et al.: The morphometry of auditory cortex in the congenitally deaf measured using MRI. NeuroImage,Vol. 20(2003),p. 1215－1225

[8] Emmorey K, Allen JS, Bruss J, et al.: A morphometric analysis of auditory brain regions in congenitally deaf adults. PNAS.Vol. 100(2003) ,p. 10049–10054

[9] Rupa V, Job A, George M, et al.: Cost- effective initial screening for vestibular schwannoma: auditory brainstem response or magnetic resonance imaging? Otolaryngol Head Neck Surg. Vol. 128(2003),p. 823-828

[10] Emmorey K, Allen JS, Bruss J, et al.: A morphometric analysis of auditory brain regions in congenitally deaf adults. PNAS.Vol.100(2003) : 10049–10054

[11] Rauschecker J P, Tian B.: Mechanisms and streams for processing of ‘‘what’’ and ‘‘where’’ in auditory cortex, PNAS .Vol.97(2000),p. 11800–11806

[12] Zatorre RJ, Belin P, Penhune VB.: Structure and function of the human auditory cortex: music and speech. Trends Cogn. Sci. Vol. 6(2002),p. 37－ 46.

[13] Schneider P, Scherg M., Gu¨nter DH, et al.: Morphology of Heschl's gyrus reflects enhanced activation in the auditory cortex of musicians Nat. Neurosci. Vol. 5(2002), p. 688–694.

[14] MacSweeney M., Woll, B, Campbell, R., et al.: Neural systems underlying British Sign Language and audio-visual English processing in native users, Brain, Vol. 125 (2002) , 1583–1593.

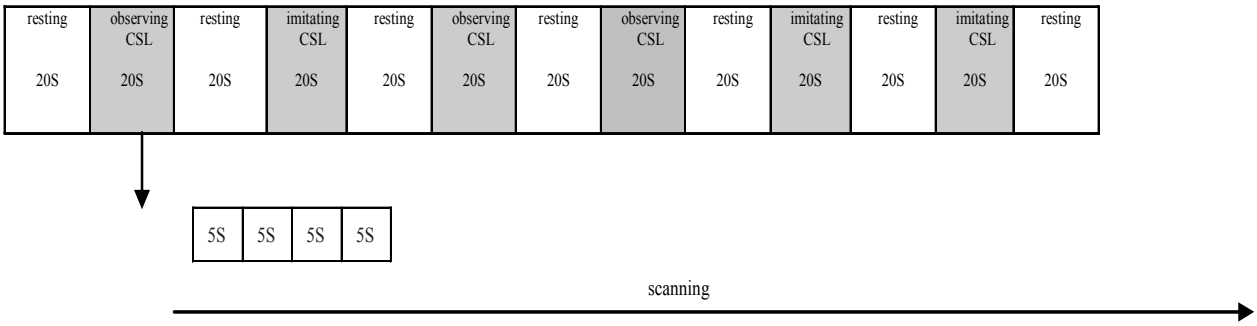

Figure1. The stimulus modality diagram

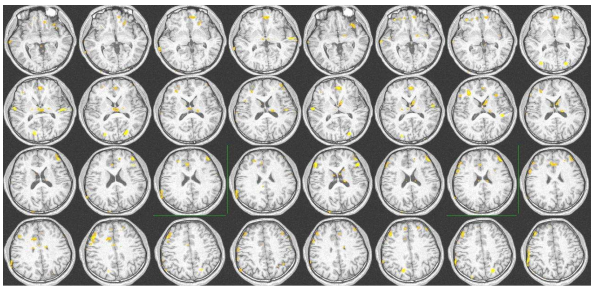

Figure3. The comparing of the volume of some activated areas during observing(left) and imitating(right) sign language in group Ⅰ. The volume of bilateral inferior frontal gyrus, superior parietal lobule and left middle temporal gyrus in imitating task was greater than those in observing task. There was no difference about the volume of bilateral superior temporal gyrus during observing and imitating tasks.

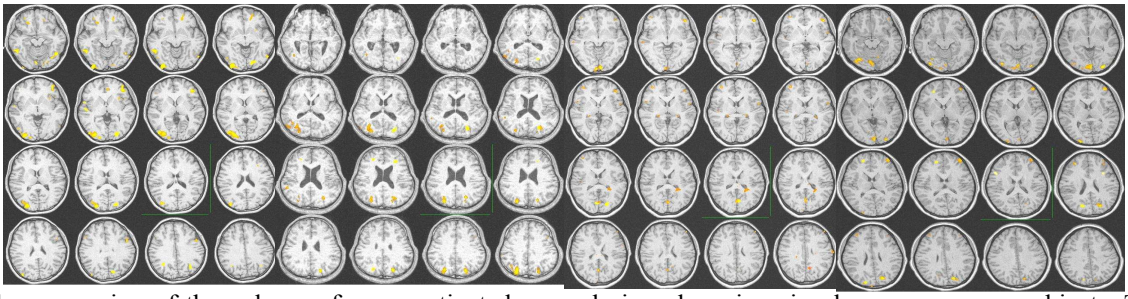

Figure2. The comparing of the volume of some activated areas during observing sign language among subjects. The volume of bilateral inferior frontal gyrus in group Ⅰ (left top) was greater than that in group Ⅲ(left lower) and Ⅳ(right lower). The volume of bilateral superior temporal gyrus in group Ⅰ was greater than that in group Ⅲ. The volume of bilateral superior parietal lobule, cuneate lobe and lingual gurus in group Ⅰ was greater than that in other groups.

Advanced Materials Research Vols. 204-210 (2011) pp 11-16

doi:10.4028/www.scientific.net/AMR.204-210.11

Overall Design of the Forming System for Squeeze Casting

Jianxin Deng [1, a] and Ming Shao [2,b]

[1] School of Mechanical Engineering, Guangxi University, Nanning, Guangxi, 530004, China

[2]School of Mechanical and Automotive Engineering, South China University of Technology, Guangzhou, Guangdong, 510640, China

[a]dengjxin@163.com, [b]shaoming@scut.edu.cn

Keywords: Squeeze Casting, Forming System, Overall Design.

Abstract. As a forming process, squeeze casting is completed in the corresponding manufacturing system. The paper deals with the overall design of the manufacturing system-the forming system for squeeze casting. To construct a practical manufacturing system for this technology, the forming control process of squeeze casting is analyzed, where the key factors are identified to determine the production quality. Then the design principles for the forming system for squeeze casting are built and its functional requirements are attained. And an overall structure for this forming system is presented including the die design system, the design and management system of process parameters and the squeeze casting equipment system. This structure decreases the difficulties and the cost of building the physical system.

Introduction

Squeeze casting (SC) is an advanced manufacturing process where molten metal is subjected to high applied pressure during cooling and solidification [1]. It can be adopted to fabricate components with improved mechanical properties at high integrity and with very low defect levels particularly aiming at minimum porosity [2].This process is completed in its manufacturing system, generally named forming system. A forming system for squeeze casting is defined as the organic integration of all hardware and software involved in squeeze casting forming process.

In the past decades, a lot of investigations about forming systems have been made which improved the production quality and advanced the technology. Liu, et al [3] investigated the multi-point forming method and developed an integrated control forming system for this process mainly based on CAD (Computer Aided Design) /CAM (Computer Aided Engineering) software and bus techniques. In order to achieve the best possible resolution of the Sumy microprobe at the high beam current mode, Magilin, et al [4] designed the integrated probe-forming system for the Sumy nuclear microprobe. A new hot forming system for high-alloy metals with poor workability was proposed by Yanagimoto and Izumi [5]. Wang, et al [6] studied a vacuum forming system based on reconfigurable screw-pin tooling technology. The system integrated reverse engineering, screw-pin tooling, CNC (Computerized Numerical Control) machining and vacuum forming to manufacture products for aerospace and plastics industries in a rapid and cost-effective way. But so far, it appears that very limited works have been carried out to study the forming system for squeeze casting.

According to the definition of the forming system for squeeze casting, it is evident that there are many composition elements and these elements change with its functions and objectives. The overall design is the very important part of a system development that is closest to its objectives and requirements and decides the composition details and development cost. Thus, In order to develop a practical forming system for squeeze casting, this paper focuses on the overall design of this forming system. An overall structure is put forward.

Forming Control Process of Squeeze Casting

The conventional forming process of squeeze casting points the string of procedures on squeeze casting equipment including: (i) pour molten metal into a die; (ii) activate press to close off the die cavity; (iii) exert and hold on pressure till metal solidification; (iv) take out the component after opening the die [7]. Following the above process, components can be produced, but whose quality and properties cannot be guaranteed, also thus the advantages of squeeze casting cannot be attained. This is because some key elements are not emphasized and controlled in the forming process.

After deep investigation of squeeze casting, there are four main factors have effects on the forming quality of the component, namely the die, the process parameters, the shape control accuracy of the die cavity and the control accuracy of the process parameters by squeeze casting machines. The relationships among the four factors are illustrated in Fig.1.The die D is designed and manufactured depending on the component geometry G, at the same time taking into account machining allowance, air vent and other factors; in addition, the selection of die material is very important. So the die cavity geometry G' can be expressed by $G' = f(D)$. Then a geometric error $\Delta E1$ must exist between the component geometry and the die cavity, which is given by

$$\Delta E1 = G - G' . \tag{1}$$

After the die is fixed on the squeeze casting machine, the mechanical pressure supporting metal solidification and fixed error will also cause another geometric error $\Delta E2$ of the die cavity.

$$\Delta E2 = G'' - G' \tag{2}$$

Where, G'' is the effective shape of the die cavity by the squeeze casting machine during production, thus it can be given by $G'' = c(f(D))$.

The key to squeeze casting is control of the processing variables represented by $X1$. The most important squeeze casting process parameters that affect the quality of castings are intensity of applied pressure, melt temperature and die preheating temperature [8]. Many studies have been carried out on squeeze casting parameters, but no universal methods have been proposed to get these squeeze casting parameters accurately for a specific component. At last, all the process parameters should be translated into running data $X2$ of the squeeze casting machine then controlled by its control system, where the control results $X3$ are the effective parameters. Probably, a parameter control error $\Delta E3$ also exists between $X1$ and $X3$. It is evident that the last two factors are determined by the performance of the squeeze casting machine.

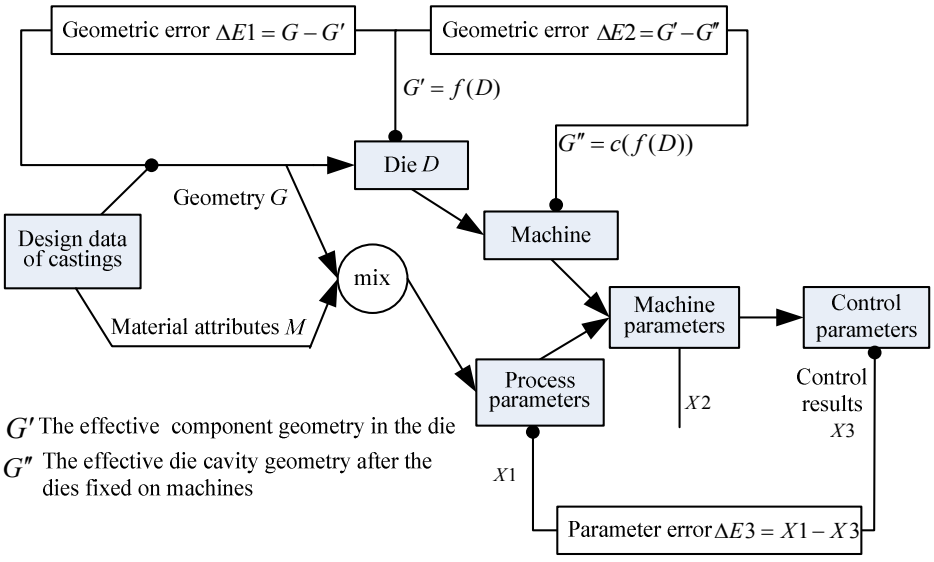

Fig.1 Relationships of the factors affecting squeeze casting forming process

Hence, in order to produce components with optimal quality and properties by squeeze casting according to the original design data or customer's requirements, it is essential to control the above four factors and their relationships, besides following the conventional process steps. Accordingly, it is defined the integral forming process of squeeze casting as the integration of all procedures related to the four factors mentioned above, including process parameter design, die design, machine running data design, melting metal, machine selection and the conventional procedures, as well as other aided procedures like machine trouble shooting. The process parameter design, the die design and the machine running data design change with the preformed component, which makes the squeeze casting production more close to customers and coordinates better. This integral definition expands the conventional squeeze casting process in terms of system engineering, reflects the fact and highlights control of key factors in squeeze casting production.

Design Principles

It is important to control the functions and mutual effects of the subjects and factors in the integral forming process of squeeze casting to have the same defined objectives, and then win competition. The forming system for squeeze casting is presented to achieve these objectives.

The forming system for squeeze casting acting as the a manufacturing system of completing squeeze casting, points the organic integration of all the hardware and software involved in the forming process of squeeze casting. According to the integral forming process of squeeze casting, squeeze casting equipment, dies and other assist tools may be included in the hardware subsystem; the theory of squeeze casting, the technology for process parameter design, die design toolkits, process design system and information are elements of the software subsystem. However, the actual elements and structure of this forming system rely on the detailed design and should be adjusted according to the application environment.

The following principles should be observed to design the forming system for squeeze casting successfully:

- Firstly, integrate necessary elements and at least provide functions to control the dies, process parameters, equipment and machine running parameters so as to realize the process of squeeze casting.
- Secondly, keep the transition of information and data among the forming system smoothly, rational and accurate, at the same time utilize advanced technology or tools to optimize all the transition processes.
- Thirdly, make the forming system configurable and flexible and can be easily adjusted into a new system at low cost.
- Fourthly, avoid starting from scratch through trying best to utilize the old tools and system, considering the relevance between squeeze casting and other forming processes like die-casting.
- Finally, keep the designed system with the characteristic of purpose, systematicness, level, adaptability and coordination.

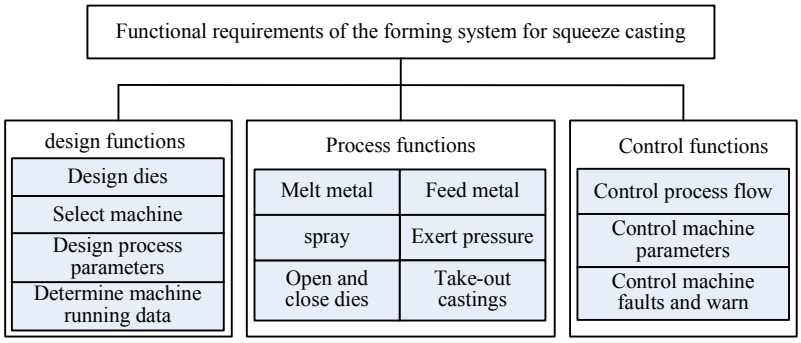

Fig.2 Functional requirements of the forming system for squeeze casting

Functional Requirements

Functional requirements are the basis of designing any system. The functional requirements of the forming system for squeeze casting are attained according to the integral forming process of squeeze casting and its objectives, as listed in Fig.2.They comprise three types of functions: design functions, process functions and control functions. The design functions include die design, process parameter design, machine selection and machine running data design. The function of process parameter design gets the parameters such as applied pressure, melt temperature and die preheating temperature according to the geometry and material of the preformed component. The machine selection determines the optimal squeeze casting machines among a group of squeeze casting equipment, according to the process parameters, equipment performance, cost, due time and so on. The machine running data design assumes the tasks of translating the process parameters into running control parameter in line with the control features of the selected machine. The process functions consists of melting metal, pouring metal, closing and opening dies, exerting pressure, taking-out components and spraying. The control functions include control of process flow and process parameters, fault diagnosis and so on.

Overall Structure of the Forming System

On the basis the functional requirements in Fig.2 and under the guidance of the design principles, we propose an overall structure of the forming system, as shown in Fig.3. In the overall structure, the forming system starts from preformed castings and integrates many elements such as the features of preformed castings, dies, CAD software, furnace, casting simulation software, squeeze casting equipment and components. In term of logics, these elements can be mainly classified into three parts, namely, the die design subsystem, the design and management subsystem of process parameters and the squeeze casting equipment system. Besides them, there are some other aid parts such as the furnace.

The first part, the die design subsystem, is made of CAD software and designs the dies for the preformed casting, which firstly gets the geometric information from the preformed casting design data by some graphic exchange standard like STEP (Standard for the Exchange of Product Model Data) and imports into the CAD system for die design, then build the structure of the dies under the guidance of die design specifications. After that, this system outputs the die data and prints the graphic paper as the basis of manufacturing dies. This part completes the control of and in Fig.1.

The second part, the design and management system of process parameters, has the functions of determining and optimizing squeeze casting process parameters, determining machine running data and managing them. It completes the control of and in Fig.1. This part includes a process knowledge management system, a casting simulation software and the rules and implementation of squeeze casting machine selection. The process knowledge management system mange lots of squeeze casting process knowledge such as process parameters, casting materials, casting properties by building knowledge repository, on the other hand, the process parameters of the specific casting can be achieved through data mining. Here, a new approach to get process parameters based on this system is presented. But the process parameters attained from the knowledge system by reasoning is not optimal. So the casting simulation software is introduced to finish optimization of process parameters, which imports the process parameters from the knowledge system and the die data, then simulates so as to shoot troubles in the process and optimize the process parameters. After that, the process parameters are more optimal which can improve quality. Actually, there are many squeeze casting machines in any foundry company, optimal selection of squeeze casting is important to help the company win competition. In this part, the rules of selecting squeeze casting machines are integrated and implemented as a toolkit. And then, combining the selected squeeze casting machine with the optimal process parameters, the machine running data exported to the last part are determined to control the machine completing the actual process.

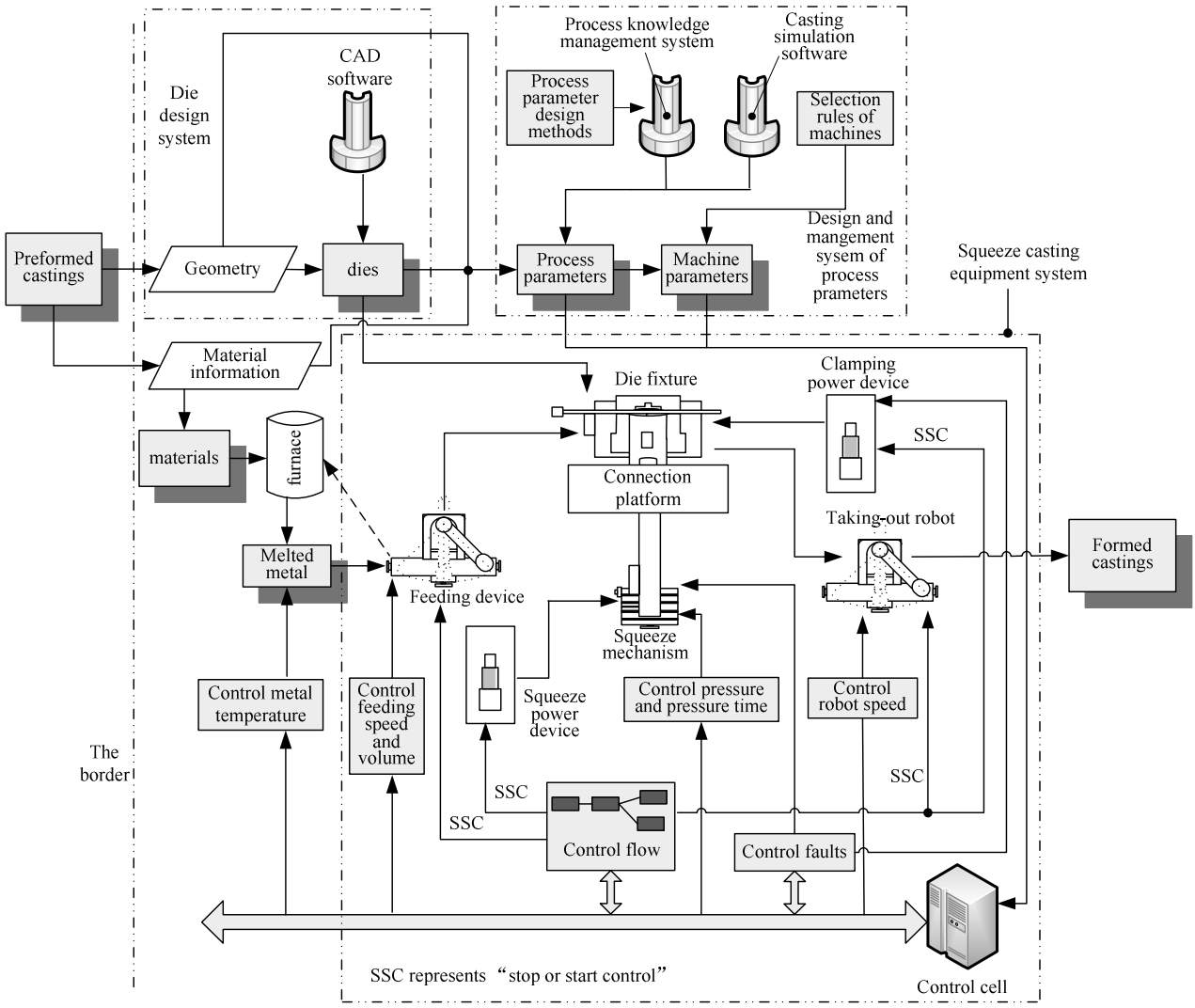

Fig. 3 The overall structure of forming system for squeeze casting

The last part named equipment system, the most important part; manufactures the physical components, which makes the squeeze casting forming process add values and the objectives come true. It is made up of a dies fixture, a power device of closing dies, a squeeze mechanism, a power device of squeeze, a feeding mechanism, a take-out robot, a control system and other components. It feeds the melt metal by the feeding mechanism into the die cavity, and forms the metal into casting shape by the squeeze mechanism, then takes out the shaped casting by the take-out robot for the continual processes. The squeeze casting process parameters are organically integrated in this process. The equipment system implements the types of process and control functions and it completes the control of $X3, G'', \Delta E2$ and $\Delta E3$ in Fig.1. Thus, the whole performance of the equipment decides forming quality of castings to a large degree.

In the first part, the die design subsystem can utilize current popular CAD software such as Proe, UG, which are applied to design moulds in the production of die-casting and injection; In the second part, there are some applicable casting simulation software like ProCAST, Anycasting that simulate squeeze casting process, at the same time the rules of selecting squeeze casting machines can refer to the rules of selecting die casting machines. Therefore, only should the process knowledge management system and the squeeze equipment system be developed.

It is obvious that the presented overall structure of the forming system for squeeze casting meets all the main core functional requirements and it utilizes many old or popular systems, which decreases the difficulties and the cost of building the physical system.

Conclusions

This paper analyzed the forming process of squeeze casting and designed the corresponding forming system. The dies, the process parameters, the shape accuracy of the dies and the control accuracy of the process parameters by squeeze casting machines are the main factors affecting the squeeze casting production quality. Besides the conventional procedure steps on the squeeze casting machine, process parameters design, die design and other corresponding procedures should be the parts of the integral forming process of squeeze casting. This integral forming process constructs the relationships with the actual production in a systematic manner. In order to support the integral forming process of squeeze casting, the functions that the forming system at least has comprises three types of functions: design, process and control functions. An overall structure for the forming system is presented, where the forming system is cut into three parts of the die design subsystem, the design and management subsystem of process parameters and the squeeze casting equipment system in terms of logics. According to this design, we have developed the practical forming system successfully, which not only controls production quality well, but also controls cost.

Acknowledgment

The author would like to thank the Scientific Research Foundation of Guangxi University of China for supporting this work (Grant No.XBZ100568).

References

[1] J.R.Morton and J. Barlow: J. Inst. Brit. Foundryman, Part 1 Vol. 87 (1994), p. 23–28.

[2] P. Vijian and V.P. Arunachalam: Journal of Materials Processing Technology Vol. 180 (2006), p. 161–166.

[3] Chunguo Liu, Mingzhe Li and Zhen Sui, in: Proceedings of the 6th World Congress on Intelligent Control and Automation, IEEE (2006), p. 6601-6605.

[4] D.V. Magilin , A.G. Ponomarev, V.A. Rebrov, N.A. Sayko, K.I. Melnik, V.I. Miroshnichenko, et al: Nuclear Instruments and Methods in Physics Research B Vol. 267 (2009), p. 2046–2049.

[5] Jun Yanagimoto, Ryo Izumi: Journal of materials processing technology Vol. 209 (2009), p. 3060–3068.

[6] Zhijian Wang, Yan Wang and Nabil Gindy,in: ICRM 2007-4th International Conference on Responsive Manufacturing, University of Nottingham(2007).

[7] M. R. Ghomashchi and A. Vikhrov: Mater. Process. Technol Vol. 101(2000), p. 1–9.

[8] A. Maleki, B. Niroumand and A. Shafyei: Materials Science and Engineering A Vol. 428 (2006), p. 135–140.

Advanced Materials Research Vols. 204-210 (2011) pp 17-20

doi:10.4028/www.scientific.net/AMR.204-210.17

Integrated Design of Airborne Radar Servo System Based on MATLAB/SIMULINK

Dingzhen Li[a]， Ruimin Jin[b]

Department of Electronics and Electrical Engineering , Nanyang Institute of Technology, Nanyang，Henan, China

[a]email: lidingzhen.student@sina.com, [b]email: jinruimin2004@163.com

Keywords: Radar Servo System， Electromechanical Coupling Model， Genetic Algorithm， Integrated Design， Simulation

Abstract: This thesis is according to the pitching part of airborne radar servo system. The electromechanical coupling model and optimization model which includes structure parameters and control parameters are built up based on model of mechanism transmission system and electricity control system. The dynamics model of mechanism transmission system includes the nonlinearity of backlash and is considered the influence of parameters for dynamics properties in structure of the mechanism transmission system. The method of integrated structure and control design is applied on the optimization model using GA. Simulation is done based on MATLAB/SIMULINK. Simulation results show that the method of integrated structure and control design is feasible and effective in servo system.

Ⅰ. INTRODUCTION

Airborne radar servo system includes machine system and electrical control system [1]. Traditional design methods make the structure and control of radar servo system as a separate module, after the structure design is optimized, then add the optimal controller to the structure. It is very difficult to achieve the global optimum. To overcome this shortcoming, the design uses a method that makes the structure and control integrated, during the process of the design, synchronize the optimization of structure parameters and control parameters. The simulation results show that the method can improve the synthetic performance of radar servo system effectively.

Ⅱ. INTRODUCTION OF THE OPTIMIZATION ALGORITHM

The model of Radar Pitch servo system are considered the influence of backlash nonlinear factors, and because of the multiple constraints of structure and control, the optimization design is more difficult, the optimization problem is finally reduced to the solution of a nonlinear function which is constrained. The genetic algorithm (GA) is based on the fitness function, by manipulating implementation for the genetic of all individuals of the population to achieve restructuring within the group iterative process of individual search method. And the search does not depend on gradient information, especially for dealing with complex problems and nonlinear problems that traditional search methods can not solve [2], and get optimal solution of the global system, so it has been widely used in the structure/control integrated design. So we select the genetic algorithm theory.

Ⅲ. Establish of Electromechanical Coupling Model

We establish a servo system electromechanical coupling model which combine the mechanical system and control system [3]. In order to show the coupling model clearly, we can use MATLAB/SIMULINK technology-related to group the function-related modules as subsystems and establish multi-level hierarchical model. Figure 1 is the pitch servo system electromechanical coupling model established. As in the basic design the parameters of PWM controller time constant and the loop filter constants are very small, has very little effect on the results of the simulation system, we ignore these factors in the coupled model [5].

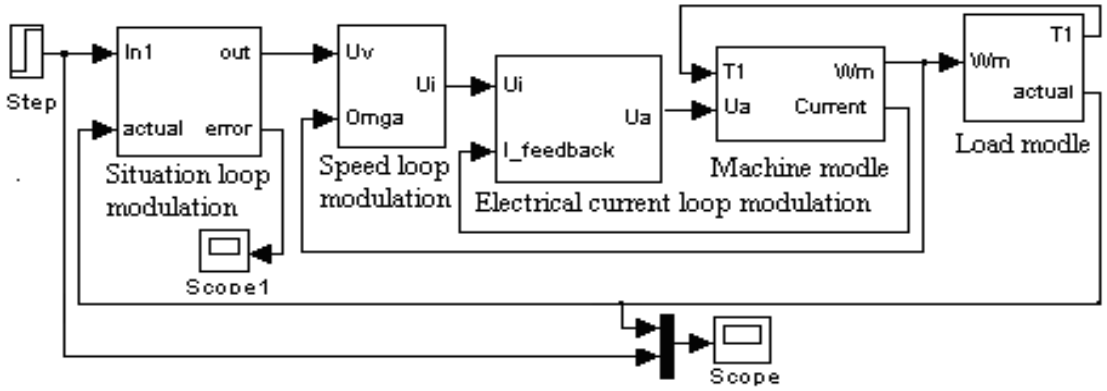

Fig.1. Diagram of electromechanical coupling model

Ⅳ. Establish of Optimization Model

We take an example of the stage signal to do the integrated design of the radar servo system.

A. Determination of the Objective Function

Structure/control integrated design optimizes the maximum gear gap value [6]. There are two levels of gear gap in the designed servo system model: high speed and low speed [7]. So the objective function is taken as: $F = \lambda_1 b_1 + \lambda_2 b_2$ .The impact of the low-level backlash is larger than the high level in the second gear transmission mechanism, so the weight factor is taken as: $\lambda_1 = 0.2, \lambda_2 = 0.8$.

B. Design Variables and Constraint Conditions

1) Selection of design variables

The select of design variables on structure: the teeth number of each gear Z_1,Z_2,Z_3,Z_4, semi-backlash are b_1 and b_2. We take tricyclic PI controller parameters K_i, Tao_i, K_v, T_v, Kp and the corresponding drive parameter K_A, PW, K_B as the design variables on controlling.

2) Specific constraints of the design variables satisfied

a) Specific constraints of variables:

b) Constraints of reduction ratio:

c) Performance constraints: The rise time of the system t_r, the transition time t_s, the peak time t_p and the maximum overshoot M_{max} should have their own limitations.

$$find$$

$$X = (K\_i, Tao\_i, K\_v, Kp, Ti, K\_A, PW, K\_B, Z_1, Z_2, Z_3, Z_4, b_1, b_2)$$

max

$$F = \lambda_1 b_1 + \lambda_2 b_2$$

$$s.t.: \begin{cases} g_1 : 2(r_1 + r_2) - W \le 0 \\ g_2 : r_2 + r_3 + 2r_4 - W \le 0 \\ g_3 : e - e_s \le 0 \\ g_4 : a_- \le i_{12} = r_2 / r_1 \le a_+ \\ g_5 : b_- \le i_{34} = r_4 / r_3 \le b_+ \\ g_6 : c_- \le i_{总} = \mathrm{i}_{12} i_{34} \le c_+ \\ g_7 : M_{\max} \le M \\ g_8 : t_r \le t_1 \\ g_9 : t_s \le t_2 \\ g_{10} \le t_p \le t_3 \end{cases} \quad (1)$$

g_1 and g_2 are the space constraints of the gear box, g_3 is the constraints of the system tracking accuracy, g_4,g_5 and g_6 are the constraints of the reduction ratio, g_7, g_8, g_9 and g_{10} are the constraint of overshoot response of the system, the system rise time, response time, peak time.

C. Optimization Simulation Model

Structure/control optimization mathematical model of integration, as has factor of backlash nonlinearity [8], and the model is complex, the constraints and the model are not so easy to set out to write, we do not need to write the code of the target function if we use the communication between MATLAB and SIMLINK. We take the simulation results which we receive through sim call the SIMULINK module as target function in the objective function file, while the simulation results of SIMULINK module return to the target through the out module. In this way, we make the process of integrated design easy. The call format of sim function is: [t, x, y]=sim (model, timespan, options, ut), while t, x, y is the simulation time, the system state variable and the simulation results output of calling the SIMULINK module, the input variable model is the name of the SIMULINK module called, ti is the simulation time of the module called. In addition, the user can specify the input signal of SIMULINK module through ut and set the solver used in simulation through options. In this way, we create an integration optimization simulation model. After establishing this model, we can design for integrative model using genetic algorithms.

Ⅴ. Simulation Analysis

Integrative design is done for the optimization simulation models. The simulation parameters of the design are shown in Table1, the simulation curves are shown in figure2 and figure3. We can get the results, mechanical structure parameters and control parameters of the servo system are matched with each other after the system is integrated design [9], the gear of the meshing has changed at the premise of meeting the performance index of the system, and the transmission ratio is re-assigned. The space the gear box used reduced at 2.46% after the integrated design, satisfied with the constraints on space of the airborne radar servo system. In addition, the high-level speed and the low-speed level backlash on this paper had an increase of 22.8% and 76.7%. Say that the system can contain a bigger backlash after the integrated design, so that the life of the gear is prolonged, the waste of resource and the cost of production are reduced, as a result, the combination property of the radar servo system is final promoted.

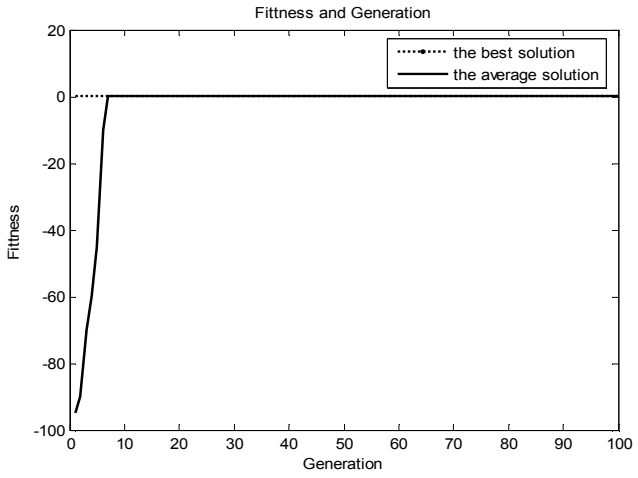

Fig.2.The best solution and the average solution of each generation

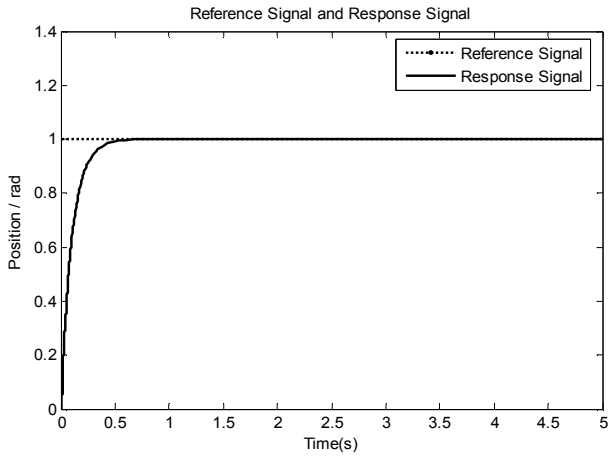

Fig.3 Optimization response curve

Ⅵ. Conclusion

The electromechanical coupling model of the airborne radar pitch servo system built based on the coupled model is the optimization model of the structure/control integration design. Using the genetic algorithms theory we designed the integrated optimization model. The simulation results showed the feasibility and effectiveness of the structure/control integration design in the servo system, and it is the stage for further research. This method can be used as new method in servo system design and can be developed in the long ran.

Table1. Optimization Results

	Parameters		*Original design value*	*Integrated Design value*
Design variable	Structure Design variable	Z_1	18	19
		Z_2	54	68
		Z_3	18	18
		Z_4	150	129
		b_1	62.5	76.778
		b_2	75	132.59
	Control design variable	K_i	5	14.682
		Tao_i	0.0028	0.36888
		K_v	47.876	21.399
		T_v	0.32265	0.08367
		Kp	59.178	58.585
		Ti	789.62	366.47
		K_A	0.3333	0.35943
		PW	4.6	2.3192
		K_B	0.5	0.23749
Performance parameter	W		0.2558	0.2495
	M_p		5%	0%
	t_r		0.4	0.21
	t_s		1	0.8
	t_p		0.8	0.7
	e		1.5e-3	2.8e-4

References

[1] Job van Amerongen,Peter Breedveld. Modelling of Physical Systems for the Design and Control of Mechatronic Systems. Annual Reviews in Control.2003, (27):87-117

[2] Chen Lunjun.mechanical optimal design heredity algorithm. Beijing: CHINE MACHINE PRESS. 2005.

[3] YU Ling，JIA Chun-qiang.Functions and Examples in Matlab GA Toolbox. Mechanical Engineer. 2004,(11):27-28.

[4] Lu Jianwei,Zhang Xianmin, Shen Yunwen. INTEGRATED STRUCTURAL AND NOISE CONTROL DESIGN FOR EIC LINKAGE MECHANISM. JOURNAL OF MECHANICAL ENGINEERING. 2003,39(3):40-43.

[5] Joseph C.Chen, Jacob Chen. Testing a New Approach for Learning Teamwork Knowledge and Skills in Technical Education. Industrial Technology .2004, 20(2): 1-10

[6] Ho Seong Lee,Masayoshi Tomizuka. Robust Motion Control Design for High-Accuracy Position System. IEEE Transaction on Industrial Electronics.1996, 2, 43(1):48-55

[7] Li Xuyu.Reaserch of the Concurrent Design Technique for Complex Mechatronic System .Zhongnan University Doctor's Degree Paper. 2004

[8] ZHAO Guo-feng，FAN Wei-hua，CHEN Qing-wei. A Survey on Backlash Nonlinearity. Acta Armamentarii. 2006,27(6)：1072-1080.

[9] Long Kai, Cheng Ying. The Research of Parameters by the Simulation of Exciting Force in Gears. Computer Simulation. 2002, 19(6):87-89.

Advanced Materials Research Vols. 204-210 (2011) pp 21-24

doi:10.4028/www.scientific.net/AMR.204-210.21

Optimal PID Control of Heat Exchanger Temperature

Xinghua Yang[1,a], Tingrui Liu[1,b] and Jing Sun[1,c]

[1] School of mechanical and electrical engineering

Shandong University of Science and Technology

Qingdao, China

[a]yxh2000@sina.com, [b]liutingrui9999@163.com, [c]sunjing@sdust.edu.cn

Keywords: heat exchanger, temperature control, PID, Simulink

Abstract: To maintain the outlet temperature at the desired set-point, a high-order outlet temperature control model is established for a shell-and–tube heat exchanger, which is based on the analysis of its heat transfer process and dynamic properties .The Optimal PID control is applied to the temerature control system on the basis of this model, and the tuning parameters of the PID controller are obtained by numerical solving of a formulated optimization problem using Matlab/Simulink. An experimental control system is set up to testify the effect of the optimal PID control. The simulation result and the practice show that the control system has a favorable control performance.

Introduction

A heat exchanger is a device which is used for transferring heat between hot and cold fluid, particularly in process industries, such as power generation and chemical plants, etc. In practice, the outlet temperature has to be maintained at a particular set-point in order to meet the practical requirements. A large number of contributions, dealing with the control of the temperature distribution for the heat exchanger, can be found in the literature[1-3], and the typical control process is based on feedback control principle. However, the control performance of the heat exchanger is limited, either because the approximate simulation model is inaccurate due to low-order, or the simulation model with high-order is not suitable for better controller design.

The paper aims to propose a theoretical high-order temperature control model for a shell-and-tube heat exchanger and apply an optimal design of PID controller.The theoretical model is based on the analysis of the heat transfer process and dynamic properties of the heat exchanger, and it can predict the outlet temperature more accurately. Then, the optimal PID controller design is provided, which is an effective alternative to classical controllers when the system model becomes complex.

Shell-and-tube heat exchanger temperature control model

The temperature control model is based on the dynamic properties of the heat exchanger, so it is necessary to analyze the heat transfer process to find the relationship between the outlet temperature and other variables. For a shell-and-tube heat exchanger, the thermal balance equation and the heat transfer rate equation give a basis for determining the theoretical temperature control function .A typical flowing process in the heat exchanger is shown as Fig.1. The hot fluid flows through the tubes of the shell-and-tube exchanger and is cooled from the shell side by another cold fluid. Hereinto, subscript 1 stands for the hot fluid and subscript 2 denotes the cold fluid. G is flow rate; c is specific heat capacity, T_i and T_o are the inlet and outlet temperature respectively. The outlet temperature T_{10} is required to be maintained at a certain set-point, and G_1 is chosen as manipulated variable.

In order to make the analysis easier, some assumption are needed:

(1) The specific heat capacity of the wall of tubes can be neglected;

(2) The hot fluid and the cold fluid are liquid, and the process belongs to laminar flow;

(3) The heat transfer coefficient and the specific heat capacity of the fluid are constant;

(4) The temperature distribution throughout any cross section is uniform.

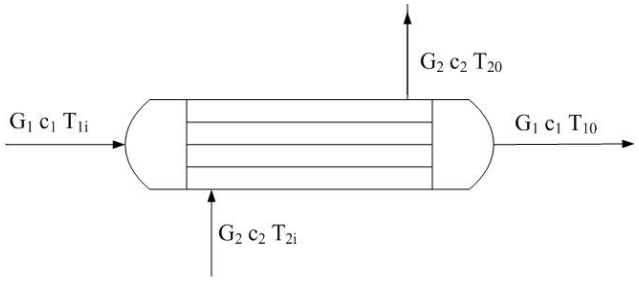

Fig. 1 Flowing process in a shell-and-tube heat exchanger

Application of the heat balance equation to this process gives that: if the heat loss is ignored, the heat absorbed by the cold fluid should be equal to that released by the hot fluid, as shown by Eq.1:

$$q = G_2 c_2 (T_{20} - T_{2i}) = G_1 c_1 (T_{1i} - T_{10}) \tag{1}$$

where q is heat transfer rate.

The heat transfer rate equation derived from the principles of heat transfer can be written as Eq.2:

$$q = UA\Delta T \tag{2}$$

where U stands for heat transfer coefficient, A is area, and ΔT is average temperature difference. For countercurrent flow, it can be replaced by logarithm average value, as listed in Eq.3:

$$\Delta T = \frac{(T_{10} - T_{2i}) - (T_{1i} - T_{20})}{\ln \dfrac{T_{10} - T_{2i}}{T_{1i} - T_{20}}} \tag{3}$$

From equation (1)-(3), an expression of the controlled parameter T10 can be obtained as Eq.4:

$$\frac{T_{1i} - T_{10}}{T_{1i} - T_{2i}} = \frac{1}{\dfrac{G_1 c_1}{UA} + \dfrac{1}{2}\left[1 + \dfrac{G_1 c_1}{G_2 c_2}\right]} \tag{4}$$

The effect on T_{10} caused by the variation of G_1, which is derived by the derivative to Eq.4, can be expressed by Eq.5. This equation describes the static state relationship between T_{10} and G_1, and will be applied to the following dynamic property analysis of the heat exchanger.

$$\frac{dT_{10}}{dG_1} = \frac{(T_{1i} - T_{2i})}{\left[\dfrac{G_1 c_1}{UA} + \dfrac{1}{2}(1 + \dfrac{G_1 c_1}{G_2 c_2})\right]^2} (\frac{c_1}{UA} + \frac{1}{2}\frac{c_1}{G_2 c_2}) \tag{5}$$

Both the theory and engineering practice show that the dynamic property of the heat exchanger can be described by a high-order system with delay, and the transfer function can be expressed as Eq.6.

$$G(S) = \frac{K}{(T_1 s + 1)(T_2 s + 1)} e^{-T_2 s} \tag{6}$$

where K is static state gain, and it can be calculated by Eq.5. T1 and T2 are time constant, whose values are related to the flow rate and the configuration size of the heat exchanger. According to the technological and mechanical design requirement, the related parameters in Eq.6 are obtained as follows: K=0.002; T1 =70.65s; T2=17.66s. So the temperature control model of the heat exchanger is,

$$G(S) = \frac{0.002}{1247.6 s^2 + 88.31 s + 1} e^{-17.66 s} \tag{7}$$

It can be seen that the time lag constant of the system is 17.66s, and it is a system with big inertia.

The optimal PID controller realization

The optimal control[4] is that, under certain concrete conditions, when special control object is achieved, the selected target reaches maximal or least. The target function used here adopts ITAE rule[5], defined as, $J_{ITAE} = \int_0^\infty t|e(t)|dt$.

When time t is relatively big, to assure the target value small, the steady error must be diminished so as to make the system enters into steady area quickly. Choose ITAE as the optimized target and build a heat exchanger Simulink model of the optimal PID illustrated as Fig.2.

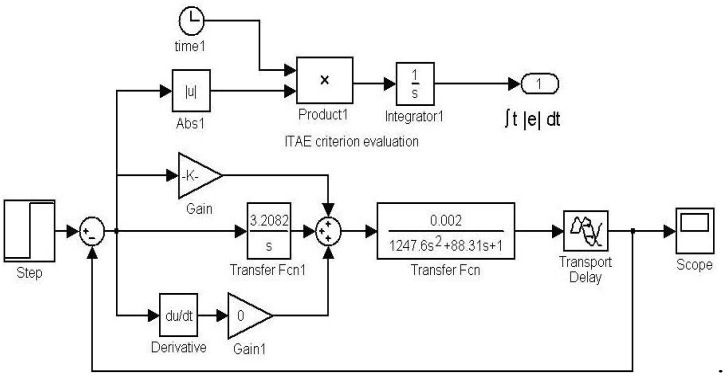

Fig. 2 Scheme of the Simulink model

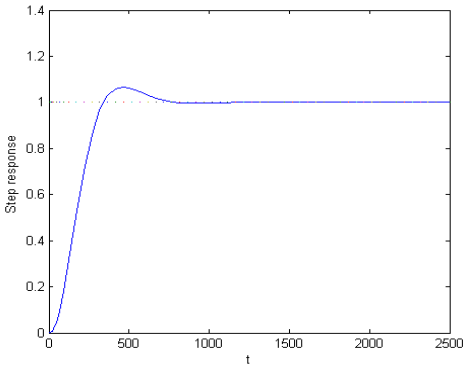

Fig.3 Unit step response consequence

Each parameter in target transfer function may be evaluated and initialized in m file. The Matlab functions, fminsearch(), fmincon(), and nonlin() were applied in background optimization. During the simulation, OCD Model[6]is used. The model permits specifying lower range and upper range of the optimized variable, automatically choosing initial value of the optimized parameters and different simulation algorithms including discrete simulation algorithm. The Matlab subprogram for creating optimal target function is as follows,

```
Function y=optfun_0(x)
assignin('base','Kp',x(1));
assignin('base','Ki',x(2));
assignin('base','Kd',x(3));
[t_time,x_state,y_out]=sim('HRQKZ.mdl', [0,2500]);
y=y_out(end);
```

Hereinto, the result of running line 2 to 4 is to evaluate the optimal simulation variable to the three pending parameters in the workspace. By running line 5, current vector x can be used to simulate the Simulink model. By running line 6, ITAE value can be evaluated to output y. So the calculation of target function is fulfilled. The sampling time is estimated as 2500, which influences the setting consequence. The optimal searching process via OCD Model may better rationalize the choices for Kp, Ki and Kd. From oscilloscope in Matlab, the dynamic optimization and its consequence can be observed, and the PID controller meeting the requirement of minimal target value of ITAE can be obtained. Here, three parameters are Kp=0.4709; Ki=3.2082; Kd=0 respectively. The unit step response consequence of the optimal PID is illustrated as Fig.3, and it can be seen that the response effect is advisable.

Realization of the control system

An experimental system used to testify the PID controller design is set up, as shown in Fig.4. it consists of motor, pump, control valve, heat exchanger, temperature transmitter(TT) , temperature controller(TC), etc. The hardware includes PLC S7－200 CPU 224 module, actuator(control valve V1), temperature sensor and its analog quantity module EM235,as shown in Fig.5.

The working process of the PID controller is that, firstly, the set-point from outside is converted to PLC inner digital value after A/D conversion of the analogue quantity module, and the feedback from the temperature sensor measurement device does the same transformation. Then the two digital values are compared and operated "minus" calculation to produce an error e(n). After the numerical PID operation inside PLC, an output M(n) of the controller is produced as a function of the magnitude of e(n). Finally, M(n) becomes to analogue value after D/A conversion, and the output M(t) is fed to the control valve(V1 in Fig.4) . As a result, the manipulated variable(G_1) is adjusted and it has a direct effect on the controlled variable(T_{10}) until the desired value is obtained.

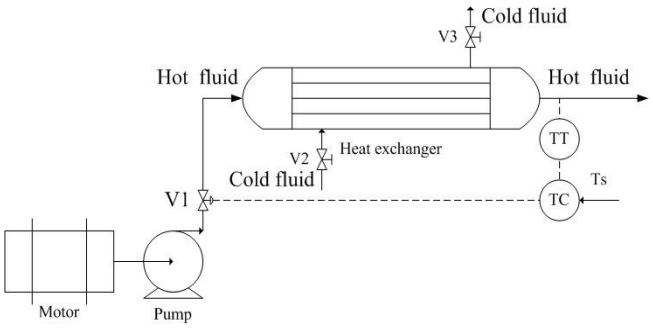

Fig.4 Scheme of the heat exchanger system

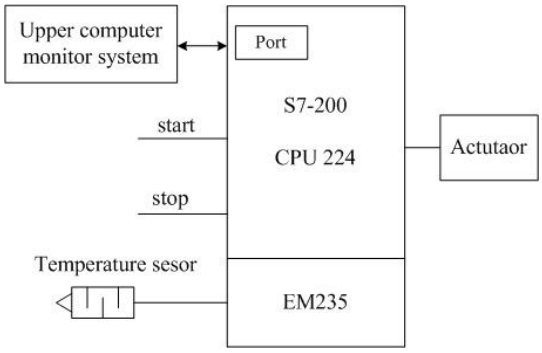

Fig.5 Hardware structure of the control system

Conclusion

(1) A high-order temperature control model based on the analysis of static state and dynamic property of a shell-and –tube heat exchanger is presented. It can be seen from the control function that it is a system with big inertia and time delay.

(2) The optimal PID controller design is applied to the temperature control system and the optimizing process via OCD Model provides better values for PID parameter Kp, Ki and Kd. For this system, they are Kp=0.4709, Ki=3.2082, Kd=0 respectively. The unit step response consequence shows that the control effect is appropriate.

(3) An experimental system is set up to testify the effect of the optimal PID control. The working process and corresponding hardware structure of the temperature control system are given , and the practice verifies its favorable control performance.

References

[1] A. Vidal, A. Banos. Reset compensation for temperature control: Experimental application on heat exchangers. Chemical Engineering Journal. Vol.159(2010), p.170

[2] A. Maidi, M. Diaf, J.Corriou. Optimal linear PI fuzzy controller design of a heat exchanger. Chemical Engineering and Processing. Vol.47(2008), p.938

[3] S. Alotaibi, M. Sen. Controllability of cross-flow heat exchanger. Int. J. Heat Mass Transfer. Vol.47(2004),p.913

[4] T.Liu, G.Chen, and J. Wang. Autocontrol of electronic expansion valve based on optimal fuzzy PD controller. WGEC(2008), p.352

[5] D. Xue: *Computer aided control systems design using MATLAB language* (in chinese). Tsinghua University Press, China,Beijing(2006) ,p.210

[6] D.Xue, Y. Chen:*Matlab solutions to mathematical problems in control*(in chinese).Tsinghua University Publishing Company, China, Beijing(2007), p.372

Advanced Materials Research Vols. 204-210 (2011) pp 25-30

doi:10.4028/www.scientific.net/AMR.204-210.25

Study of Fuzzy Control for Intelligent Cantilever Beam Based on Genetic Algorithm

JingJun Zhang [1, a], XiaoPin Guo [2, b], LiLi He [2, c], RuiZhen Gao [3, d]

[1]Department of Science Research, Hebei University of Engineering, Handan, Hebei, China;
[2]College Civil Engineering, Hebei University of Engineering, Handan, Hebei, China;
[3] Mechanical and Electrical Engineering, Hebei University of Engineering, Handan, Hebei, China
[a] santt88@163.com, [b] xiaopin04@163.com, [c] helili0910@163.com, [d]ruizhenemail@163.com

Keywords: Fuzzy controller; Fuzzy rules; Genetic Algorithm; Intelligent structure; MATLAB

Abstract. The design of fuzzy controller is the key of fuzzy control system, while the core of fuzzy controller design lies in fuzzy rules, whose performance determines the control effect of fuzzy system. General fuzzy rules are obtained from expert experience, in which much subjectivity exists. In this paper, a fuzzy controller is designed by taking an intelligent cantilever beam as the research object. And a method using the genetic algorithm to optimize fuzzy rules is proposed and the genetic coding as well as the fitness function is confirmed. Finally, the simulation model of intelligent cantilever beam is built by Matlab/Simulink, and the vibration control effects of fuzzy controller optimized by genetic algorithm are compared with those un-optimized. The simulation results indicate that the vibration amplitude of intelligent cantilever beam has a significant decrease and the vibration decay rate has a significant increase after the fuzzy rules optimized.

Introduction

Fuzzy control is a kind of control theory based on fuzzy set theory, fuzzy linguistic variables and fuzzy logic reasoning, and a kind of rule-based control [1]; it belongs to the category of intelligent control. The fuzzy control takes control object as "black box", and languages people's operating experience for "black box" into "fuzzy rules", which machines according to imitate people's operating and achieve vibration control [2].

Intelligent cantilever beam structure is one of the most commonly structures used in building engineering. For a long time, great attentions have been paid to the vibration control of the structure. Fuzzy control has achieved good results in active vibration control of flexible structures [3-6]. Fuzzy control can be viewed as a way of converting expert knowledge into an automatic control strategy without a detailed knowledge of the plant [7], and uses rules to linguistically describe the input/output relationship. Fuzzy rules often obtained by expert knowledge, for complex control tasks, obtaining the fuzzy knowledge base from an expert is often based on a tedious and unreliable trial and can't obtain the best. So the design of fuzzy rules has many problems.

Genetic Algorithm (GA) is the optimization algorithm inspired by Darwin's evolutionism and based on survival of the fittest and species genetic ideas. GA which has the advantages of little dependence on the problem has been used to design and optimize different parameters of fuzzy controllers, such as membership functions, rule base, and scaling factors. Take intelligent cantilever beam for example, the paper design a fuzzy controller and GA is used to optimize fuzzy rules to improve the control effects of fuzzy controller. Then the simulation model of intelligent cantilever beam is built by Matlab/Simulink to test the effects of fuzzy controller.

1. Study Object

In this section a model of intelligent cantilever beam structure that is suitable for control analysis is developed. The structure considered consists of a member that includes a sensor, an actuator and a main structure, as shown in Fig. 1. When exciting forces act on the free end of the intelligent cantilever beam, the structure will vibrate and cause damaging effects.

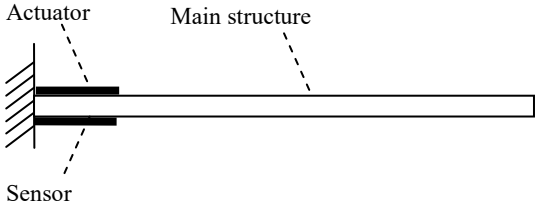

Fig.1 Physical model of the intelligent cantilever beam

Mathematical model is the mathematical expression that describes the relationship among input, output variables and the internal variables. To simulate the vibration process of system, mathematic model of the system must be established firstly. Modeling the structure by finite element method, the motion equation for intelligent cantilever beam structure is [8]

$$M\ddot{x} + C\dot{x} + Kx = F(t) \tag{1}$$

where M , C and K are total quality, total damping and total stiffness of structure, and x , $\dot{x}$, and $\ddot{x}$ are the vectors of displacement, velocity and acceleration, respectively， $F(t)$ is exciting force.

2. Design of Fuzzy Controller

Currently, fuzzy controller is usually the structure mode of two inputs and single output in structural vibration control. In this paper, the same structure mode is employed to solve the problem. The inputs and output variables are displacement, velocity and reaction force in intelligent cantilever free end which are expressed as e、ec and u respectively. Triangular membership functions of 7 linguistic variables are chosen for two inputs and one output whose fuzzy sets are defined as {NB, NM, NS, ZE, PS, PM, PB}. Relationships of inputs and output decide the fuzzy rules. The seven fuzzy sets for two inputs constitute a 7 × 7 two-dimensional fuzzy rule table:

Rule：IF $<E = e_i>$ AND $<EC = e_j>$, THEN $<U = u_{ij}>$, where $1 \le i \le 7$, $1 \le j \le 7$;

The fuzzy domain of displacement, velocity and control reaction is $E = EC$ =[-8 , 8], U =[-6 , 6]， quantification factor for displacement and velocity are K_e and K_{ec} , proportional factor for control reaction is K_u , Fuzzy reasoning method is Mandain method; De-fuzzy is gravity method.

3. Fuzzy Rules Optimization by GA

In GA, code the fuzzy rules for fuzzy controller firstly, then determine the fitness function, obtain the most adaptable population through selection, crossover and mutation until convergence.

3.1 Genetic Coding

The first problem of optimizing fuzzy control rules by GA is the coding problem of fuzzy control rules, coding is the basis. Genetic coding changes the problem objects into certain order of strings by Specific symbols, and then operates these strings.

The common coding methods are binary coding and decimal coding. Relative to the binary coding, decimal coding has shorter length of coding, saves computer memory space, improves the algorithm speed and has obvious physical meaning. So the paper use decimal coding that the fuzzy

set {NB, NM, NS, ZE, PS, PM, PB} is represented by an integer set {1, 2, 3, 4, 5, 6, 7}, which can be convenient to digitize fuzzy control table. And obtain the GA individuals by expanding two-dimensional fuzzy control rules into one-dimensional from left to right, from top to bottom. For this fuzzy controller which has two inputs that have 7 fuzzy sets, a complete fuzzy rule base should be 7×7 control rules, that is, there are 49 parameters to be searching. Such a chromosome contains 49 genes. Take a common fuzzy rule table of FLC for example [9], and the chromosome is thus obtained from the fuzzy rule table by the code string of GA illustrated by the 49 integers such as

7777644777764466664336654322554222244211114421111.

The common fuzzy rule table and the chromosome table are shown in Table 1 and Table 2.

Table 1.The Common Rule Table

OOUTPUT U		EC						
		NB	NM	NS	ZO	PS	PM	PB
E	NB	PB	PB	PB	PB	PM	ZO	ZO
	NM	PB	PB	PB	PB	PM	ZO	ZO
	NS	PM	PM	PM	PM	ZO	NS	NS
	ZO	PM	PM	PS	ZO	NS	NM	NM
	PS	PS	PS	ZO	NM	NM	NM	NM
	PM	ZO	ZO	NM	NB	NB	NB	NB
	PB	ZO	ZO	NM	NB	NB	NB	NB

Table 2. Chromosome Table

OUTPUT U		EC						
		NB	NM	NS	ZO	PS	PM	PB
E	NB	7	7	7	7	6	4	4
	NM	7	7	7	7	6	4	4
	NS	6	6	6	6	4	3	3
	ZO	6	6	5	4	3	2	2
	PS	5	5	4	2	2	2	2
	PM	4	4	2	1	1	1	1
	PB	4	4	2	1	1	1	1

3.2 Determination of Fitness Function

GA searches on the value of fitness function, so the problem of individual quality evaluation whose basis is fitness function must be solved. In the paper, the objective of the fuzzy controller performance evaluation is to find the minimal vibration amplitude for intelligent cantilever beam whose free end has an exiting load through GA searching. Take fuzzy rules which have 49 fuzzy sets in the control rule table as design variables. The objective function is selected as the maximum deflection in free end of the intelligent cantilever beam, whose expression is shown in equation (2)

$$J(x) = Abs(\max(x)) \tag{2}$$

Where x is the displacement at the free end of intelligent cantilever beam, $J(x)$ is the absolute value of maximum displacement in the free end of intelligent cantilever beam. The optimization objective is minimizing $J(x)$.

The large value of fitness function is selected priority in GA, while the control objective is to minimize the vibration amplitude and accelerate the decay speed of the intelligent cantilever beam. So the objective function needs to be translated into the maximum problems taken as fitness function. Through fitness scaling, the fitness function in the GA can be selected as

$$F(x) = \frac{1}{1 + J(x)} \tag{3}$$

Where $F(x)$ is the fitness function.

3.3 Genetic Operation

3.3.1 Selection Operation

Selection operation had been evaluated based on the fitness functions. Design variables that will become parent designs are selected according to their individual fitness ranking. In the paper,

Selection operator is proportional fitness assignment method where the selected probability of individuals is proportional to their fitness.

That is $$p_i = f_i / \sum_{i=1}^{n} f_i \quad (4)$$

Where n is population size, f_i is fitness of i individual, p_i is the probability of i individual.

3.3.2 Crossover Operation

Crossover operation is the primary means of generating new individuals in GA. This process ensures that design information is transferred from one generation to the next. Crossover is the two mutual paired chromosomes exchange some sections of its genes in some way and form two new individuals [10]. In the paper two-point crossover is used.

For example, Select two parent chromosomes S1 and S2, and generate cross-point randomly.

Parent 1: S1= (11465742567123544 | 35614577425514327722324 | 334651213)

Parent 2: S2= (15635457633457625 | 43126454122145365645445 | 356563512)

After crossover: S3= (11465742567123544 | 43126454122145365645445 | 334651213)

S4= (15635457633457625 | 35614577425514327722324 | 356563512)

3.3.3 Mutation Operation

Mutation operation is introduced via the occasional switching at a randomly selected location of the generated strings. This action is important since it guards against the premature convergence of the design towards a non-optimal solution [11]. Mutation operation is that some genes of the chromosomes are replaced by other allele genes and form new individuals. In the paper, fuzzy rules is divided into seven linguistic variables, and mutation genes are replaced by random number 1-7. For example, one or several of the 49 genes of chromosome S1 mutate randomly.

Parent 1: S1 (1) = (11465742567123544356145774255143277223243346512 13)

After mutation: S1 (2) = (11465252563123544356145474255143277233241346542 13)

3.4 Basic Steps of GA

Determined GA parameters: number of design variables is 49, number of population is 15, and number of iterations is 20. The process of optimizing fuzzy rules by GA is shown as follows:

(1) Coding individuals to create initial groups P(t)，t=0.

(2) Act the fuzzy controller whose fuzzy rules are the groups above on intelligent cantilever beam, take the vibration results of intelligent cantilever beam as objective function to evaluate the individuals of the generation, and then calculate the fitness f_i of each individual.

(3) Select individuals with higher fitness for offspring generations by optimal preserving strategy.

(4) Cross the two random generations with probability Pc to get the new two generations.

(5) Mutate the generations with probability Pm to gets new generations.

(6) Evaluate the fitness of the individuals and gets the new offspring, and then go back to (2), until certain criteria, such as a fixed number of iterations, or a time limit etc. are met. End.

Apply the GA process to the fuzzy control process in intelligent cantilever beam drawn in Fig.2.

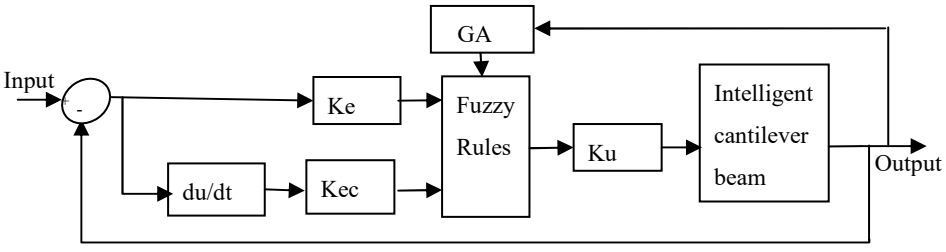

Fig.2 Fuzzy control process based on GA

4. Simulation Example

4.1 Intelligent Cantilever Beam

Take an intelligent cantilever beam shown in Fig.1 as an example, the parameters and fuzzy controller structure are same as reference [12] (Showed in table 3). Through calculations, the total mass of the intelligent cantilever beam is 0.108kg, the total stiffness is 73.8N / m, the damping is 0.05N· s / m. Interference is a period of step response which act on the free end of the beam. Initial value is 500N, the sampling time is 0.001s.

Table 3. Parameters of piezoelectric intelligent beam

Name	Code	Value	Unit
length \ width \ thickness of the beam	l\b\h	350\25\4	[mm]
length \ width \ thickness of the piezoelectric patches	l_v\b_v\t	35\25\1	[mm]
Density of beam \ piezoelectric patches	ρ_m\ρ_p	2900\8300	[kg/m^3]
Elastic modulus of beam \ piezoelectric patches	E_m \E_p	$(6.8\times10^{10})\backslash 3.8\times10^{9}$	[Pa]
Piezoelectric constant \PVDF breakdown Voltage	d_{31}/V	$21\times10^{-12}/1400$	[(C/V)·N]

4.2 Simulation Results

Establish the simulation model of intelligent cantilever beam shown in Fig.3. Different fuzzy control rules for the fuzzy logic controller module in figure can come to different control effects. GA is used to search for the optimal fuzzy rules which make the best control effects.

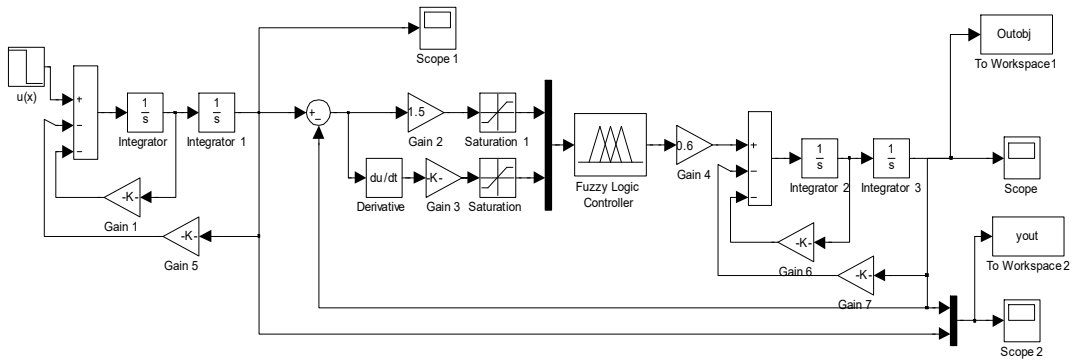

Fig. 3 Simulation model of intelligent cantilever beam

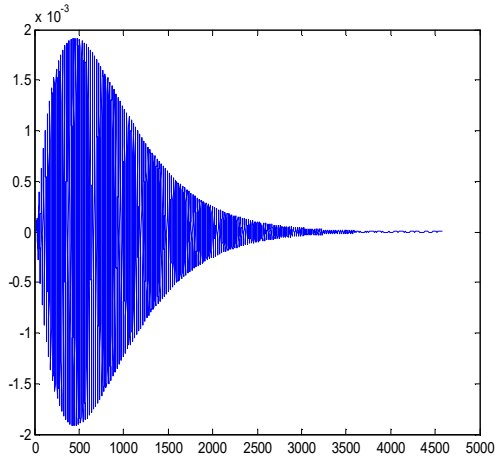

Fig.4 Displacement curve of the intelligent cantilever beam in control of fuzzy controller un-optimized

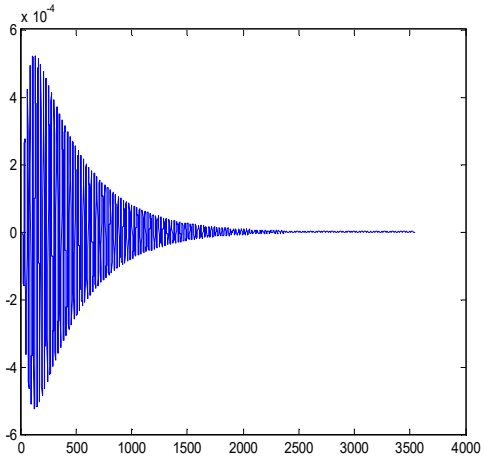

Fig.5 Displacement curve of the intelligent cantilever beam in control of fuzzy controller optimized

To compare the vibration control effects in control of optimized rules to un-optimized clearly. Take the displacement in the free end of intelligent cantilever beam as output curve. Fig.4 and Fig.5

are the displacement curves of the intelligent cantilever beam in control of un-optimized fuzzy controller and optimized. The simulation results can conclude that fuzzy controller optimized by GA have significant control effects in control maximum displacement. After optimizing, the maximum displacement of intelligent cantilever beam changes from 1.85×10^{-3} m to 5×10^{-4} m. In addition, the intelligent cantilever beam has the higher decay rate and the shorter vibration time.

5. Conclusion

The optimization problem of fuzzy control rules by GA has been discussed, and a process of GA optimize fuzzy rules is described in detail, and then obtain the control effects applying the optimized fuzzy controller to intelligent cantilever beam. From the control results of intelligent cantilever beam, the conclusions can be obtained, ① Optimize fuzzy control rules by GA is feasible. ② Fuzzy controller optimized by GA can achieve good results in vibration control of intelligent structures vibration. Therefore, GA optimizes fuzzy control rules have high practical value in preventing the displacement of some vibration in systems with high requirements.

Reference:

[1] LimMN, Rahardjm S, Gwee B H: A GA paradigm for learning fuzzy rules [J]. Fuzzy Sets and Systems, 82(2): 177-186 (1996)

[2] Shi Xinmin, Hao Zhengqing: Fuzzy control and matlab simulation [M]. Tsinghua University Press, Being Jiaotong University Press (2008)

[3] Lin J, LiuWeizheng: Experimental evaluation of a piezoelectric vibration absorber using a simplified fuzzy controller in a cantilever beam [J]. Journal of Sound and Vibration, 296: 567-582 (2006)

[4] Teng Tsoliang, Peng Chengping, Chuang Chun: A study on the application of fuzzy theory to structural active control [J]. Comput Methods Appl Mech. Engrg, 189: 439-448 (2000)

[5] Gustavo Luiz C M de Abreu, Jos F. Ribeiro: A self-organizing fuzzy logic controller for the active control of flexible structures using piezoelectric actuators [J]. Applied Soft Computing, 1: 271-283 (2002)

[6] Wei jingjun, Qiu zhicheng,Ye chunde: Experimental study of active vibration control Piezoelectric Flexible Beam Based on Fuzzy Control [J], journal of vibration and shock，27(12): 91-96 (2008)

[7] K.Parsa, T.A.Lasky, and B.Ravani: "Design and implementation of a mechatronic, all-accelerometer inertial measurement unit," IEEE/ASME Trans. Mechatronics, vol.12, no.6, pp.640-650 (2007)

[8] Wang Dezhou, Zhang Chijiang, Chen Jianjun. Hardware-in-the-loop fuzzy vibration control simulation for intelligent structures [J]. Aeronautical Computing Technique, 36(3): 93-96 (2006)

[9] Li dongxu, Large Flexible Space Truss Structures: Dynamic Analyses and Vibration Fuzzy Control [M], Science Press (2008)

[10] Lim M H，Rahardardja S , Gwee B H.A GA paradigm for learning fuzzy rules. Fuzzy sets and system (1996)

[11] C.Mares, C.Surace, An application of genetic algorithms to identify damage in elastic structures, Journal of Sound and Vibration 195 195-215 (1996)

[12] Zhang Jingjun, Cao Liya, Fuzzy control and simulation of piezoelectric intelligent structure vibration [J], engineering mechanics, 10(26): 228-232 (2009)

Advanced Materials Research Vols. 204-210 (2011) pp 31-35

doi:10.4028/www.scientific.net/AMR.204-210.31

Research on the Fouling Prediction Based on Hybrid Kernel Function Relevance Vector Machine

Lingfang Sun[1,a], Honggang Xie[1,b] and Lihong Qiao[1,c]

[1]School of Automation Engineering, Northeast Dianli University Jilin 132012, Jilin Province, China

[a]dr_sunlf@163.com,[b]zhuxi113@163.com,[c]jasmin@163.com

Keywords: Fouling Thermal Resistance; Prediction; Relevance Vector Machine; Hybrid Kernel Function

Abstract. The research on the fouling prediction of heat exchanger is significantly to improve operational efficiency and economic benefits of the plants. Based on the relevance vector machine with Gaussian kernel function, polynomial kernel function and hybrid kernel function, simulation research on the fouling prediction was introduced. We construct a six-inputs and one-output network model according to the fouling monitor principle and parameters with MATLAB, all training data came from the Automatic Dynamic Simulator of Fouling and input the network after normalized processing and reclassification. Simulations show that the root mean square error of fouling prediction with hybrid kernel function is less than simple kernel function, and has the better prediction precision.

Introduction

The heat exchanger fouling has caused a huge loss in industrial production process today. According to the investigation for the all types of three thousands heat exchangers of the New Zealand's thousands of enterprises by Steinhagen and others, over 90% of the heat exchangers have different degree issues of fouling [1]. Fouling is the gradually accumulated solid material at the solid surface contacted the fluid, and it exists as a mixture [2]. According to the investigation of the west developed countries, the heat exchanger fouling caused the loss to the industrial countries averagely accounting for 0.3% of GDP. However, for the developing country just like China, because of the lag of technology and equipment, the loss was more serious. Reducing the damage accused by fouling is a support to develop the Low-carbon energy economy.

The formation of fouling is an extremely complex process, it concludes lots of factors. Because of the complex formation of the fouling, the research on fouling relates to the other subjects, i.e. biology, physics, chemistry and others. Researches on the heat exchanger fouling conclude three indirections, that is, fouling prediction, fouling monitoring and fouling countermeasure. Fouling prediction is the basic of the fouling monitoring and fouling countermeasure. From the 1980s, Epstein had adopted matrix to the theoretical analysis and experimental research of fouling formation [3]. Recently, gray theory, neural network, fuzzy theory and others algorithm were applied into fouling prediction. Although they attained great achievements, there were some deficiencies.

Support vector machine (SVM) proposed by Vapnik and others in the 1990s is based on the statistic theory of machine learning algorithm [4]. Although SVM overcame some shortcomings of other intelligent algorithm, there were some deficiencies. The choice of kernel function must obey the rules of Mercer. The choice of kernel function in SVM is restricted to some single kernel function, either local kernel function or global kernel function, and then it limits some aspects of SVM. Hybrid kernel function not only has the advance of the local kernel that being good at interpolation and collecting local sample's property, but also acquires the global sample's property [5].

Relevance Vector Machine(RVM) based on the frame of Bayes was proposed by Tipping M. E. in 2001[6-8]. Compared to SVM, RVM not only get the binary output, but also a probability output. The choice of kernel function isn't limited by Mercer. The time of training sample is shorter. This paper

combined RVM with hybrid kernel function and applied the Hybrid Kernel Function RVM into the prediction of the heat exchanger fouling.

Hybrid Kernel Function RVM

Hybrid Kernel Function. Kernel function is the crucial part of SVM. Kernel function improves the SVM capacity of dealing with non-linear. According to kernel function, SVM implements the optimal separating surface in the high dimensional feature space. Kernel function achieves the non-linear learning algorithm in the input space and replaces dot product of the original space. Through a nonlinear change Φ , kernel function maps a stochastic vector x in the n -dimensional vector space to high dimensional feature space. The following parts are the relational concepts and definitions.

Definiton2.1 (feature space) assumed the mode x belonging to input space, i.e. $x \in$ X, through Φ , mapping the input space to a new space $F = \{\Phi(x) : x \in X\}$, F is the feature space.

Difiniton2.2 (Gram matrix) given a function $k : X^2 \to K$ ($K = C$ or $K = R$, C means complex set, R means set of real numbers) and mode $x_1,...,x_m \in X$, then the $m \times m$ matrix $K_{ij} = k(x_i, x_j)$ is called Gram matrix for $x_1,...,x_m$.

Definition2.3 (positive definite matrix) a $m \times m$ matrix K is the positive definite matrix, if $\forall_{c_i} \in C$, then $\sum_{i,j} c_i \overline{c}_j K_{ij} \geq 0$.

Definition2.4 (positive definite kernel) X is a nonempty set, k is a function based on $X \times X$, if k is suitable for all $m \in N$ and $x_1,...,x_m \in X$ generates a Gram matrix, and then we call it for positive definite kernel, kernel for short.

Mercer theorem assuming(X, μ) is a finite measure space, if $k \in L_\infty(X^2)$ is a symmetric real-valued function and the formula (1) is positive , i.e. $\forall f \in L_2(X)$, $\int_x k(x,y) f(x) f(y) d\mu(x) \mu(y) \geq 0$

$$T_k : L_2(X) \to L_2(X), (T_k f)(x) := \int_x k(x,y) f(y) d\mu(y). \quad (1)$$

Gaussian kernel function is a classical local kernel function. Gaussian kernel function influences the samples which their distances are close to σ , nevertheless, when sample distance is larger than σ its value will tend to 0. Gaussian kernel function can attain good local properties of sample. Polynomial kernel function is a staple global kernel function. It is mainly used to extract the sample global property. K_m stands for hybrid kernel function, K_g stands for global kernel function, K_l stands for local kernel function. K_m can be represented by the following equation:

$$K_m = \alpha K_l + \beta K_g. \quad (2)$$

here $\alpha + \beta = 1$.

Relevance Vector Machine（RVM）. Given the input sample $\{x_n\}_{n=1}^N$ and the output sample $\{t_n\}_{n=1}^N$, with t_i independently distribute. We based on the input samples, output samples of data and the prior probability to design a system. When there was the new input x_i , to predict the output t_i . The prediction model can be represented by the following equation:

$$y(x : \omega) = \sum_{i=1}^{N} \omega_i k(x, x_i) + \omega_0. \quad (3)$$

N means the number of sample, ω_i means weights， $k(x, x_i)$ means kernel function. So the prediction value is

$$t_i = y(x_i, \omega) + \varepsilon_i \ . \quad (4)$$

ε stands for the additional noise and independently distribute, with the variance is σ^2 ,the mean is 0. Assumed t_i independently distribute, then

$$p(t_i|\omega,\sigma^2) = N\left(y(x_i,\omega_i),\sigma^2\right) . \quad (5)$$

The likelihood function of all samples is:

$$p(t|\omega,\sigma^2) = \prod_{i=1}^{N} p(t_i|\omega,\sigma^2) = (2\pi\sigma^2)^{-N/2} \exp\{-\frac{1}{2\sigma^2} \| t-\Phi\omega \|^2\} . \quad (6)$$

here $t = (t_1,...,t_n)^T$, $\omega = (\omega_0,...,\omega_N)^T$, $\Phi = [\varphi_{(x_1)},...,\varphi_{(x_n)}]^T$, $\varphi(x_i) = [1, k(x_i,x_1),...,k(x_i,x_N)]^T$

to avoid over learning, weighs ω given the prior probability distribution:

$$p(\omega|a) = (2\pi)^{-\frac{M}{2}} \prod_{m=1}^{M} a_m^{\frac{1}{2}} \exp(-\frac{1}{2} a_m \omega_m^2) . \quad (7)$$

as the prior probability and likelihood distribution, then the posterior probability distribution of ω is:

$$p(\omega|t,a,\sigma^2) = \frac{p(\omega|t,\sigma^2)p(\omega|a)}{p(\omega|a,\sigma^2)} = N(\omega|\mu,\Sigma) . \quad (8)$$

with $\mu = \sigma^{-2}\sum\Phi^T t$, $\sum = (\sigma^{-2}\Phi^T\Phi + A)^{-1}$, $A = diag(a_0,a_1,...,a_n)$.

Fouling Prediction Based on Hybrid Kernel Function RVM

Sample Data Acquisition. In the study of formation process of fouling, we found fouling resistance reflect the degree of the scale of the forming. We took the fouling resistance as our goal output. On the monitoring principle of fouling resistance, we found that six measuring parameters influenced fouling directly, i.e. input temperature of working fluid, output temperature of working fluid, flow velocity of working fluid and three temperatures of heat exchanger tube wall. We took these 6 parameters as the independent variable and the fouling resistance value as the dependent variable. The data we acquired used for the research were from the Automatic Dynamic Simulator of Fouling [9]. Each minute we would collect a group of sample data, altogether 1700 groups of data continuously. The former 1000 groups of data were used as the training samples, and the whole data were used to forecast confirmation. The samples data would be normalized by the prestd function in matlab.

Parameters Set. The Gaussian kernel function was chosen as K_l in the hybrid kernel function, as well as the polynomial kernel function was chosen as K_g. Here $q = 1$, $\alpha = 0.9, \beta = 0.1$. We conducted an experiment comparison respectively based on hybrid kernel function, gassian kernel function and poly kernel function of RVM. The width of hybrid kernel function was 0.33, the width of Gaussian kernel function was 0.3, the width of the poly function, which was a quadratic polynomial, was 1.

Evaluation Criterion. The quality of regression results can be verified through a variety of ways, in this paper, we evaluate the results by root mean square (RMS) and root mean square error (RMSE):

$$RMS = \frac{1}{n}\sum_{t=1}^{n}\left|\frac{y_t - \hat{y}_t}{y_t}\right| , \quad RMSE = \sqrt{\frac{1}{n}\sum_{t=1}^{n}(y_t - \hat{y}_t)^2} .$$

Experimental Results and Analysis

We used 1700 samples for the simulation in MATLAB7.1, respectively, via hybrid kernel function, Gaussian kernel function, and polynomial kernel function of RVM.

Fig.1 is the real fouling resistances curve. Fig.2, Fig.4 and Fig.6 are the comparison Figures between the real curve and prediction curve under hybrid kernel function, Gaussian kernel function and poly kernel function of RVM. It could be seen; all they accurately predicted the tendency of fouling resistance. Compared to Fig.4 and Fig.6, Fig.2 had a better effect. Fig.3, Fig.5 and Fig.7 are

the relative error curves that under the corresponding kernel function RVM. Compared to Fig.5 and Fig.7, Fig.3 had a smaller relative error range.

Table 1 enumerates the experimental results of the root mean square (RMS) and root mean square error (RMSE) under hybrid kernel function, Gaussian kernel function and poly kernel function of RVM. It can be seen, RMS and RMSE under the hybrid kernel function RVM are smaller than those under Gaussian kernel function and poly kernel function of RVM.

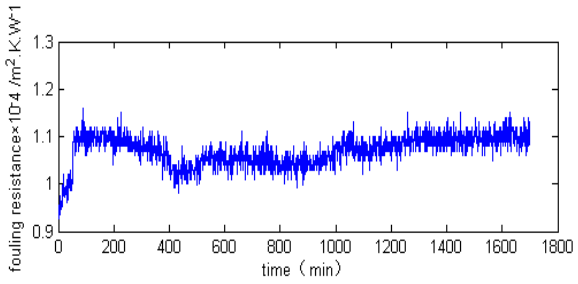

Fig.1 The real fouling resistance curve

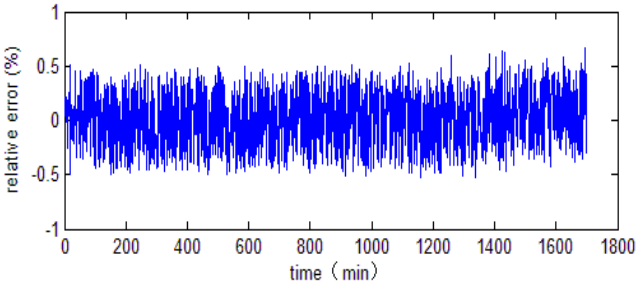

Fig.5 Relative error curve of Gaussian kernel function SVM

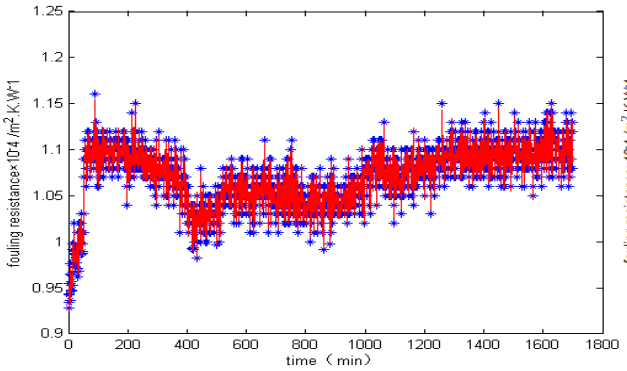

Fig.2 Real curve (*) and prediction curve , with hybrid kernel function SVM(-)

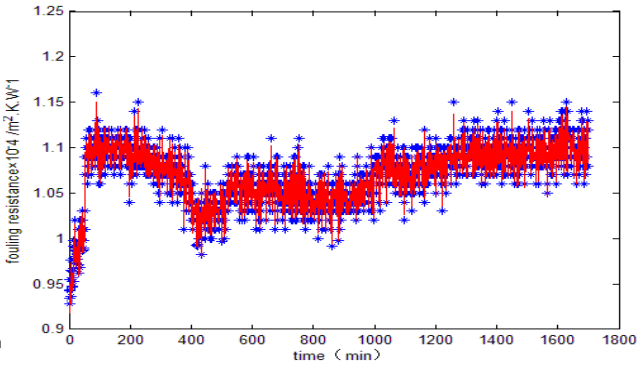

Fig.6 Real curve (*) and prediction curve with poly kernel function SVM(-)

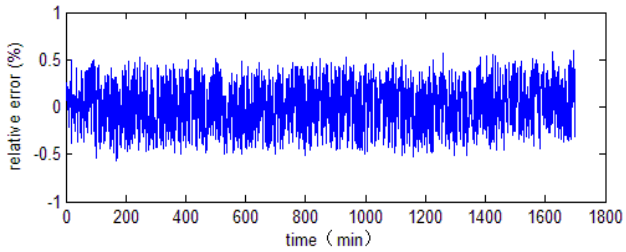

Fig.3 Relative error curve of hybrid kernel Function SVM

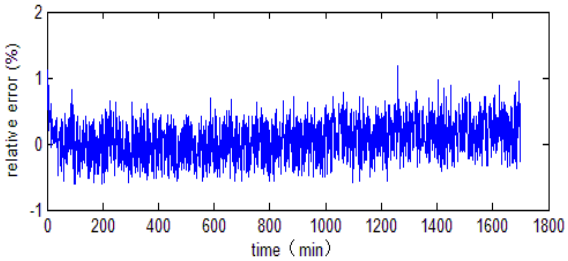

Fig. 7 Relative error curve of poly kernel function SVM

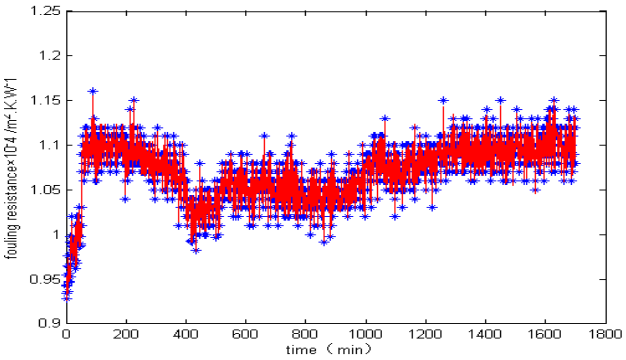

Fig.4 Real curve (*) and prediction curve with Gaussian kernel function SVM(-)

Table 1 The error of different kernel function

	Hybrid kernel function	Gaussian kernel function	Poly kernel function
RMS	0.00233456	0.00234192	0.00261182
RMSE	0.00289565	0.00291296	0.00337553

Conclusions

The research shows that the Hybrid Kernel Function RVM has the best fouling prediction precision than the single kernel functions, i.e. Gaussian kernel function SVM and the poly kernel function SVM, and the method can provide more output information, such as probability output and confidence interval output, and so on.

However, some problems still need to solve, such as the weight of every single kernel function, decrease of the training time of RVM with complex input sample, we will do the further study in the following work.

Acknowledgment

Supported by National Basic Research Program of China (2007CB206904).

References

[1] Steinhagen R, Steinhagen H M, Maani K. Problems and Costs due to Heat Exchanger Fouling in New Zealand Industries. Heat Transfer Engineering, Vol. 14(1993), p. 19-30

[2] Shanran Yang, Zhiming Xu, Lingfang Sun. Heat Exchanger Fouling and Its Countermeasure, 2nd Ed, Science Press, Beijing, 2004.

[3] Epstein N. Thinking about Heat Transfer Fouling: A 5×5Matrix. Heat Transfer Engineering, Vol. 4(1983), p. 43-56

[4] Zhimin Yang, Guangli Liu. Uncertainly Principle and Application of Support Vector Machine, Science Press, Beijing (2007)

[5] Xiao Huang. The Study on Kernels in Support Vector Machine,[Master Thesis], Soochow University, Su Zhou(2008)

[6] Tipping M E. The Relevance Vector Machine//Proc. of Advances in Neural Information Processing Systems. Cambridge, Mass: MIT Press(2000)

[7] Tzikas D G, Likas A, Galatsanos N P, et al. Relevance Vector Machine Analysis of Functional Neuroimages. Arlington, VA: IEEE(2004)

[8] Nikolaev N. Sequential Relevance Vector Machine Learning from Time Series. Proceedings of International Joint Conference on Neural Networks. Montreal, Canada(2005)

[9] Lingfang Sun , Shanyang Yang, Yukun Qin, Zhiming Xu. Evaluation of Antifouling Performance for Ion-rod Water Treater with Automatic Dynamic Simulator of Fouling, Journal of chemical industry and Engineering, Vol. 56(2005),p. 668-671

Advanced Materials Research Vols. 204-210 (2011) pp 36-41

doi:10.4028/www.scientific.net/AMR.204-210.36

Rank reversal and Rank Preservation in TOPSIS

Feng Kong

Department of Economics and Management, North China Electric Power University, Baoding,P. R. China, 071003

wenfeng3596@sina.com

Keywords: MADM，TOPSIS, rank reversal, rank preservation

Abstract. TOPSIS has been in use for more than 20 years in many fields. However, few researches have studied its defect of rank reversal. This paper, by studying the fundamental cause for the rank reversal problem in TOPSIS, put forward an improvement on TOPSIS based on the decision maker's subjective preferences, which can, proved by a numerical example, overcome the rank reversal problem and lead to more scientific decision result that is in more agreement with the decision makers' subjective intensions.

Introduction

TOPSIS, put forward by Hwang and Yoon (1981), is a technique for order preference by similarity to the ideal solutions to solve multi-attribute decision making (MADM) problems. This method is to order alternatives according to their relative closeness, which is defined as the distance between an alternative and the positive and negative ideal solutions. TOPSIS has been in use for more than 20 years in many fields. However, since the 1980s, rapid developments in researches on rank reversal revealed that it is not desirable to study practical decision problems merely from mathematical models, without consideration of the actual decision behaviors of human beings. Therefore, decision results may deviate greatly from the decision makers' intensions. Rank reversal generally refers to the fact that, when adding new alternatives or deleting some old ones, the ranking of alternatives may change. Researches in this aspect give two causes for rank reversal: one is the change in decision makers' preferences or judgments when alternatives are being added or deleted; the other is that the algorithm of the model was wrong.

This paper is to study the rank reversal of TOPSIS caused by the model itself. Our paper aims to reveal the cause for rank reversal in TOPSIS by numerical analysis. We put forward an improvement on TOPSIS based on the decision maker's subjective preferences, which can overcome the rank reversal problem and ensure good agreement in decision results.

Procedure for traditional TOPSIS

TOPSIS is to rank alternatives according to the closeness of each alternative to the ideal points which is defined by the space distance. It's calculation steps as follow.

If a multi-attribute decision making problem has *m* alternatives, each of which has *n* attributes, then the decision matrix is: $D = \{y_{ij}\}$. Where y_{ij} represents the original value of the *j*-th attribute for alternative *i*.

Step 1 Normalize the decision matrix, $X = \{x_{ij}\}$

Where x_{ij} represents the normalized value of the *j*-th attribute for the *i*-th alternative, and

$$x_{ij} = \frac{y_{ij}}{\sqrt{\sum_{i=1}^{m} y_{ij}^2}}, \quad i = 1,2,...,m; \ j = 1,2,...,n. \tag{1}$$

Step 2 Derive the weighted normalized decision matrix, $Z = \{z_{ij}\}$

Where $z_{ij} = w_j \bullet x_{ij}$, w_j represents the weight of the *j*-th attribute of the *i*-th alternative.

Step 3 Determine the positive and negative ideal points.

Let x_j^+ and x_j^- be the values of the *j*-th attribute of the positive and negative ideal point (solution) respectively. According to TOPSIS, for the positive ideal point, there is:

$x_j^+ = \max_i x_{ij}$, for benefit type attributes; $x_j^+ = \min_i x_{ij}$, for cost type attributes.

For the negative ideal point, there is;

$x_j^- = \min_i x_{ij}$, for benefit type attributes; $x_j^- = \max_i x_{ij}$, for cost type attributes.

Step 4 Calculate the distances between each alternative and the ideal points.

The distance between alternative and the positive ideal point and the negative ideal point is give by

$$d_i^+ = \sqrt{\sum_{j=1}^{n} (x_{ij} - x_j^+)^2} \quad , \quad d_i^- = \sqrt{\sum_{j=1}^{n} (x_{ij} - x_j^-)^2} \tag{2}$$

Step 5 Calculate the relative closeness of each alternative to the ideal points.

$$C_i = \frac{d_i^-}{d_i^- + d_i^+} \tag{3}$$

The rank reversal problem in traditional TOPSIS

The rank reversal problem in traditional TOPSIS can be illustrated with an example as follow.

Consider a decision problem with five alternatives, each of which has two attributes. Suppose both attributes are benefit type and of the same weights, i.e.. The data for the alternatives and the ranking result derived by TOPSIS method is shown in Table 1.

When we add some new alternatives to the original alternatives, the ranking of the five old alternatives will change, even when the new alternative added is the same as one of the old ones. Table 2,3 gives the ranking of the alternatives when one new alternative is added. Table 3 gives the ranking of the alternatives when two new alternatives are added.

From table 1, we see originally, the ranking of the five alternatives is: $A \succ C \succ D \succ B \succ E$.

Table.1 Data for the original five alternatives and their ranking

		Original attribute values		Weighted normalized attribute values		d^+	d^-	C	Ranking of the original alternatives
		a	*b*	*a*	*b*				
Original alternatives	A	33	7	0.3469	0.1140	0.195	0.242	0.553	1
	B	20	12	0.2103	0.1955	0.178	0.133	0.428	4
	C	12	18	0.1262	0.2932	0.221	0.180	0.449	2
	D	10	19	0.1051	0.3095	0.242	0.195	0.447	3
	E	23	8	0.2418	0.1303	0.208	0.138	0.398	5

When one new alternative is added to the five old ones, the ranking of the five alternatives will change. As table 2 shows, when alternative F_1, F_2, F_3, and D is added respectively, their ranking becomes $C \succ D \succ A \succ B \succ E$, $A \succ B \succ E \succ C \succ D$, $A \succ D \succ C \succ B \succ E$, and $A \succ B \succ E \succ C \succ D$.

When two alternatives, i.e., A1 and A1, or F1 and F_1, or F_2 and F_2, are added respectively to the five old ones, the ranking of the five alternatives becomes $C \succ D \succ A \succ B \succ E$, $C \succ D \succ B \succ A \succ E$, and $A \succ E \succ B \succ C \succ D$ respectively.

The rank reversal problem is obvious: when some alternatives are added, the ranking of the old ones change so that their new ranking disagrees with their original ranking.

Table. 2 Data for the original five alternatives and their ranking when a new alternative is added

		Original attribute values		Weighted normalized attribute values		d^+	d^-	C	Ranking of the original alternatives
		a	*B*	*a*	*b*				
When a new alternative, F_1, is added	A	33	7	0.2520	0.1140	0.216	0.209	0.492	3
	B	20	12	0.1527	0.1955	0.222	0.210	0.486	4
	C	12	18	0.0916	0.2932	0.253	0.294	0.538	1
	D	10	19	0.0764	0.3095	0.267	0.310	0.537	2
	E	23	8	0.1756	0.1303	0.246	0.164	0.400	5
	F_1	45	0	0.3436	0.0000	0.310	0.267	0.463	——
When a new alternative, F_2, is added	A	33	7	0.3469	0.0970	0.166	0.347	0.676	1
	B	20	12	0.2103	0.1662	0.168	0.221	0.569	2
	C	12	18	0.1262	0.2493	0.221	0.198	0.472	4
	D	10	19	0.1051	0.2632	0.242	0.197	0.449	5
	E	23	8	0.2418	0.1108	0.185	0.242	0.567	3
	F_2	0	19	0.0000	0.2632	0.347	0.166	0.324	——
When a new alternative, F_3, is added	A	33	7	0.2794	0.0955	0.178	0.195	0.522	1
	B	20	12	0.1693	0.1638	0.167	0.109	0.394	4
	C	12	18	0.1016	0.2457	0.197	0.151	0.434	3
	D	10	19	0.0847	0.2593	0.212	0.164	0.436	2
	E	23	8	0.1947	0.1092	0.193	0.111	0.365	5
	F_3	35	20	0.2964	0.2730	0.000	0.276	1.000	——
When a new alternative, D_1, is added	A	33	7	0.3395	0.0970	0.166	0.237	0.587	1
	B	20	12	0.2058	0.1662	0.165	0.124	0.429	2
	C	12	18	0.1235	0.2493	0.216	0.154	0.415	4
	D	10	19	0.1029	0.2632	0.237	0.166	0.413	5
	E	23	8	0.2366	0.1108	0.184	0.134	0.422	3
	D_1	10	19	0.1029	0.2632	0.237	0.166	0.413	——

Table. 3 Data for the original five alternatives and their ranking when two alternatives are added

		Initial attribute values		Weighted normalized attribute values		d^+	d^-	C	Ranking of the original alternatives
		a	*b*	*a*	*b*				
When two alternatives, A_1, are added	A	33	7	0.2476	0.1085	0.186	0.173	0.481	3
	B	20	12	0.1501	0.1861	0.146	0.108	0.425	4
	C	12	18	0.0900	0.2791	0.158	0.171	0.520	1
	D	10	19	0.0750	0.2946	0.173	0.186	0.519	2
	E	23	8	0.1726	0.1240	0.186	0.099	0.346	5
	A_1	33	7	0.2476	0.1085	0.186	0.173	0.481	——
	A_1	33	7	0.2476	0.1085	0.186	0.173	0.481	——
When two alternative, F_1, are added	A	33	7	0.2077	0.1140	0.210	0.184	0.468	4
	B	20	12	0.1259	0.1955	0.194	0.205	0.514	3
	C	12	18	0.0755	0.2932	0.208	0.294	0.585	1
	D	10	19	0.0629	0.3095	0.220	0.310	0.584	2
	E	23	8	0.1447	0.1303	0.226	0.154	0.405	5
	F_1	45	0	0.2832	0.0000	0.310	0.220	0.416	——
	F_1	45	0	0.2832	0.0000	0.310	0.220	0.416	——
When two alternatives, F_1, are added	A	33	7	0.3469	0.0858	0.147	0.347	0.702	1
	B	20	12	0.2103	0.1471	0.161	0.219	0.576	3
	C	12	18	0.1262	0.2206	0.221	0.185	0.455	4
	D	10	19	0.1051	0.2329	0.242	0.181	0.428	5
	E	23	8	0.2418	0.0981	0.171	0.242	0.586	2
	F_2	0	19	0.0000	0.2329	0.347	0.147	0.298	——
	F_2	0	19	0.0000	0.2329	0.347	0.147	0.298	——

In all, when different alternatives are added to the original alternatives, different ranking of the original ones may result. When we remove one or some of the original alternatives, similar ranking reversal may also result. In such cases, it is hard for us to tell which of the above ranking is correct.

Causes For Rank Reversal In Topsis

One cause for the rank reversal in TOPSIS is the method used to normalize the decision matrix method. When we use this method to normalize the decision matrix, correlation or dependent functions may result between the alternatives.

In fact, this normalization procedure could be considered as giving each of the initial attribute values a weight of $1/\sqrt{\sum_{i=1}^{m} y_{ij}^2}$. Hence, the drawback of this normalization method is obvious: the independence between alternatives may be affected and alternatives may have some relationship with one another after Normalization .

In the above example, the values of the five alternatives in respect to attribute a are: (33, 20, 12, 10, 23) respectively. After normalization, the above attribute values become (0.6938, 0.4206, 0.2524, 0.2102, 0.4836). Therefore, Vector Normalization procedure is equivalent to giving each of the initial attribute values a weight of 0.02102.

When we add a new alternative, for example, alternative F_1, the values of attribute a become (33, 20, 12, 10, 23, 45), while the values of attribute b remain to be (0.504, 0.3054, 0.1832, 0.1528, 0.3512, 0.6872). Since the new added alternative takes the value of 45 for attribute a, and 0 for attribute b, the initial attribute values change in respect to attribute a and remain the same in respect to attribute b. This is the drawback in the Vector Normalization method.

Not only the normalized values will change when alternatives are added or deleted, but also the ideal solution will change. This can been seen from the ideal solution Equation. Therefore, rank reversal will preveal since the distances between the ideal solution and each alternative will always change as a result of the change of the ideal solution.

Improvement Over Topsis

To overcome the drawback of TOPSIS, we should make sure that the normalization procedure should retain the independence between the alternatives and at the same time keep the ideal solution constant.

According to utility theory, the ideal points are the most satisfactory alternative (or the most unsatisfactory alternative) which comprises all attribute values that are most satisfactory (or the most unsatisfactory). With the attribute value that is most satisfactory being normalized to be 1 and the one that is most unsatisfactory being normalized to be 0, attribute values in between the most satisfactory and the most unsatisfactory can be transformed one by one to normalized values according to some utility function which can be either linear or non-linear.

For example, initial attribute values could be normalized according to the following linear function:

$$x_{ij} = f(y_{ij}) = \frac{y_{ij} - y_j^-}{y_j^+ - y_j^-} \text{ (For benefit type) ; } x_{ij} = f(y_{ij}) = \frac{y_j^+ - y_{ij}}{y_j^+ - y_j^-} \text{ (For cost type)} \quad (6)$$

where y_j^+ and y_j^- represent the value of the j-th attribute of the postive and negative ideal solution respectively. They are determined by the decision maker according to his judgments or experience. Generally, there is: $y_j^+ \geq \max_i y_{ij}$, (For benefit type attributes) ; $y_j^- \leq \min_i y_{ij}$. (For cost type attributes)

Obviously, according to the above method, the ideal points will never change whether alternatives are added or deleted. That is, the above method can ensure the coordinates of the ideal points do not change as the number of alternatives changes.

Still take the previous example to illustrate. Suppose the decision maker, according to his experience, decided the positive ideal point to be with values of 45 and 25 in respect to attribute a and b respectively, and the negative ideal point to be with values of (0, 0). Table 4 gives the normalized attribute values, the relative closeness and the ranking of the five alternatives. From table 4, we see that when a new alternative is added to the five old ones, the normalized values of attributes are not affected, which are always (0.3667, 0.2222, 0.1333, 0.1111, 0.2556) in respect to attribute a and (0.1400, 0.2400, 0.3600, 0.3800, 0.1600) in respect to attribute b. Further, the ranking of the five alternatives remains the same as $A \succ C \succ D \succ B \succ E$.

Table.4 Data for the original five alternatives and their ranking according to improved method

		Initial attribute values		Weighted normalized values		d^+	d^-	C	Ranking of the original alternatives
		a	*b*	*a*	*B*				
Original alternatives	A	33	7	0.3667	0.1400	0.384	0.392	0.506	1
	B	20	12	0.2222	0.2400	0.380	0.327	0.462	4
	C	12	18	0.1333	0.3600	0.392	0.384	0.494	2
	D	10	19	0.1111	0.3800	0.407	0.396	0.493	3
	E	23	8	0.2556	0.1600	0.419	0.302	0.419	5
When a new alternative, F_1, is added	A	33	7	0.3667	0.1400	0.384	0.392	0.506	1
	B	20	12	0.2222	0.2400	0.380	0.327	0.462	4
	C	12	18	0.1333	0.3600	0.392	0.384	0.494	2
	D	10	19	0.1111	0.3800	0.407	0.396	0.493	3
	E	23	8	0.2556	0.1600	0.419	0.302	0.419	5
	F_1	45	0	0.5000	0.0000	0.500	0.500	0.500	——
When a new alternative, F_2, is added	A	33	7	0.3667	0.1400	0.384	0.392	0.506	1
	B	20	12	0.2222	0.2400	0.380	0.327	0.462	4
	C	12	18	0.1333	0.3600	0.392	0.384	0.494	2
	D	10	19	0.1111	0.3800	0.407	0.396	0.493	3
	E	23	8	0.2556	0.1600	0.419	0.302	0.419	5
	F_2	0	19	0.0000	0.3800	0.514	0.380	0.425	——
When a new alternative, F_3, is added	A	33	7	0.3667	0.1400	0.384	0.392	0.506	1
	B	20	12	0.2222	0.2400	0.380	0.327	0.462	4
	C	12	18	0.1333	0.3600	0.392	0.384	0.494	2
	D	10	19	0.1111	0.3800	0.407	0.396	0.493	3
	E	23	8	0.2556	0.1600	0.419	0.302	0.419	5
	F_3	35	20	0.3889	0.4000	0.149	0.558	0.789	——
When a alternative, D_1, is added	A	33	7	0.3667	0.1400	0.384	0.392	0.506	1
	B	20	12	0.2222	0.2400	0.380	0.327	0.462	4
	C	12	18	0.1333	0.3600	0.392	0.384	0.494	2
	D	10	19	0.1111	0.3800	0.407	0.396	0.493	3
	E	23	8	0.2556	0.1600	0.419	0.302	0.419	5
	D_1	10	19	0.1111	0.3800	0.407	0.396	0.493	——

Summary

TOPSIS has been in use for more than 20 years in many fields. However, few researches have studied its defect of rank reversal. Though some have questioned about TOPSIS, they did not give any correct improvement. This paper, by studying the fundamental cause for the rank reversal problem in TOPSIS, contributes the rank reversal problem to: (1) the method we use to normalize the decision matrix-the Vector Normalization method; (2) the change in ideal points.

This paper puts forward an improvement on TOPSIS based on the decision maker's subjective preferences, which can, proved by our numerical example, overcome the rank reversal problem and lead to more scientific decision results that are in more agreement with the decision makers' subjective intensions.

Acknowledgement

This paper is supported by “ the Fundamental Research Funds for the Central Universities”(09MR41)

References

[1] Hwang, C. L and Yoon, K.: *Multiple attribute decision making: Methods and Applications*, (Springer-Verlag. Berlin, 1981).
[2] Lai, Y. J, Liu, T. Y and Hwang, C. L.: TOPSIS for MODM. European Journal of Operational Research, Vol. 76 (1994),p. 486-500.
[3] Agrawal, V. P, Kohli, V and Gupta,S.: Computer aided robot selection: The multiple attribute decision making approach. International Journal of Production Research, Vol 29(1991), p. 1629-1644.
[4] Shanian A., Savadogo O.: TOPSIS multiple-criteria decision support analysis for material selection of metallic bipolar plates for polymer electrolyte fuel cell. Journal of Power Sources, Vol. 159(2006), p. 1095-1104.
[5] Wang Ying-Ming, Taha M.S. Elhag: Fuzzy TOPSIS method based on alpha level sets with an application to bridge risk assessment. Expert Systems with Applications, Vol. 31(2006), p. 309-319.
[6] Jahanshahloo G.R., Hosseinzadeh F.: Extension of the TOPSIS method for decision-making problems with fuzzy data. Applied Mathematics and Computation, Vol. 181(2006), p.1544-1551.
[7] Hsu-Shih Shih: Incremental analysis for MCDM with an application to group TOPSIS. European Journal of Operational Research, Vol.186(2008), p. 720-734.
[8] HU Yong-hong: The Improved Method for TOPSIS in Comprehensive Evaluation. A Chinese Journal of Mathematics in Practice and Theory, Vol. 132(2002), p. 572-575.
[9] YU Yan, LIANG Liang: Extensions of the TOPSIS for Multiple Criteria Decision Making, A Chinese Journal of Systems Engineering, Vol.21(2003), p. 98-111.

Advanced Materials Research Vols. 204-210 (2011) pp 42-45

doi:10.4028/www.scientific.net/AMR.204-210.42

Negative Selection Algorithm Based on Double Matching Rules

Yu Hu[1, a] and Bin Li[2, b]

[1]Measuring and Controlling Technology Institute, Taiyuan University of Technology, Taiyuan 030024, China

[2]College of Computer Science and Technology, Taiyuan University of Technology, Taiyuan 030024, China

[a]huyutyut@163.com, [b]412928782@qq.com

Keywords: artificial immune, intrusion detection, detectors, double matching, negative selection

Abstract. The theory of artificial immune had been widely used in the research of network intrusion detection. Nowadays, the existing detector generating algorithms based on negative selection usually use a certain matching rule, as a result, too many detectors may generate, and the false alarm rate will become more serious. This paper proposes an improved negative selection algorithm using double matching rule: candidate detectors should be selected by the improved Hamming distance matching first, then the remaining detectors go through the segmented r-chunks(rch) matching rule. Experiments show that compared with traditional algorithms, this method brings a small number and more efficient detectors, reduces the false alarm rate and guarantees the efficiency of detectors.

Introduction

The detection rate of IDS based on artificial immune is decided by the quality of detectors, and Negative Selection Algorithm (NSA) is the most commonly used way to generate detectors. In 1994, Forrest etc. from New Mexico University of USA put forward the idea of NSA [1], established a detection model to distinguish self patterns and non-self patterns, and then applied the model to IDS. Mature detectors are generated by NSA; so to speak, NSA is the core of AIS. The matching rule which directly affects the efficiency of detectors is the foundation of NSA, and its performance is of important significance to the whole system [2]. After a deep research on commonly used matching rules in NSA and their disadvantage, this paper proposes a new type of NSA based on double matching rule. The new rule integrates Hamming matching rule and rch matching rule, and then makes an improvement on the integration. Through experiments a conclusion is made that NSA based on double matching rule can efficiently generate the needed detectors，evidently enhance the detection rate and reduce the false alarm.

In NSA, the most commonly used matching rules are Hamming matching and r-continuous bits (rcb) matching rule [3], in addition, rch matching rule can be occasionally mentioned. Mature detectors generate through negative selection, different matching rules' emphases are different, and as a result, the mature detectors' quantity, quality and efficiency will be different with different rules.

Double matching rule

Based on the analysis of the several matching rules, it proves that each rule has its own respective shortcoming when individually used. In order to avoid these drawbacks, a double matching rule is presented in this paper which assimilates each rule's advantages and improves the quality and efficiency of the mature detectors.

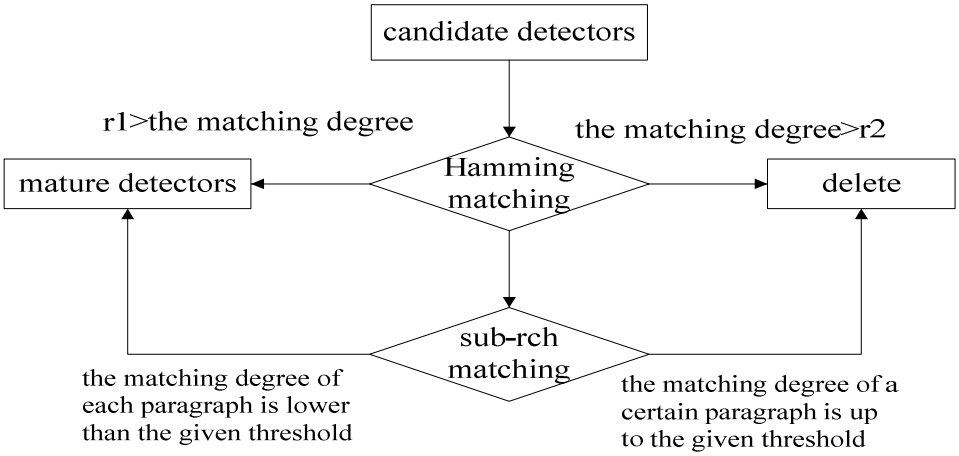

Fig.1. Negative selection based on double matching rule

Process of double matching rule. As shown in Figure.1.

1) First, use Hamming matching rule to process the candidate detectors. If the matching degree between a candidate detector and any self pattern is up to the threshold r2, then this candidate detector will be deleted. The threshold r2 here should be a little big, so that the candidate detectors which match self pattern in a high degree will be deleted. If the matching degree between a candidate detector and each self pattern is lower than the threshold r1, then this candidate detector will become a mature detector. The threshold r1 here should be a little small, so that the candidate detectors that changed into mature detectors are very different from all self patterns.

2) The major work of negative selection is carried on in this stage. As the network data stream are composed of a series of fields, if rch matching rule is simply applied in the system, some candidate detectors that with a large number of contiguous matched bits but low similarity to self patterns will be deleted incorrectly. So the matching degree calculated by rch matching rule can not accurately reflect the real similarity between two strings. In this paper, sub-rch matching rule is proposed: every self pattern is divided into several paragraphs according to every field's implications, each paragraph has a threshold. A candidate detector can change into a mature detector only if the matching degree of each paragraph is lower than the given threshold. Once the matching degree of one paragraph is higher than its threshold, the matching process will stop, and the candidate detector here will be deleted.

Algorithm analysis. The core of the double matching rule is to make an effective combination of Hamming matching rule and rch matching rule, the two rules can be complementary through some further improvements, and more effective mature detectors can be generated. After the Hamming matching, some candidate detectors that have high similarity to self patterns will be filtered out, and some candidate detectors will change into mature detectors directly. This phase can prevent the vulnerabilities that easy to produce in the next phase, and alleviate the burden of the whole system. This paper adopts sub-rch matching rule rather than rch matching. By using sub-rch matching, the candidate detectors with a large number of contiguous matched bits but low similarity to self patterns can not be arbitrarily removed like before. So this phase make valuable contributions to protect the excellent detectors and improve the quality of the mature detectors.

In regard to time complexity, the sub-rch matching used in this paper and rch matching is the same. Some candidate detectors are directly change into mature detectors and some are removed through Hamming matching, all these detectors do not need to participate in next phase. For a certain candidate detector in sub-rch matching, the process will stop immediately when one paragraph matches the corresponding paragraph of a self pattern, and the remaining paragraphs of this candidate detector will not continue to carry on the rule. Something else, with same number of candidate detectors, mature detectors generated through double matching rule are fewer than through any other rules. Consequently, it will be very helpful to reduce the matching operations and save a lot of time. The above analysis shows that using double matching rule will not increase much more time than using rch matching rule, the time efficiency is quite similar.

Experimental results and analysis

In view of the fact that the real network data sets are too enormous; the simulation using Matlab is performed in this paper. Select KDDCUP 99 classic data set as the experimental data, each record of this data set is composed of 42 attributes. The last attribute which is classified into normal and abnormal is the behavioral attribute. When creating a self set, select the records that the last attribute is “normal”, and the establishment of an invasion set need to select the opposite records. To facilitate the analysis, 11 representative features are selected: protocol_type, service, flag, src_bytes, dst_bytes, Hot, num_file_creations, count, srv_count, dst_host_count, dst_host_srv_count. These 11 features are encoded to a 37-bit binary string.

To verify the performance of the algorithm, this paper carried out three tests. Experimental procedures are as follows:

1) Extraction of experimental data. Select 3000 invasion records and 7200 self records from KDDCUP 99 data set according to the method described above, and encode these records to 37-bit binary strings. The invasion records should include all types of invasions.

2) The selected 11 features are divided into two paragraphs according to data character and network traffic character. protocol_type, service, flag, src_bytes, dst_bytes and Hot belong to data character, as the first paragraph. its length is 22, and the threshold is set to 8. num_file_creations, count, srv_count,dst_host_count and dst_host_srv_count belong to network traffic character, as the second paragraph. its length is 15, and the threshold is set to 6.

3) The two thresholds r1, r2 used in Hamming matching of double matching rule are set to 6, 20.

4) Select 200 records from the self records of 1) as the self patterns used in the phase of tolerance.

5) Create 3 groups of data sets as candidate detectors; each data set includes 3000 37-bit binary strings that randomly generated.

6) Respective implement of negative selection. Apply Hamming matching, rcb matching, rch matching and double matching proposed in this paper to the candidate detectors generated from the last step. After negative selection with the self patterns of 4), 3 groups of mature detectors will be generated, and each group includes 4 different kinds of mature detectors generated by different matching rules. Then calculate the average numbers of the 4 kinds of mature detectors, and give the comparison of their sizes. As shown in Table 1.

Table 1. the quantity of mature detectors generated by different rules

matching rule	Hamming matching	rcb matching	rch matching	double matching
the quantity of mature detectors	459	287	311	242

7) Set the 3000 invasion records and the 7000 remaining self records of 1) as a testing set. Test the 3 groups of mature detectors in 6); give the average detection rate and false alarm rate. As shown in Figure.2.

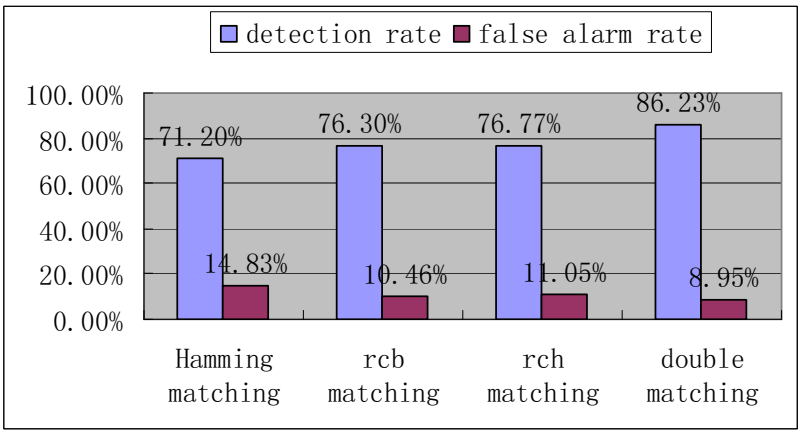

Fig.2. the average detection rate and false alarm rate

Table 1 shows that, with the same number of candidate detectors, the number of mature detectors generated by double matching is obviously smaller than by any other ways. It will effectively alleviate the operation burden of the system in the detection phase. Judging from the quality of mature detectors, as shown in Figure 2, the mature detectors generated from double matching have the best detection rate with the smallest quantity, and reduce the false alarm rate.

Conclusions

This paper presents an improved NSA based on double matching rule. Based on analyzing and comparing several matching rules in common use, this article integrates Hamming matching and rch matching rule，then some improvement is made to the unity to make the two matching rules complement one another and avoid their respective drawbacks. Analysis and experimental results indicate clearly that the mature detectors generated from double matching are more efficient, the detection rate is improved and the false alarm, detection failures are reduced. The work of this paper lays a good basis for the research of exploring more efficient detectors.

Acknowledgment

The authors would like to thank the Natural Science Foundation of Shanxi Province (2009011019-2) for the financial support.

References

[1] FORREST S, HOFMEYR S, SOMAYAJI A. Computer Immunology [J].Communications of the ACM, 1997, 40(10):88-96.

[2] E Esponda, S.Forrcst. Positive and negative detection. IEEE Transactions 0n Systems, mall andcybernetics, 2002, 34：65-69.

[3] D.Dasgupa, S.Forrest. Novelty detection in time series data using ideas from immunology.5th International Conference of Intelligent Systems, Reno,Nevada,1996:19-21.

Advanced Materials Research Vols. 204-210 (2011) pp 46-53

doi:10.4028/www.scientific.net/AMR.204-210.46

Empirical Study on Ordering Policy for Multi-Products in Fresh Food Supply Chains

[1]Yin Huang[a, 1], Xiamiao Li[b, 2], Dapeng Liu[c, 3]

[a]School of Transportation and Traffic Engineering, Central South University, Changsha, Hunan, China

[b]School of Transportation and Traffic Engineering, Central South University, Changsha, Hunan, China

[c]Transportation Bureau of Putian,Fujian, China

[1]share0122@126.com; [2]xmli@mail.csu.edu.cn; [3]liudabird@163.com

Key words: Perishable goods; Ordering policy; Multi-product; Supply chain; Inventory control; Agglomeration effect.

Abstract: Food supply chain is a complex process. The author develops a model that will provide both researchers and practitioners with a means of determining the optimal ordering policy for multi-products in fresh food supply chain. By using computer simulation. this paper conduct for a numerical analysis to the ordering policy of products of a food company in Hubei province to analyze the properties of total cost functions under each of the six different ordering policies and proposes an approximate optimal ordering policy of multiple products. Based on the models and analysis, it is found that agglomeration effect plays an important role in determine ordering policy of multiple products.

---

[1] Yin Huang works in School of Transportation and Traffic Engineering of Central South University as a teacher. She graduated from this school with PhD degree in logistics engineering in June, 2010. Her primary research focuses on inventory control (especially for perishable products inventory), ordering process and medical logistics.

1. Introduction

Perishable goods, such as food products, vegetables, flowers and ready-mix concrete, often deteriorate during the process of delivery and inventory. More and more researchers are paying attention to perishable inventory in order to reduce the loss of profit due to deterioration of perishable goods.

Among these perishable goods, fresh food products usually deteriorate most rapidly. The value or quality of perishable food products will decrease rapidly when being stored. Inventory problems for multi-products have been studied extensively by many researchers from time to time. However, Very little research has been reported in the perishable product area. This study focuses on the ordering policy of multi-products in the fresh food supply chain [1].

2. Related Work

Papachristos and Skouri (2000) proposed a continuous review inventory model with varying deterministic demand and constant deterioration rate. This inventory model allows for shortages, which are partially backlogged at a negative exponential rate with waiting time. They provided an optimal solution to minimization of the total cost. However, they don't include the cost of lost sales and the purchase costs for a non-constant order quantity into the total cost [2]. Teng et al. (2002) added the costs of lost sales and the purchase costs into the total cost suggested by Papachristos and Skouri [3]. They (1999) considered four possible replenishment policies for deteriorating items over a fixed planning horizon where the demand function is taken to be positive and fluctuating with time which is more general than increasing, decreasing and log-concave demand patterns [4].

This paper introduces six ordering policies and conducts a numerical analysis of the ordering policy of products of food company in Hubei province (in China) to analyze the properties of total cost functions under each of the six different ordering policies and proposes an approximate optimal ordering policy of multiple products. The inventory models are on the basis of theoretical results of Chopra et al. [5] (2002) , Yu YG et.al [6] (2004) and Wen XW et al. [7] (2007).

3. Assumptions and notation

The mathematical model of the inventory replenishment is based on the following assumptions:

1. The planning horizon of the inventory here is finite and is taken as $\boldsymbol{H}$ time units.
2. Shortages are not allowed for.
3. There exists a lead time and the replenishment rate is A.
4. The initial inventory level is zero.
5. The inventory holding cost per unit per unit time for every piece of production is the same.

6. The product begins to deteriorate when it is put into the inventory and the rate of deterioration is a constant.
7. The demand rate for the same product is constant.
8. If the objective is to minimize the costs, then we assume that the cost of lost sale is because of loss in stock. The total cost is the sum of ordering cost, the cost of lost sale due to deterioration, and inventory holding cost.

For convenience, the following notations are used throughout this paper:

n the number of replenishments over $[0.H]$ (a decision variable)

w_j the j th good

B_k the k th chain store

Q_{kj} purchasing order quantity

$I_{kj}(t)$ the level of inventory at time t

D_{kj} the demand rate

n_{kj} order-placing frequency

T_{kj} the optimum order cycle

θ_j the rate of deterioration

h the inventory holding cost per unit per unit time

C_j the purchasing cost per unit

s the ordering cost per unit

s_j additional cost per order

z_j the total cost under ordering policy i

The objective of the inventory here is to determine the optimal ordering policy to minimize the total relevant cost.

4. Description of the Inventory Model

In the food supply chain, the core enterprise owns r retailers in chain supermarkets $B_k(k=1,2,...,r)$ The suppliers provide m products $Wj(j=1,2,...,m)$ to the retailers. Their rates of deterioration are $\theta_j(j=1,2,....,m)$ respectively. Since the inventory is depleted with the combined

effect of demand and deterioration, the inventory level at time t during i the replenishment cycle as above is governed by the following differential equation:

$$\frac{dI_{kj}(t)}{dt}+\theta_j I_{kj}(t)=-D_{kj}, 0\le t\le T_{kj}(j=1,2,\cdots,m,k=1,2,\cdots,r)。 \quad (1)$$

Suppose that U_{kj} is the order quantity B_k order W_j, then the time of replenishment of product W_j is $U_{kj}=A_{kj}\cdot t_p, t_p$. A_{kj} is the replenishment rate of product W_j.

Owing to the existing of replenishment period, the maximum inventory is Q_{kj}, its initial condition is

$$I_{kj}(0)=0, I_{kj}(t_p)=Q_{kj}, I_{kj}(T_{kj})=0.$$

According to the above analysis $t_p=U_{kj}/A_{kj}$

Solving the differential equation (1), we get

When $0\le t\le U_{kj}/A_{kj}$

$$I_{kj}(t)=\frac{D_{kj}}{\theta_j}(e^{-\theta_j t}-1) \quad (2)$$

When $U_{kj}/A_{kj}<t_p\le T_{kj}$

$$I_{kj}(t)=\frac{D_{kj}}{\theta_j}[(\frac{\theta_j Q_{kj}}{D_{kj}}+1)e^{\theta_j(t_p-t)}-1] \quad (3)$$

So $$Q_{kj}=I_{kj}(\frac{U_{kj}}{A_{kj}})=\frac{D_{kj}}{\theta_j}(e^{-\theta_j\frac{U_{kj}}{A_{kj}}}-1) \quad (4)$$

The total cost of the inventory system during the planning horizon *H* under the following policies are:

Policy 1: Each supermarket has its order and each order includes only one product

$$z_1=\sum_{k=1}^{r}\sum_{j=1}^{m}n_{kj}(S+S_J)+h\sum_{k=1}^{r}\sum_{j=1}^{m}n_{kj}\int_0^{T_{kj}}I_{kj}(t)dt+\sum_{k=1}^{r}\sum_{j=1}^{m}n_{kj}C_jQ_{kj} \quad (5)$$

Now there exists $n_{kj}.T_{kj} = H$, hence, $T_{kj} = \frac{H}{n_{kj}}$. The maximum inventory during the planning horizon H is Q_{kj}. Hence, $n_{kj}\int_0^{T_{kj}} I_{kj}(t)dt = \frac{1}{2}H \cdot Q_{kj}$. So (5) can be simplified to be

$$z_1 = \sum_{k=1}^{r} n_{kj}(S + S_j) + \frac{1}{2}h\sum_{k=1}^{r}\sum_{j=1}^{m} HQ_{kj} + \sum_{k=1}^{r}\sum_{j=1}^{m} n_{kj}C_jQ_{kj} \quad (6)$$

Policy 2: Each supermarket has its own order and each order includes all the products:

In this case, suppose the order frequency of B_k is n_k

$$z_2 = \sum_{k=1}^{r} n_k(S + \sum_{j=1}^{m} S_j) + h\sum_{k=1}^{r}\sum_{j=1}^{m} n_kC_j\int_0^{T_{kj}} I_{kj}(t)dt + \sum_{k=1}^{r}\sum_{j=1}^{m} n_kC_jQ_{kj} \quad (7)$$

As above, each supermarket orders all products every time. Given to the policy of the total order being equal, $n_k\int_0^{T_{kj}} I_{kj}(t)dt = \frac{1}{2}H.Q_{kj}$.So (7) can be simplified to be

$$z_2 = \sum_{k=1}^{r} n_k(S + \sum_{j=1}^{m} S_j) + \frac{1}{2}hC_j\sum_{k=1}^{r}\sum_{j=1}^{m} HQ_{kj} + \sum_{k=1}^{r}\sum_{j=1}^{m} n_kC_jQ_{kj} \quad (8)$$

Policy 3: Each supermarket has its own order and each order includes only some of the products

In this case, we suppose the order frequency of B_k is n_k . Obviously, $n_k = \max\{n_{kj}\}$, and n_k can be divided by n_{kj} exactly. So the total cost of the inventory system under this policy is:

$$z_3 = \sum_{k=1}^{r} n_kS + \sum_{k=1}^{r} n_{kj}S_j + h\sum_{k=1}^{r}\sum_{j=1}^{m} n_{kj}C_j\int_0^{T_{kj}} I_{kj}(t)dt + \sum_{k=1}^{r}\sum_{j=1}^{m} n_kC_jQ_{kj} \quad (9)$$

Given to the policy of the total order is equal, $n_k\int_0^{T_{kj}} I_{kj}(t)dt = \frac{1}{2}H \cdot Q_{kj}$. So (9) can be simplified to be

$$z_3 = \sum_{k=1}^{r} n_{kj}S + \sum_{k=1}^{r} n_{kj}S_j + \frac{1}{2}hC_j\sum_{k=1}^{r}\sum_{j=1}^{m} HQ_{kj} + \sum_{k=1}^{r}\sum_{j=1}^{m} n_kC_jQ_{kj} \quad (10)$$

Policy 4: All the supermarkets send orders together and each order includes only one product.

Suppose the number of order is n， the total cost function is

$$z_4 = nS + \sum_{j=1}^{m} n_{kj}S_j + hC_j\sum_{k=1}^{r}\sum_{j=1}^{m} n_{kj}\int_0^{T_{kj}} I_{kj}(t)dt + \sum_{k=1}^{r}\sum_{j=1}^{m} n_{kj}C_jQ_{kj} \quad (11)$$

Given to the policy of the total order being equal, $n_{kj}\int_0^{T_{kj}} I_{kj}(t)dt = \frac{1}{2}H \cdot Q_{kj}$ So (11) can be simplified to be

$$z_4 = nS + \sum_{j=1}^{m} n_{kj}S_j + \frac{1}{2}hC_j \sum_{k=1}^{r}\sum_{j=1}^{m} HQ_{kj} + \sum_{k=1}^{r}\sum_{j=1}^{m} n_{kj}C_jQ_{kj} \tag{12}$$

Policy 5: All the supermarkets send orders together and each order includes all the products:

Suppose the number of order is n， the total cost is

$$z_5 = n(S + \sum_{j=1}^{m} S_j) + nh\sum_{k=1}^{r}\sum_{j=1}^{m} n_{kj}C_j \int_0^{T_{kj}} I_{kj}(t)dt + n\sum_{k=1}^{r}\sum_{j=1}^{m} C_jQ_{kj} \tag{13}$$

According to the policy of the total order being equal, $n\int_0^{T_{kj}} I_{kj}(t)dt = \frac{1}{2}H \cdot Q_{kj}$ So (13) can be simplified to be

$$z_5 = n(S + \sum_{j=1}^{m} S_j) + \frac{1}{2}hC_j \sum_{k=1}^{r}\sum_{j=1}^{m} HQ_{kj} + \sum_{k=1}^{r}\sum_{j=1}^{m} n_{kj}C_jQ_{kj} \tag{14}$$

Policy 6: All the supermarkets send orders together and each order includes many products

Suppose all the supermarkets send orders together and the number of order is n, then the total cost function is

$$z_6 = nS + \sum_{j=1}^{m} n_jS_j + h\sum_{k=1}^{r}\sum_{j=1}^{m} n_{kj}C_j \int_0^{T_{kj}} I_{kj}(t)dt + \sum_{k=1}^{r}\sum_{j=1}^{m} n_{kj}C_jQ_{kj} \tag{15}$$

According to the policy of the total order being equal, $n_{kj}\int_0^{T_{kj}} I_{kj}(t)dt = \frac{1}{2}H \cdot Q_{kj}$. So (15) can be simplified to be

$$z_6 = nS + \sum_{j=1}^{m} n_jS_j + \frac{1}{2}hC_j \sum_{k=1}^{r}\sum_{j=1}^{m} HQ_{kj} + \sum_{k=1}^{r}\sum_{j=1}^{m} n_{kj}C_jQ_{kj} \tag{16}$$

5. The results of numerical analysis

The original data are from a food company in Hubei province (in China).

From the program and simulation, we get:

The total amount of the cost of Policy 1 is 8806490.5334 yuan，that of Policy 2 8773946.6322 yuan，that of Policy 3 8775289.1645 yuan，that of Policy 4 11447911.6549 yuan, that of Policy 5 8809536.4826 yuan，and that of Policy 6 8770352.0413 yuan.

6. Conclusion

Obviously, Policy 1 and Policy 4 are two extreme conditions. No agglomeration effects can be achieved in these two policies. In practice, the companies seldom make use of such two policies. With Policy 5, each order involves all the products. The Agglomeration effect is stronger than that in the former policies. However, the disadvantage is taking together products of high capacity and those of low capacity. For the products of low capacity, more additional ordering costs will be involved, so the buyers should weigh tradeoff between ordering cost and agglomeration effect. Policy 6 makes use of the difference between the products of high capacity and those of low capacity and the products are classified by numerical simulation. It is concluded that the company should adjust order-placing frequency of different products reasonably by ordering in classification. It is good for saving the total cost. Another thing we come to know is that agglomeration effect plays an important role in determining ordering policy of multiple products in fresh food supply chain.

Reference:

[1] Chen HK, Hsueh CF and Chang MS. Production scheduling and vehicle routing with time windows for perishable food products. Computers&Operations Researech. Vol.10 (2008), p.1~9.

[2] Papachristos S, Skouri K. An optimal replenishment policy for deteriorating items with time-varying demand and partial---exponential type---backlogging. Operational Research Letter. Vol.27 (2000), p.175~184.

[3] Teng JT, Chang HJ, Dye CY and Hung CH. An optimal replenishment policy for deteriorating items with time-varying demand and partial backlogging. Operational Research Letter. Vol.30 (2002), p.387~393.

[4] Teng JT, Chern MS, Yang HL, Wang YJ. Deterministic lot size inventory models with shortages and deterioration for fluctuating demand. Operational Research Letter. Vol.24 (1999), p.65~72.

[5] Chopra.S and Peter.MP., Supply Chain Management: Strategy, planning and operation. Prentice-Hall.Inc. (2002) in press.

[6] YU YG, Liang L, Wang C and Wang ZQ. An Integrated Vendor- Managed - Inventory Model for Deteriorating Item. Chinese Journal of Management Science. Vol.2 (2004), p.32-37.

[7] Wen XW and Da QL. Ordering Policy and Empirical Study of Multi-Product in a Supply Chain. Vol.21 (2007), p.56~60.

Advanced Materials Research Vols. 204-210 (2011) pp 54-57

doi:10.4028/www.scientific.net/AMR.204-210.54

Research on the Relationship between Yarn Path and Yarn Tension in Tufting Carpet Equipment System

Yang XU [a], Zhi-jun SUN [b], Zhuo MENG [c] and Yi-ze SUN [d]

School of Mechanical Engineering, Donghua University, china

[a]xuyang@dhu.edu.cn, [b]sunzj@dhu.edu.cn, [c]mz@dhu.edu.cn, [d]sunyz@dhu.edu.cn

Keywords: Tufting carpet, Yarn path, Yarn flexing, Yarn tension

Abstract. The yarn tension is a key factor to accurately control carpet pile height, which changes with the yarn path and the path flexing. The purpose of this paper is to find the relationship between yarn path and yarn tension and provide a basis for the yarn tension controller design. Firstly, tufting equipment system components and basic principle of tufting carpet is introduced. Then, the yarn path during weaving tufting carpet including yarn feeding parts, yarn guiders and tufting needle is constructed and yarn flexing in the yarn path is analyzed. After discussing yarn tension change caused by the path flexing, it is concluded that yarn tension changes with the tufting needle position and periodic change with the yarn flexing periodic change.

Introduction

Tufting carpet is rich in color, pattern and variety, which accounts for 80% in the total carpet market [1, 2]. Varieties of pile height can make tufting carpet have sculptured effect. Generally, the range of pile height is from 1 mm to 16 mm. Fig.1 shows a sculptured-style jacquard carpet with five kinds of pile height.

Fig.1 Sculptured-style jacquard carpet

During weaving tufting carpet, the yarn tension is a key factor to accurately control carpet pile height, which changes with yarn path and yarn flexing. So analyzing the relationship between yarn path and yarn tension is very important. In this paper, tufting equipment system components and basic principle of tufting carpet is firstly introduced. Then, the relationship between yarn path and the total path flexing is constructed. According to periodic yarn path flexing result, yarn tension change caused by the path flexing is discussed. Finally, it is concluded that yarn tension periodic change with the yarn flexing periodic change.

Basic principle of tufting carpet

A typical tufting equipment system mainly consists of fabric feed parts, tufted fabric parts, level loop yarn feed parts, jacquard parts, tufting needles, the hoopers and so on.

The basic working principle of carpet tufting is shown as followings. Thousands of tufting needles are driven by the main axis system to move up-and-down reciprocally. At the same time, the looper hooks the yarn and makes it form loop on the rear of backing which coordinating with the tufting needle movement precisely. By controlling the yarn-feeding, different loop-height can be obtained. Through the horizontal movement of hackle, the variety of carpet pattern can be realized [3].

Yarn flexing in the yarn path

Pile yarn has a long path before threading the tufting needle. During weaving tufting carpet, with the distance periodic changes between tufting needle and the backing, yarn flexing in the yarn path show a periodic change. Fig. 2 shows the schematic diagram of path flexing in the yarn path.

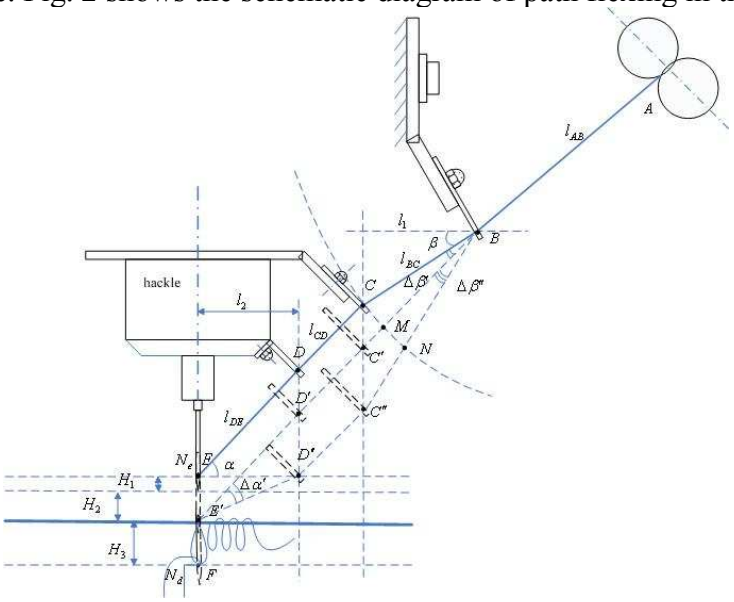

Fig.2 Yarn flexing in the yarn path

Where, the symbol A represents puller-rollers. B is fixed yarn guider. C and D are respectively adjustable yarn guiders, which are with fixed pitch and motion along with the hackle. N_d is the looper and N_e is the tufting needle. l_1 is the distance between fixed yarn guider B and adjustable yarn guider C. l_2 is the distance between adjustable yarn guider D and tufting needle N_e. E represents the highest position of tufting needle. F is the lowest position of tufting needle. E' is the contact point when the tufting needle motions downward to contact with backing. C' and D' are positions of adjustable yarn guider C and D that the tufting needle motions downward to the contact point E'. C'' and D'' are positions of adjustable yarn guider C and D respectively that tufting needle motions downward to the lowest position F. H_1 is the distance between tufting needle hole and needlepoint. H_2 is the distance between needlepoint and backing. H_3 is the sum of loop-height and spring back of yarn. α is the angle between line l_{DE} and the horizontal line . β is the angle between line l_{BC} and the horizontal line. α' is angle variation of α when the tufting needle motions downward. $\Delta\beta'$ is angle variation of β when the tufting needle motions downward to the contact point E'. $\Delta\beta''$ is angle variation of β when the tufting needle motions downward to the lowest position F.

According to weaving process of tufting carpet, yarn path can be analyzed through two parts:

(1)Yarn path before tufting needle enters the backing

When the tufting needle is in the highest position, defined that the yarn path length is L_1. When the tufting needle move downward to the contact point E', defined that the yarn path length is L_2.

As shown in Fig. 2, L_1 can be expressed as

$$L_1 = l_{AB} + l_{BC} + l_{CD} + l_{DE} \tag{1}$$

L_2 can be expressed as

$$L_2 = l_{AB} + l_{BC'} + l_{C'D'} + l_{D'E'} \tag{2}$$

Yarn guider C and yarn guider D are fixed pitch, so $l_{CD} = l_{C'D'}$, $l_{C'D'} = l_{C''D''}$, $l_{DE} = l_{D'E'}$. Thus, when yarn path changed from L_1 to L_2, yarn variation Δs_1 can be expressed

$$\Delta s_1 = l_1\left(\frac{1}{\cos(\beta + \Delta\beta')} - \frac{1}{\cos\beta}\right) = C'M \tag{3}$$

(2) Yarn path after tufting needle enters the backing

When the tufting needle enters the backing, defined that the yarn path length is L_3. L_3 can be expressed as

$$L_3 = l_{AB} + l_{BC''} + l_{C''D''} + l_{D''E'} \tag{4}$$

Comparing L_3 and L_1, yarn variation Δs_2 can be expressed as following

$$\Delta s_2 = l_1\left(\frac{1}{\cos(\beta + \Delta\beta' + \Delta\beta'')} - \frac{1}{\cos\beta}\right) + l_2\left(\frac{1}{\cos(\alpha - \Delta\alpha')} - \frac{1}{\cos\alpha}\right) \tag{5}$$

For a typical tufted carpet machine, $\alpha \approx 31°$ and $\beta \approx 13.1°$. By analysis on yarn path before tufting needle enters and after tufting needle enters the backing, periodic yarn path flexing can be obtained, as shown in Fig. 3. Generally, a pile-loop is formed when main axis rotates one circle. From Fig. 3, it is known that when tufting needle is the highest position, yarn path flexing is zero and main axis rotation angle is about 143°. When the tufting needle move downward to backing, main axis rotation angle is about 205° and yarn path flexing is 2.32mm. When the tufting needle moves downward from backing to the lowest position, main axis rotation angle is about 327° and yarn path flexing is 0.84 mm. Due to the constant yarn feeding in a unit time, the yarn tension inevitably changes along with the needle position alternately.

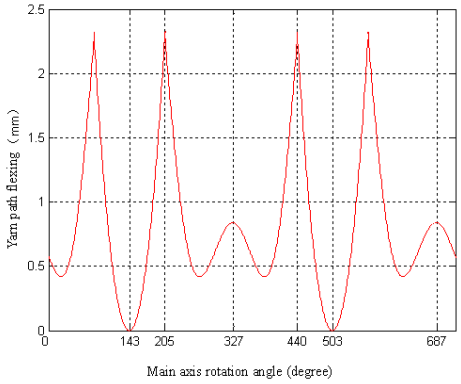

Fig. 3 Periodic yarn path flexing

Analyzing Fig. 3, it may be concluded that yarn path is always positive during weaving tufting carpet process, greater than the initial value. The yarn path flexing shows a periodic change corresponding with the periodic change of formed loop process.

Analysis on yarn tension during weaving tufting carpet

In this section, yarn tension is analyzed according to running position of tufting needle, shown as in Fig. 4. Concrete process can be divided into the following four stages:

(1) In the first stage, shown as Fig. 4a), motion range of tufting needle is from the highest position to contact point with backing. Tufting needle is upon the backing and yarn tension is T_1.

(2) In the second stage, motion range of tufting needle is from contact point with backing to loop-height position, shown as Fig. 4b). Tufting needle is under the backing and the looper just doesn't work. Yarn tension is T_2.

(3) In the third stage, tufting needle is under the backing, which motion range is from loop-height position to the lowest position, shown as Fig. 4c). When tufting needle arrives at the lowest position, the looper just hooks the yarn. Yarn tension is T_3.

(4) In the forth stage, tufting needle motions upward. When tufting needle is at the highest position, the looper is just out of the yarn shown as Fig. 4d). At this time, yarn path is the smallest and yarn is without any tension.

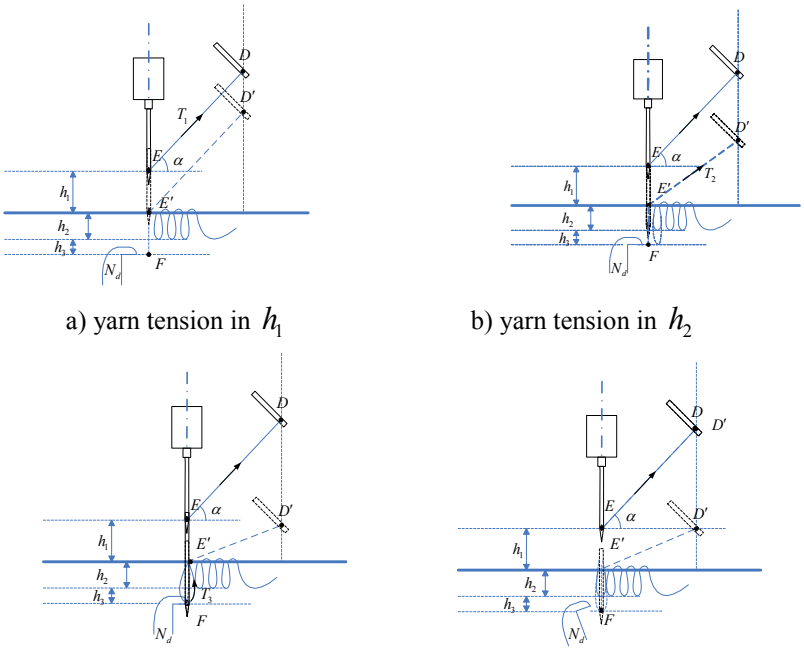

a) yarn tension in h_1 b) yarn tension in h_2

c) yarn tension in h_3 d) yarn tension when needle in highest position

Fig. 4 Analysis diagram of yarn tension

Analyzed from Fig. 4, it is known that the yarn is subject to tension control in the first three stages. Only when tufting needle is at the highest point, yarn is without any tension.

Summary

In this paper, by analyzing path flexing in the yarn path and yarn tension of the tufting equipment system, a conclusion can be educed that yarn tension changes with the tufting needle position alternately. When the tufting needle is in different position, the yarn tension is different. Yarn tension periodic change with the yarn flexing periodic change.

Acknowledgement

This project is supported by National Science Foundation of China(No. 50775033) and by the Fundamental Research Funds for the Central Universities(9D10304, 9D10310).

References

[1] S.X.Xue: Machine-made Carpet, Beijing: Chemical Industry Press, (2003), pp.1-6.

[2] Y. Xu, Z. J. Sun, Z. Meng, Y. Z. Sun, G. F. Chen, Yarn Tension Analysis in Typical Carpet Tufting Equipment System，Key Engineering Materials, (2010)

[3] Meng zhuo, Sun Jingjing and zhou tingze etal: Research on the influence that stop position of carpet tufting machine to yarn tension and the method of eliminating stop mark. Key Engineering Materials, (2008), p.724-728

Advanced Materials Research Vols. 204-210 (2011) pp 58-61

doi:10.4028/www.scientific.net/AMR.204-210.58

Development of Biodegradable Wood Fiber Foam Packaging Material

Chen Li[1], ShengLing Xiao [1,a], Hong Lin [1]

[1]Key Laboratory of Forest Sustainable Management, Environmental Microorganism Engineering of Heilongjiang Province, Northeast Forestry University, Harbin 150040, China

[a] Corresponding author: shenglingxiao@yahoo.com.cn

Keywords: Wood fiber; Foam; Packaging Material; Biodegradable.

Abstract. In daily life, expanded polystyrene foams (EPS) are widely used as packaging material and waste EPS has caused lots of environmental pollutions because it cannot be decomposed in nature. In this study, the machining process is developed of a reinforced foam packaging material by hot press molding, potato starch and birch fiber as the main raw materials. Analysis of the dosage of the birch fiber, starch adhesive and foaming agent and how do they affect the mechanical properties. Experiments show that material compressive strength is good and foam well-distributed, when the birch fiber content is 20%-25%, adhesive content is 30%-35%, and birch fiber amount is 10%-15%, the material has fine performance, and the cells are well distribute.

1. Introduction

With the economic development, rational utilization of the earth's resources and environment protection have been increasingly global concerned. Protecting resources and environment, and creating a favorable survival and development space are the basic strategy to realize the sustainable development of global economy. At present, the world plastic production has been more than two million tons. In this plastic garbage, packaging rubbish accounts for 30% of the total.

Cushion material plays the role of mechanical protection in order to effectively protect product and it is also indispensable. But its waste can't be degraded and recovered completely, which makes serious environment pollution. Many advanced countries have limited the use of the plastic foam materials and prohibit the imported product using it by legislation. Thus, a green revolution have been on the rise in cushion packaging materials and the developing of the biodegradable foam packaging materials has been the main stream of sustainable development.

Wood residues are precious biomass resources. The rational utilization is the essential condition of sustainable development of forestry. For forest resources are decreasing and the reserved resources are seriously shorted, serious shortage of the reserve resources, the development and utilization of wood residues appears more urgent. Using wood residues to develop the biodegradable foam packaging materials has a broad market prospect.

2. Research status

At present, Europe, Japan and other developed countries are seeking for new environmental-friendly packing material. They are dedicating the research the plant fiber foam technology and expecting for the new packaging materials which can replace the expanded polystyrene foams being widely applied to the shockproof pads of industrial productions.

Abdulkadir Kan studied on a new recycling process development of the waste EPS foams by using heat treatment [1]. Lawton used the aspen fiber to develop a biodegradable foam material[2]. The results showed that trays containing between 15%and 30% fibers had no significant difference in tray strength. Trays containing more than 30% fiber had lower tray strength. Salgado conducted study showed the biodegradable food packaging trays made from cassava starch[3], sunflower proteins and cellulose fibers by a foam baking process. Soykeabkaew conducted study on the Starch-based composite foams[4]. Orientation of fibers was shown to have a strong effect on both the flexural

strength and the flexural modulus of elasticity of SCFs. Averous studied on the properties of biocomposites based on lignocellulosic fillers[5]. Glenn obtained that baked foams made of a composite of starch and fiber and equilibrated to a moisture content of approximately 11% have better physical and mechanical properties than foams made only of starch or starch and $CaCO_3$[6]. Curvelo introduced the advantages of thermoplastic starch reinforced with cellulosic fibers[7].

Lv YanNa researched on the vegetable fiber cushion material of waste paper fiber and potato starch[8]. Ding Yi used the extrusion and swelling technique and the prepress principle to develop a new biodegradable cushion packaging materials[9]. Chen Yan adopted wet foaming method which stirred the vegetable fiber in water to get fibrillation[10]and then mold. GaoDe studied on the preparation technology with the main components of corn straw and starch[11]. Li JiZhu mixed up the plant fiber, PS and starch for multi-component cross linking[12].

Some scholars also had similar studies, there were also some patents that introduced the method of manufacturing the foam packaging materials using the plant fiber. According to the research situation, we have made some achievements in using plant fiber to manufacture foam packaging material. But the study of using the wood residues is very little, this paper introduces the development of the foam packaging material with the wood residues, which has excellent buffering properties and characteristics of natural degradation.

3. Experimental program and processing

3.1 Raw materials

Wood fiber. Wood fiber has high mechanical strength, modulus and lower density, and it is suitable for the reinforcement of the composite materials. It is the skeleton of the product. This experiment selects of northeast common birch fiber, the fiber and length is 40-60 mesh.

Adhesive. Adhesive can make the joint surface have enough strength. This experiment selects polyvinyl alcohol (PVA) and mixed starch solution as adhesive.

Foaming agent. Foaming can make the cushion packaging material have superior cushion properties. With the temperature rising, foaming agent begins to decompose gas and make the mixture expand and foam. This experiment selects NH_4HCO_3, $NaHCO_3$ and AC as foaming agent.

Other addition agent. In order to improving the physical properties, mechanical performance and service performance, it is necessary to add various trace additives.

3.2 Material preparation process

(1)Putting the birch sawdust into the pulverizer through the screen of 40-60 mesh.

(2)Using 10% sodium hydroxide solution to soak wood powder for 24 hours, washing the wood powder after alkali treatment into neutral, drying moisture content below 5% in the oven.

(3)Making the polyvinyl alcohol (PVA) dissolve in the mixer at 95℃, perpetrating solid content 8% PVA solution and cooling to room temperature.

(4)Stirring the esterified starch for 1.5 to 2 hours until complete dissolution at 48℃ by mixer.

(5)Mixing up the starch solution and PVA solution, adding foaming agent, additives and wood powder, stirring uniformly, place it for half an hour at normal temperature.

(6)Putting the mixture into the oven, pre-dry for a period of time at 50-60℃ to control the moisture content, and preventing the loss of adhesive at forming.

(7) Filling the prepared paste mixture in the mould, and compression molding by hot press.

4. Material performance analysis

There are many uncertain factors in the process of preparation, including the selection of raw material, dosage and processing condition. This paper explores the influence of the dosage of wood fiber, adhesive and foaming agent on the compressive strength of the material.

4.1 The dosage of wood fiber

Starch material has low intensity and easy to crack and poor waterproof after drying. Adding proper birch fiber can improve the properties. Birch fibers constitute three-dimensional mesh, the structural strength depends on the strength of fiber bundles themselves and the connection strength among the fiber bundles. Birch fibers can increase the strength as skeleton of the foam material, but the increasing quantity of birch fiber will reduce the matrix viscoelasticity, which lead to decline the surface tension of glue membrane, causes other components can't joint connection, affecting the foaming quality and the performance of the material. The experiment studied the birch fiber content from 5% to 45%, how to influence of the compressive strength.

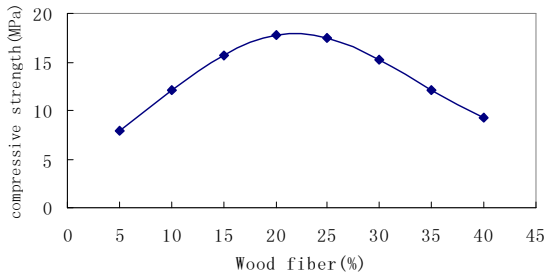

Fig.1 **Effect of birch fiber content on compressive strength**

Figure 1 shows that the compressive strength of the material is raising then falling with the raising of birch fiber dosage. The compressive strength is less if birch fiber adding little, adding too much (about 35%) material appeared collapse phenomenon. The main reason is too much fiber dosage cause the bonding strength of matrix drop, So as to structure relax and low intensity. Experiments show that material compressive strength is good and foam well-distributed, when the birch fiber content is at 20%-25%.

4.2 The dosage of starch adhesive

The experiment mainly adopts starch as adhesive, in order to improve the performance of adhesive, the joining polyvinyl alcohol (PVA) is used as crosslinking agent to enhance the effect of adhesive.

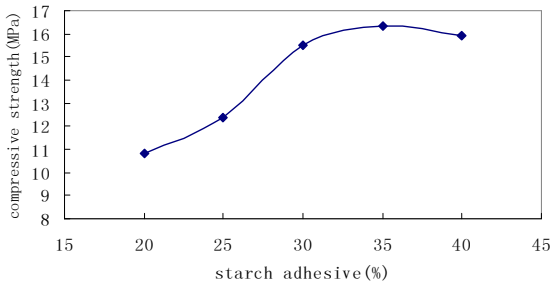

Fig.2 **Effect of starch adhesive content on compressive strength**

In figure 2, we can see, with the adhesive increasing, compressive strength increases, but as the dosage of adhesive reaches to 40%, material strength declines. Because the adhesive is PVA and starch copolymerization, as the content below 35%, starch particles embeds in polymeric scaffold, and closely, so as to improve the mechanical properties of the material. When more than 35% of adhesive, excess starch of adhesive can't enter into the polymeric scaffold, starch molecular chain is easy to tangled, forming round-shape. Starch is brittle material after drying, starch content increasing, brittle of the composite materials also increase. Thus, the content of adhesive in 30 to 35% is appropriate.

4.3The dosage of blowing agent

This study chooses the mixture of NH_4HCO_3 and $NaHCO_3$, azodicarbonamide (AC) as foaming agent because that they are cheaper and little impact on environment. NH_4HCO_3 decomposition is at low temperature (about 60 degrees Celsius), produces too much gas and hard to control. $NaHCO_3$ foaming agent decomposition is at high temperature (about 70℃-110℃), gas production release uniformly, with the temperature increase, in favor of control foaming , so this experiment select the mixture of NH_4HCO_3 and $NaHCO_3$ as foaming agent. In addition, certain content of water also play a role of the foaming agent, at baking temperature, water becoming into steam homogeneous dispersion in material, forming uniform bubbles.

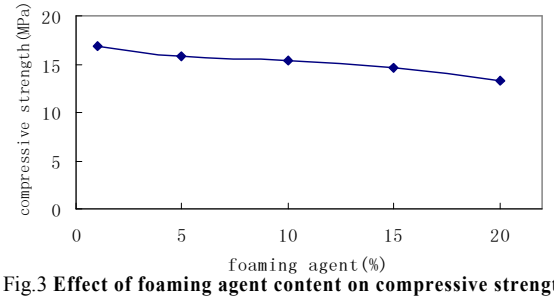

Fig.3 **Effect of foaming agent content on compressive strength**

Figure 3 shows the compressive strength is decreased with the amount of the foaming agent increasing, but the material has the cushioning properties gradually. As small amount of the dosage, such as rigid material, it hasn't basically buffer performance. As increasing the dosage, the rigid is decrease, bubble is uniform gradually, and cushioning performance becomes better. Excessive dosage

of the foaming agent, producing a lot of gas with the temperature rising, the volume of a gas expanding constantly, causing the diaphragm of internal gas chamber being thinner till to break, so the gas overflows and matrix collapse internal. The dosage of the foaming agent and compressive strength show nonlinear relationship. When the amount of birch fiber is 10%-15%, the material has fine performance, the stomata well distribute.

5. Summary

This paper studied on the preparation method of a biodegradable foam material by hot press molding, adding the birch fiber into starch based material can improve the characteristics of the mechanical strength, fragile and moisture absorption alone starch material. Tested the material properties and obtained the optimal proportion range of wood fiber, starch adhesive and foaming agent, under the condition of ensuring a good performance of the material. The conclusion laid a foundation for the further study.

6. Acknowledgements

This work was financially supported by the Fundamental Research Funds for the Central Universities(Grant No. DL09AB05).

References

[1] Abdulkadir Kan, Ramazan Demirbog. A new technique of processing for waste-expanded polystyrene foams as aggregates. journal of materials processing technology,2009:2994-3000.

[2] J.W. Lawton, R.L. Shogren, K.F. Tiefenbacher. Aspen fiber addition improves the mechanical properties of baked cornstarch foams. Industrial Crops and Products, 2004, (19): 41–48.

[3] Pablo R. Salgado,et al. Biodegradable foams based on cassava starch, sunflower proteins and cellulose fibers obtained by a baking process. Journal of Food Engineering, 2008, (85): 435 - 443.

[4] Nattakan Soykeabkaew, Pitt Supaphol, Ratana Rujiravanit. Preparation and characterization of jute- and flax-reinforced starch-based composite foams. Carbohydrate Polymers, 2004, (58): 53–63.

[5] L. Ave'rous, F. Le Digabel. Properties of biocomposites based on lignocellulosic fillers. Carbohydrate Polymers, 2006,(66) :480 - 493.

[6] G.M. Glenn, W.J. Orts, A.R. Nobes. Starch, fiber and CaCO3 effects on the physical properties of foams made by a baking process. Industrial Crops and Products, 2001, (14): 201–212.

[7] A.A.S. Curveloa , A.J.F. de Carvalhoa, J.A.M. Agnelli. Thermoplastic starch±cellulosic fibers composites: preliminary results. Carbohydrate Polymers, 2001, (45):183-188.

[8]LU Yan-na,ZHANG Yun-zhan, OU Jian-zhi. Study on Making Buffer Packaging Material by Wastepaper. Packaging Engineering, 2004,(6):78-82.

[9]DING Yi,LI Yao,ZENG Shan-qi,et al. Development of plant fiber cushion packaging material. Packaging Engineering, 2006,26(2):50-51.

[10]Yan Chen. A Cushiony Package Material Composite with Wood Fiber by Foam-dilating and Dry Technology. Fujian :Fujian Agriculture and Forestry University,(2004).

[11]GAO De, CHANG Jiang,GONG Xue. Research on Corn Straw Cushion Packaging Material. Packaging Engineering, 2007,28(1):27-29.

[12]Li Jizhu,Xie Taihe, Cai Yihui. Development of Degradable Cellulose Reinforced Starch Foamed Plastics Dishware. China Plastics Industry, 2002,(5):45-46.

Advanced Materials Research Vols. 204-210 (2011) pp 62-68

doi:10.4028/www.scientific.net/AMR.204-210.62

Optically powered Sensor for Measuring Differential Pressure with Optical Fiber Data Link

Xiaohong Ni[1,a], Jing Yuan[2,b], Jinyu Wang[3,c], Yutian Wang[4,d]

[1]Cangzhou Teachers College, Cangzhou, Hebei China 061001

[2;4]Yanshan University, Qinhuangdao, Hebei China 066004

[3]No.5711 Aviation Industry Corporation of China, Qinhuangdao, Hebei China 066004

[a]nixiaohong2005@163.com, [b]love-sky-yj@163.com, [d]y.t.wang@163.com

Keywords: Two wave-length detection, LD Light power, Micro-power consumption probe, Optical fiber data link

Abstract. The paper describes the operation principle of optically powered sensor to measure differential pressure. Its probe powered by LD light only consumes tens micro watt .The optical source for power and signal can be transmitted to and fro by a single multiple mode optical fiber. The power and signal lights have different wave length. The system design is introduced and its parameters are selected. The signal and power are transmitted by fiber, and the probe is low power consumption, so this pressure measuring system can work in flammable and explosive environment. Adopted differential measuring signal processing technology, its anti-noise ability is improved. Experimental results show that this system has high precision and high reliability.

Introduction

With the development of electronics and photoelectric technology, we can use the photo-electric conversion to bring optical power through the optical fiber for long-distance transmission to drive the micropower circuit, in order to realize the work of optically powered electric sensor. At present, the research in the optical fiber transmission power drive mode mainly focus on three aspects[1]: optically powered fiber telephone communications; pneumatic and hydraulic optically powered executive device; optically powered sensor. Studying the fiber optically powered sensor mainly in order to solve the compatibility between fiber coupling and conventional electric sensor, not only assure the precision, but also assure the sensor apply to the measurement applications in the special circumstance ,for example the high electromagnetic influence, using the fiber-coupled high-voltage insulation and the passive characteristic of measuring terminal.

There are two basic modes of the power offered by fiber and the bi-directional signal transmitting having been achieved:the single-fiber using the beamsplitter and the double-fiber system.Though these two basic modes are different in the form of fiber coupling, the optical power adopts the non-modulation system, and it realized the photo-electric conversion to make the probe work with the silicon photocell. The fiber-coupled optical powered sensor uses the single multi-mode fiber to offer the channel of measuring signals and double-wavelength power[2]. The LD optical power peak wavelength is 1300nm which is from the instrument to the probe, and the measuring singal peak wavelength is 850nm which is from the probe to the instrument. The light power signal transmission by using a square wave modulation, with the PD detector of 1:13.5 step-up

transformer to realize the transformation between electric and light, to generate the standard voltage required by the probe. Due to the micro-consumption electronic circuit design of the probe and the highly efficient coupling between LD illuminant and the fiber, the optical power comes from 200m long fiber is enough to make the probe work stably. The probe and the instrument are linked by a fiber, and the probe can be regarded as a "black box". Although it using the traditional electrical sensor method, due to the light source offered by fiber, generally speaking, it is consistent with the goal of the all-fiber optical sensor, and because the special signal detection and the design of modulation system make it not only keep the inherent characteristics of the electrical sensor, but also be superior to the optical method of sensors.

Optical power propulsion system and channel parameters selection

The single fiber system frame is shown in Fig.1， which has the optically powered function and the bi-directional transceiver function. It consists of two parts, one part is the instrument which provides LD square-wave modulation signal and measures the signal processing, and the other part of the sensor is the probe of the optically powered sensor, with 200m long single fiber coupled in between. The pulse signal PAM formed by the driving circuit units drives the laser diode(LD) luminesce focus on the two surfaces of the power sensing fiber and the optical feedback fiber, and the full-duplex coupler forms X biforked fiber which will convey PAM to the pulse transformer in the probe. It will be changed into a certain voltage of electric power. After the rectification of the low power diode, there will be 3.5 V constant DC voltage output, which supplies the detector probe and the transmission circuit power. The probe detection circuit adopts the micro-consumption design.The power supply voltage of 3.5V,which needs current of 30μA and power of about 100μW.

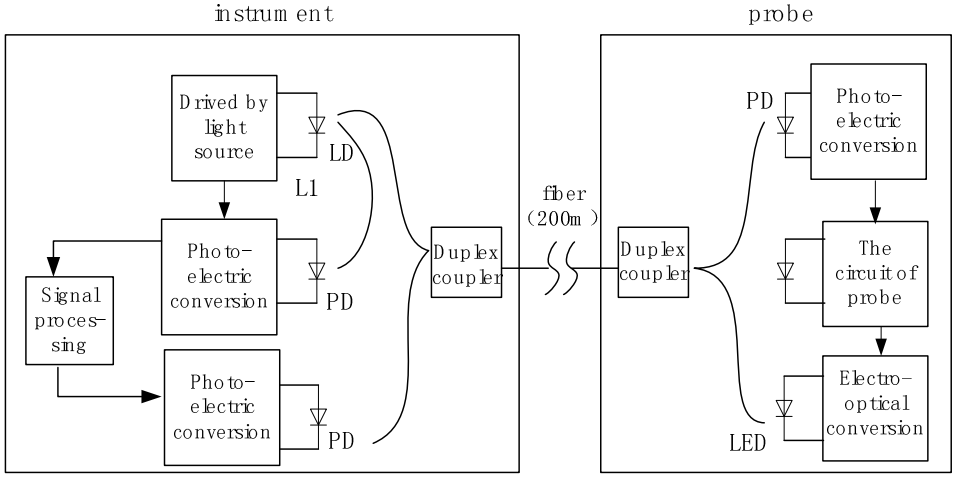

Fig.1 The system block of fiber transmission promoted by the optical power

LD and its drive circuit. Take the InGaAsp/InP double heterojunction LD as the power source[3]. After the fiber coupling with LD, testing I-P, V-I and the spectral characteristics, the test results are shown in Fig.2.

Test results show that, when the applied reted thermal current of LD increases from 10mA to 30mA , its output of optical power presents the linear change from 1 to 5mW , without peak shift. The other parameters of LD: the centre wavelength is λ=1.3μm, the half-width of the spectrum is $\Delta\lambda$=3nm ,the cut-off frequency is greater than 1GHZ, and the coupling efficiency is 40~50%.

The driver and the optical feedback circuit of LD are showed in Fig.3.In Fig.3,the square signal of LD optical power is driven by NE555[4],taking R_B=1KG, $R_{A=}$10KG, C=0.01μF, the drived signal frequency is:

$$f = 12KHZ \tag{1}$$

LD output power P is the function of its driving foward current I. When I increases, the output optical power is then increased to. It also causes LD fever, making its junction temperature rise and optical power output decrease. LD works in the repeat pulse current turntable, and the range of LD junction temperature is:

$$\Delta Q_J = Q_{jman} - Q_{j\min} = P_D R_T (1 - e^{-\frac{T_P}{R_T}}) \tag{2}$$

Where P_D, R_T and T_P are the loss power, the thermal resistance of LD junction relative to the environment, and the pulse width of the drive current, respectively.
There is the relationship between the decline of LD optical power and the junction temperature:

$$P_D = 1 - e^{K\Delta Q_1} \tag{3}$$

Where K is the factor which is relevant with the LD materials.
The experiment and theory of LD analysis indicates that thermal characteristics of LD is the main factor of the working status. When the working temperature field of LD is from 25°C to 60°C,the decline of power is approximately 25%.
To ensure the output power of LD constant and the system of the measurement precision, there are three adopted technical measures: add cooler for LD, in order to make its junction temperature field constant; Use the amplitude of output power of optical feedback stabilization LD; The sensing probe uses the differential mode to reduce the power supply fluctuation and other isotropic interference.

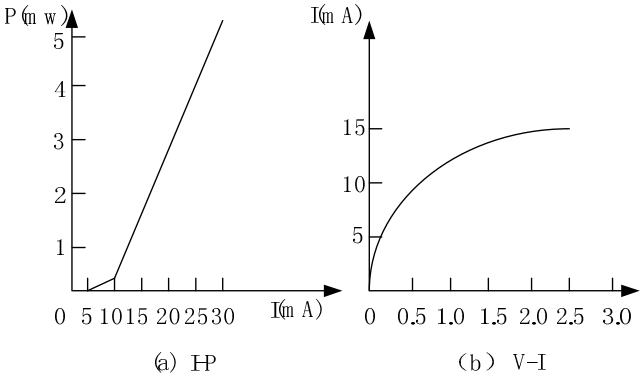

Fig.2 Photoelectric properties of LD

In Fig.3, The PAW signal from LD, one way is supplied for the power fiber, another way is couplied with the 0.2m long feedback fiber, after the optical/electricity transformation and the phase-sensitive detection, then it connected with the drive current Settings and feedback circuit of LD which is formed by A_1~A_3, G and so on. In Fig.3, the driving current for LD is:

$$I = \frac{V_A}{R} = \frac{K}{R}(V_s - V_f) \tag{4}$$

Where V_s and V_f are the given voltage to drive LD and the optical feedback voltage, respectively.

Eq.4 showed that when the LD thermal characteristic is changed and influenced by other

disturbances including the temperature, the luminous intensity is changing, that is to say V_f is changing. When V_f increases, the drive current I diminishes, and the luminous intensity of LD decreases; When V_f is reduced, I increases, and the luminous intensity of LD increases. Therefore, no matter how the luminous intensity of LD have changed, the stable source photoelectric negative feedback system will keep the luminous intensity from changing,thereby maintaining the stability of the output light intensity of LD.

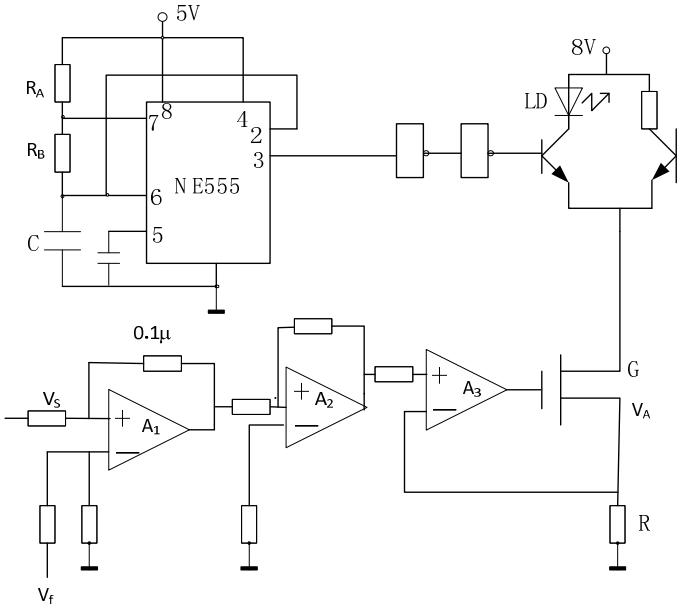

Fig.3 The circuit of the driving LD and the optical feedback

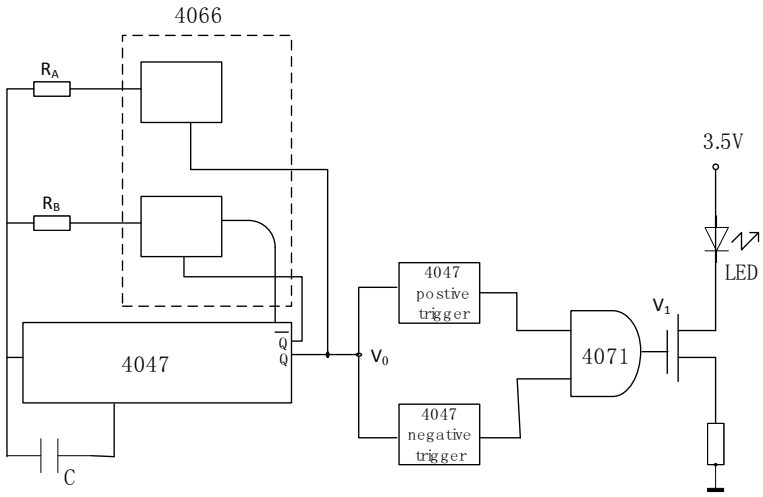

Fig.4 The sensitive probe circuit

The differential sensitive probe. Using the strain gauge which has the semiconductor piezoresistive effect to form the differential pressure sensing probe of differential operating mode, whose transformation of the pressure-pulse width modulation (PWM)- pulse position modulation

(PPM) is shown in Fig.4.

The circuit of the sensitive probe is supplied with the optical power. In fig. 4, the multivibrator of 4047 is feedback controlled by the electronic switch of 4066. The differential pressure measuring resistances R_A and R_B of the diffused silicon are in turn fixed into the fixed width capacitance C to get the PWM signal. The positive and the negative triggers triggered by the monostable time delaying convert PWM signal to PPM signal by 4071. LED emits the light of which the peak wavelength is 0.85μm, coupled to the transmission fiber. The period of PWM square-wave output of 4047Q is:

$$T = -2R_{AB}C\ln\frac{V_{TR}(V_{DD}-V_{TR})}{(V_{DD}+V_{TR})(2V_{DD}-V_{TR})} \tag{5}$$

Where V_{DD} and V_{TR} are the power supply voltage and the transfer voltage, respectively. When V_{TR} is 0.5 times of V_{DD}, and the diffused silicon resistances, R_A and R_B ,are working in differential mode, there are:

$$t_1 = 4.4R_AC \tag{6}$$

$$t_2 = 4.4R_BC \tag{7}$$

Eq.5 shows that the period of PWM square-wave output of 4047Q is proportional to the R_A and R_B, respectively. As long as R_A and R_B are linear with the measured quantity, the transform from the reisistance to the voltage is a linear relationship showed in Fig.4. After the measuring signal is converted to the PPM position, it is transferred to the instrument through the fiber optic transmission, then converted to PWM signal by the circuit (Fig.5).

The function of the circuit in Fig.5 is as follow: PD is to realize the shift from the optical pulse to the electrical pulse, with two monostable 4047 and the trigger D for the recovery of the pulse position-pulse width. The 6μs frontier and the 30ms trailing edge of the triggered monostable determine the pulse width of the PPM-PWM transformation and the uniqueness of polarity.

The waveform of the circuit in the Fig.4 and Fig.5 is showed in the Fig.6, respectively.

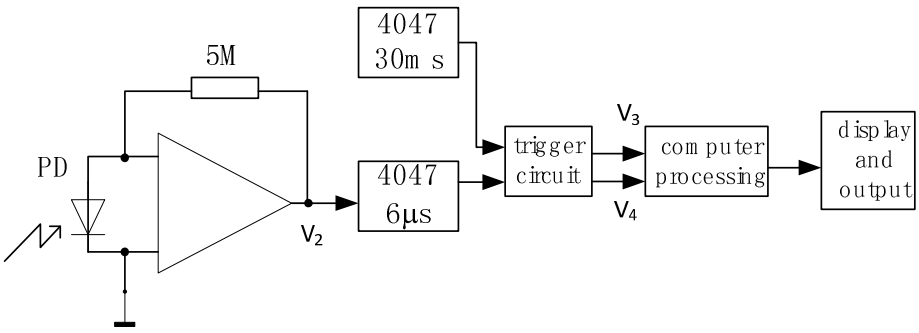

Fig.5 The PWM-PPM recovery and signal processing

Eq.8 is the subtract and ratio operation for the PWM signal by the microcomputer signal processing system[5].

$$S = A\frac{t_1 - t_2}{t_1 + t_2} = AN\frac{R_A - R_B}{R_A + R_B} \tag{8}$$

Where A and N are the factor related to the computing pulse and the constant, respectively.
After the operation shown in the Eq.8, the system output is only related to the measured quantity , R_A and R_B ,but it has nothing to do with the power supply voltage and all kinds of the isotropic interference.

The calculation of power. Power channels: The attenuation of the 200m-long optical is 1.5 dB; The attenuation of the both full-duplex coupler is 1.5 dB; The attenuation of other couplers is 7dB;The attenuation of the signal channel is about 7dB.

The test of the performance index about the instrument

The probe power test. The current/voltage conversion is got by the high-precision OP-AMP[6]. When the probe is for the differential pressure measurement, it measures V_0 is 35mV, and the calculated power of the probe is 120μw.

The differential pressure test. The instrument is testing the differential pressure for the measurement range from 100.0 to 900kPa. The pressure counts as a standard of this instrument and the test results are shown in Table 1.

Table 1 Results of measure based on differential pressure

Readings of the standard pressure meter [KPa]	100	200	300	400	500	600	700	800	900
The output of this instrument [KPa]	100.1	197.2	298.3	397.1	499.6	597.8	600.2	799.8	900.1

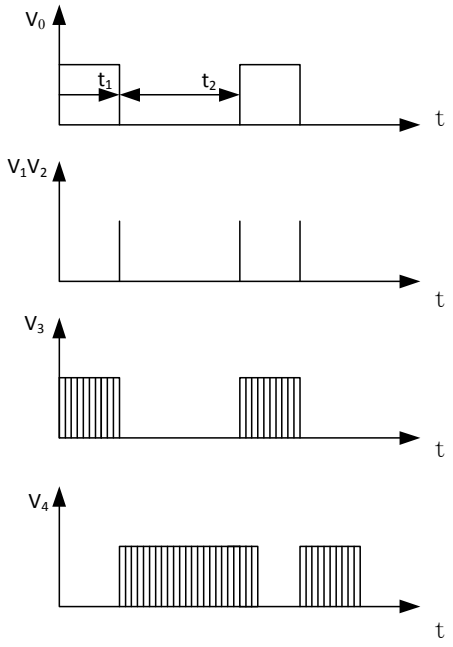

Fig.6 The signal waveform

Summary

1. The optic power driving sensed system using the time-sharing double wavelengths realizes bidirectional transmission between the power and the signal. The sensitive probe is considered to be passive. As the black box, it is a all-optical sensor for the outside, and this working mode has theoretical and practical significance in the application of the conventional power sensor which is inflammable, explosive and in the situation including the strong electromagnetic interference source, and promoting the development and practicability of the fiber optic sensor.
2. The optical power working mode of InGaAsP/Inp luminescent device LD can realize the fiber transmission of the more long-distance optical power. The fiber for the experiment is 200m long in this instrument. As the experiment in the function of the probe and LD and the analysis for the coupling efficiency show that, when the pushing distance is km, the output power can be greater than 1Mw , and also make the probe work.
3. The sensitive probe with the micro-consumption PWM/PPM transformation is the key to realize the optical power supply and long-term work steadily. Using the differential pressure sensitive probe which is diffused silicon resistance, the total power is less than 150μW, which not only realize that the optical power offers probe enough energy and the signal is transmitted undistortedly, but also because the difference and division operations of the measuring signal, which are the mutual reference channels, it reduces the power supply fluctuation and various isotropic interference in system, and improves the accuracy of the instrument.

Acknowledgement

This paper is supported by the National Science Foundation Under Grant No.60974115 and No.61071202, and it is supported by the Hebei Science Foundation (F2010001312).

References

[1] Guo Li, Zhang Qingmin, Research Progress of the Residue Analytical Method of Carbamate Pesticides . Journal of Tianjin Agriculture College. 2001,8(4): 15-21
[2] Guo Deji, Sun Hongfei, *Analytic Approach of the Spectrum* . Publishin Company of Chongqing University.1999.
[3] ShiJinShan, etc., *Optoelectronics and Application* , P576, machinery industry press, 1991.
[4] Wang Yutian, Liu Rui, Study of Fiber-Optical Fluorescence Spectrometer for monitoring Carbamate Pesticides. Sensing Technological Journal. 2003,16(3):318-320.
[5] Salah Ha ssoon, Israel Schechter, In Situ Fluorimetric Determination of Pesticides on Vegetables. Analytica Chimica Acta, 2000,405(2):9-15.
[6] Zhang Jiyan, Yang Guohong, Zhang Baoquan etc., Research of the Small-Scale Flat Focal Field Grating Spectrometer. Optics Journal.2001,21(9):1099-1103.

Advanced Materials Research Vols. 204-210 (2011) pp 69-72

doi:10.4028/www.scientific.net/AMR.204-210.69

Intelligent Building System Based on Sensor Network of IPV6

Jian-ming CUI[1,2,a]

[1]School of Information Engineering, Chang'an University, Xi'an 710064, China

[2]Shaanxi Road Traffic Detection and Equipment Eng. Research Center, Xi'an 710064, China

[a]cjianming@gmail.com,

Keywords: Intelligent Building. IPv6. Sensor Network. Construction System

Abstract. With living standards improve, more and more attention of intelligent building. Follow that, required facilities of life, entertainment, security and other more and more to connect into the network. The IP address of the traditional IPv4 space is facing the depletion, facing a crisis of a large number of the access device; The IPv6 addresses solve such crisis. In this paper, framework an intelligent building system based on Ipv6, to achieve access to smart sensors, and to intelligent home facilities purposes.

Introduction

In the past few decades, but the new demand for intelligent building has more requirements [1]. Constantly developing new technologies has brought new means to the development of intelligent buildings, makes the need for access into internet more and more the equipment. In different agreement, the common use of different resources, these are the evils of obvious. To address such issues, the introduction of IPv6 protocol will be a good idea. Between IPv6 and IPv4 conversion to achieve [2] can use IPv6 protocol after a simple transformation the composition network of the original IPv4.

2 IPv6 advantages in intelligent building

2.1 Reduce duplication of investment

With the application of information appliances and development of home network[3], and increased penetration of home networks, Coexistence of a variety of network technologies and standards in a residential area or the home will become universal. But the coexistence of a variety of network technology has brought us repeat investment and resource conflicts. If using IPv6 technology, the coexistence of a variety of home networking technologies will substantially improve the current situation. Intelligence technology from the current mainstream view, supported by the subsystem for the main application can be divided as follows: intelligent control, media (audio and video) sharing, security alarm, video surveillance and others. From the data flow direction perspective, can be divided two broad categories data flow as follows: within the family and the family home outside. The flow of data outside the family including home appliances remote control, media data sharing between homes, the three Meters(water ,electronic, gas) away copy, telemedicine, security and management of property outside the flow of data; The flow of data within the family, including transfer of DV, DVD, TV and other media equipment resources within the family, the terminal of intelligent control within the family, light automatic adjustment within the family section, curtains automatically open, and the flow of data within the family and et. . The development state of now

home network is: Whether the flow of data within the family or the family Application of the flow of data using an independent external IP address of the IPv4 technology, independent of the data channel is more difficult to realize there are bottlenecks. To achieve interoperability and integration of multiple technologies information, IPv6 technology is the best choice.

2.2 Separate address and improve safety

The technical aspects of interoperability, IPv6 and IPv4 networks have the same advantages. However, this particular network in the home environment, IPv6 network is superior than the IPv4 network, mainly in two, those are for each home appliances assigned an IP address and provide a more secure home network to use.IPv6 address space is a huge technology advantage to support each appliance gets a real IPv6 address in the global. In theory, every IPv6 home appliances can exchange any form data with any other IPv6 Internet hosts or other IPv6 home appliances. Such a broad technology base for any wish to make to the data exchange for the support of home networking applications can provide extensive support and realization.

3 Function of intelligent building IPv6-based

The core of intelligent Building design based on IPv6 is set up an open network platform, use this platform to achieve interoperability between the various subsystems by the Family Services gateway, and provide a unified interface to use all functions.

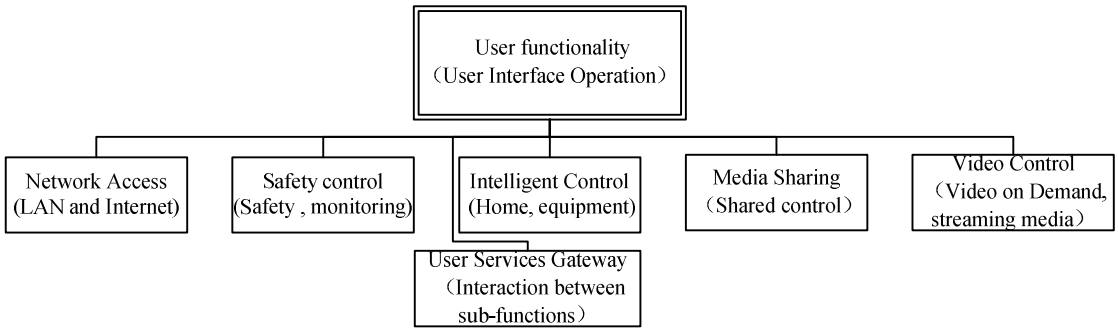

Fig.1 Intelligent building systems based on IPv6

The whole system model includes several features about: user functionality, Network Access, Security control, intelligent control, Media Sharing Module, video Control Module, user Services Gateway.

Shown in Figure 1, the user control module manages several other modules. Although the function of each module is relatively independent, but combining to each module through a unified user interface of families, the maximum cost reduction, improved system operational.Family Service Gateway is the core of the system, It completed the acceptance of user commands, processing instructions, sends control commands to the intelligent control module, simultaneous acquisition status of Intelligent Control Module, and returned to the user. At home, to facilitate control computer, PDA, remote control, electronic wall switch, video intercom and other indoor family services by a unified gateway.

In addition, the system provides two ways that are computer remote control and control of GPRS mobile phones, using Internet connected to the home service gateway by Web mode, centralized control and management the home device.

Network Access. Network access is divided into two parts that are LAN area access and internet access, these access methods can achieved seamless switching of intelligent building system access. Community LAN access is for browsing the cell information, announcements, internal control and other functions; Internet access module is for connecting public network and to reach the remote control.

Security control. In the security module design, full use the powerful features of the intelligent building platform to enable this security system has many unique features: System not only sends alarm message, and send control image; Households alarm at any time through a variety of ways, and view the log of home security system through the browser and images, avoid the owner of the home away from home safety concerns. Once alarm occurred, the camera will automatically capture and save images on the server, and can be see it the future. As illustrated in Fig. 2

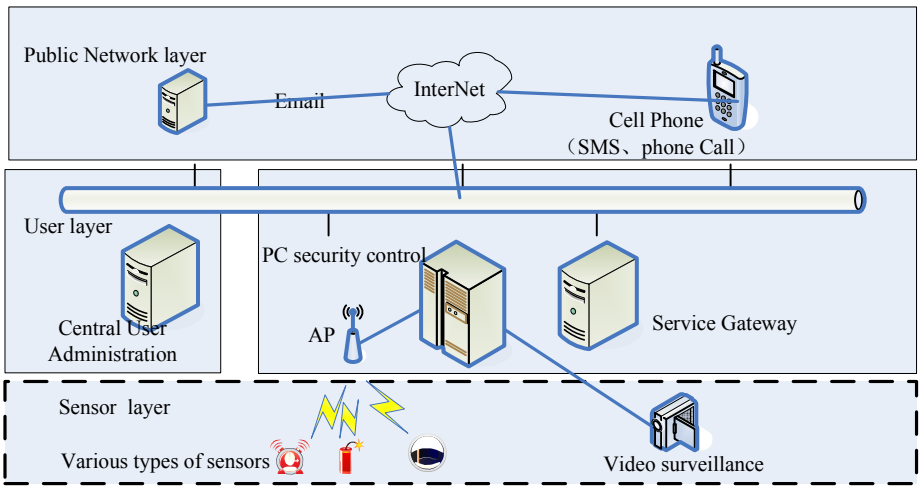

Fig.2 Security control function

Intelligent control. Intelligent control module is a remote operation, intelligent household appliances complete management solution for independent IP address for the equipment, the implementation of intelligent control easier, more convenient operation, as show Fig.3. The main of control have follows form:

a. **The individual device control.** Users can select different and controlled separately that lighting in the room, curtains, televisions, kitchen appliances and each power outlet, able to demonstrate the state of the controlled object while control. Drive the truck into the gate, for example, system can be sent ahead of time the order to open the garage door through intelligent control module, so no need to wait, you can directly enter the garage.

b. **Profile mode control.** The system according to the family's daily life set a different profile. The daily profile is divided into a number of different equipment operation instruction set, to complete a default profile.

c. **Model schedule.** Model schedule is automatically start time based on users daily work schedules and some of the profiles.

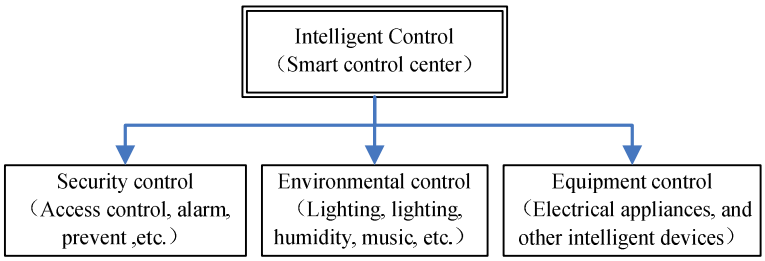

Fig.3 Intelligent Control form

Media Sharing Module. Media sharing is one of the typical applications of the intelligent network architecture in the family, IPv6 directly optimize and service quality assurance the media of information transmission in IP layer. In IPv6 networks, media information will be faster transmission between families within, outside and the each of family, that improve their reading for the quality of media information and real-time transmission requirements. Limitations by the time

of technical produced, some standards and technologies not fully meet the needs of the development of home network because they produced in time are earlier time and some standards exist in name only. With development the application of information appliances and home network, and raise in the level of family networks widespread, more and more vendors would developed information appliances with the network interface chip to support IPv6, this family visit to the sharing media data will become more easy and popular.

Conclusions

IPv6 does not fundamentally solve the QoS problem of IPv4[4], only made some degree of expansion based on the IPv4.In order to better resolve the QoS issue of IP network, IETF (internet engineering task force) made a variety of Qos mode and mechanisms, to satisfy the requirements of Streaming media applications for QoS.

Comprehensively promote in IPv6 technology the intelligent building is still a long process, with the perfect IPv6 protocol technology, IPv6 protocol on the application of intelligent building will further improve and expand scope of use. View of the current multi-network integration and the pressing issues of interoperability, to IPv6 technology-based, by designing a common family services IPv6 gateway connecting a variety of heterogeneous network and interoperability that is a transition program. With continues to expand to IPv6 protocol application in transition program, IPv6-based intelligent building to replace IPV4-based intelligent building is only a matter of time.

Acknowledgements

The Project was Supported by the Special Fund for Basic Scientific Research of Central Colleges(CHD2010JC035), Chang'an University, by the Special Fund for Basic Research Program of Chang'an University and by the open Fund for Shaanxi Road Traffic Detection and Equipment Engineering Research Center.

References

[1] Everett, Richard, "The 'building colleges for the future' program. Delivering a green and intelligent building Agenda", New Review of Information Networking, v 14, n 1, p 3-20, May 2008

[2] Atefeh Ahmadi , R. Berangi , "Automatic Location Update using IPV6 Addressing Format for Next Generation Network ", JCIT: Journal of Convergence Information Technology, Vol. 4, No. 2, pp. 132 ~ 137, 2009

[3] Yu, Chen, "Research and design of intelligent building distributed circumstance monitor system based on wireless communication", Proceedings - 2008 2nd International Symposium on Intelligent Information Technology Application, IITA 2008, v 2, p 750-754, 2008

[4] Hocheal Kim, "An Enhancement of FMIPv6 for the Packet Radio Networks which Supports the QoS Provisioning on the MIPv6 ", JDCTA: International Journal of Digital Content Technology and its Applications, Vol. 3, No. 2, pp. 33 ~ 41, 2009

Advanced Materials Research Vols. 204-210 (2011) pp 73-78

doi:10.4028/www.scientific.net/AMR.204-210.73

Geometry Covering Theory in Biomimetic pattern cognition

Wenming Cao, XiongFeng Li

School of Information Engineering, Shenzhen University Guangdong,518060,China;

Email: wmcao@szu.edu.cn

Key words—Biomimetic Pattern Recognition Mapping, manifold space, covering subset

Abstract — We describe a new pattern recognition method which is based on the concept of geometry theory. The method identifies subsets of the data which are embedded in arbitrary oriented lower dimensional space. We definite a kind of mapping, and study its property. Covering subsets of points are repeatedly sampled to construct trial geometry space of various dimensions. The sampling corresponding to the feature space having the best cognition ability between a mode near zero and the rest is selected and the data points are partitioned on the basis of the best cognition ability. The repeated sampling then continues recursively on each block of the data. We propose this algorithm based on cognition models. The experimental results for face recognition demonstrate that the correct rejection rate of the test samples excluded in the classes of training samples is very high and effective.

1.Introduction

The method is "High-Dimensional Space Complex Geometrical Shape Cover Recognition Method [3-6]". It studies some kinds of samples' distribution in feature space and gives reasonable cover, so the samples can be "recognized". In the theory of BPR , in feature space Rn , to judge whether the points belongs to set Pa, a n-dimensional geometrical shape in the feature space covering set Pa need be constructed with the software and hardware methods. This geometrical shape is the topological product of a low-dimensional manifold and n-dimensional hypersphere. In this paper we describe a new model which is based on the concept of manifolds theory. The method identifies subsets of the data which are embedded in arbitrary oriented lower dimensional manifolds space. Covering subsets of points are repeatedly sampled to construct trial manifolds space of various dimensions. The sampling corresponding to the feature space having the best cognition ability between a mode near zero and the rest is selected and the data points are partitioned on the basis of the best cognition ability. The repeated sampling then continues recursively on each block of the data. We propose geometry covering theory based on biomimetic pattern recognition. The experimental results demonstrate that the correct rejection rate of the test samples excluded in the classes of training samples is very high. It proves the proposed method for face recognition is effective.

2.Biomimetic Pattern Recognition Mapping and its Property

We will move in the category of topological spaces. We will not define those, but assume the reader to have a basic knowledge. We will designate by $\Omega(x)$ the neighbourhood filter of a point $x \in X$.

Definition 2.1[3]. A map $f: Y \to X$ is called BRP mapping if $\forall y \in Y \exists V \in \Omega(y)$ with $U = f(V) \in \Omega(f(y))$ and $f \mid V : V \tilde{\to} U$ is homeomorph.

These local isomorphisms are also called sometimes *immersions.*

Definition 2.2. A map $f: Y \to X$ is called *separated* if $\forall y_1 \neq y_2$ with $f(y_1) = f(y_2) \exists V_1 \in \Omega(y_1)$, $V_2 \in \Omega(y_2)$ with $V_1 \cap V_2 = \varnothing$.

Definition 2.3. A map $f: Y \to X$ is called *proper* if f is *closed* with *quasi-compact* fibers $f^{-1}(x) \subset Y$, $x \in X$.

Definition 2.4[1-2]. A map $f: Y \to X$ is called a *covering* if $\forall x \in X$ the fiber $f^{-1}(x)$ is discrete and there exists a neighbourhood U of x and a homeomorphism h with

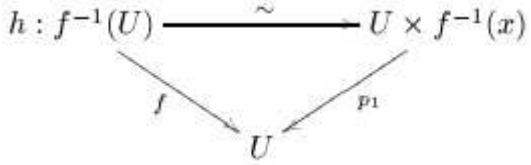

Fig 1. *covering*

Where you can assume that $h(y) = (f(y), y) = (x, y)$ for $y \in f^{-1}(x)$.

Otherwise put a covering is a *locally trivial bundle* with a *discrete* fiber. In an equivalent description you have $f^{-1}(U) = \bigcup_{y \in f^{-1}(x)} V_y$ disjoint, $V_y \in \Omega(y)$ and $f \mid V_y \tilde{\to} U$ In particular, a covering is separated and BRP, Obviously, BRP mappings $f: Y \to X$ are open, as this is a local property. But this dose also hold for their sections:

Lemma 2.1. *Let* $U \subset X$ *be open,* s **:** $U \to Y$ *be a section of* f **.** *Then* $V = s(U) \subset Y$ *is open.*

Proof. Take any $y \in V$, say $y = s(x)$, therefore $f(y) = x$. Let $W \in \Omega(y)$ be such that $f \mid W : W \tilde{\to} f(W) \subset U$ and consider $y \in f^{-1}s^{-1}W \cap W$. For $z \in W \cap f^{-1}s^{-1}W$, we have $f(s \circ f(z)) = f(z)$, which implies $s \circ f(z) = z \in s(U) = V$, therefore $W \cap f^{-1}s^{-1}W \subset V$ and V is a neighbourhood of y.

Lemma 2.2. *Let* s, t *be section* $U \to Y$ *with* $s(x) = t(x)$ *at one point* $x \in U$. *Then* $\exists$ *a neighbourhood* U_1 *of* x *such that* $s \mid U_1 = t \mid U_1$.

3. Separated Mapping

An equivalent statement to the definition 1.2 of '$f: Y \to X$ is separated' is obviously that the diagonal $\Delta_Y \subset Y \times X$ is closed.

Proposition 3.1. *separated maps are stable under base change:*

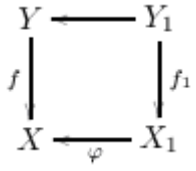

Fig .2 *separated map*

where $Y_1 = Y \underset{X}{\times} X_1$. *If* f *is separated, then* f_1 *is separated.*

Proposition 3.2. *In a diagram* $Z \xrightarrow{g} Y \xrightarrow{f} X$ *we have* f, g *are separated* $\Rightarrow f \circ g$ *is separated* $\Rightarrow g$ *is separated*

If all fibers of a covering are finite, then the map $X \to N$, $x \mapsto card\ f^{-1}(x)$ is locally constant on X. These coverings are called locally finite. The following converse is true

Proposition 3.3. A separated BRP morphism $f: Y \to X$ such that $x \mapsto card\ f^{-1}(x)$ is locally constant, is a locally finite covering.

Proof: Without loss of generality assume $n = \# f^{-1}(x)\ \ \forall x \in X$ (restricting to such a neighborhood). $f^{-1}(x) = \{y_1, \cdots, y_n\}$. There are open neighborhoods $V_1, \cdots, V_n$ of $y_1, \cdots, y_n$, pairwise disjoint, with $f\big|V_i$ is homeomorph to its image. Define $U := \bigcap_i f(V_i)$, then with $W_i := f^{-1}(U) \bigcap V_i$ we have $f(W_i) = U$ and $f^{-1}(U) = \bigcup_i W_i$ disjoint.

Theorem 3.1. $f: Y \to X$ *is a locally finite covering if and only if f is BRP, separated and proper.*

Lemma 3.1. Let X be connected, $x \in X$,

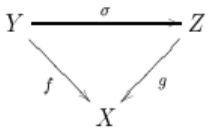

Fig .3 connected

f, g *be finite coverings and* $\sigma_x : f^{-1}(x) \tilde{\to} g^{-1}(x)$ *bijective. Then* σ *is a homeomorphism.*

Proof. According to (5.3) σ is locally finite covering. If we had $Z - \sigma(Y) \neq \varnothing$ then this open and closed set would imply $g(Z - \sigma(Y)) = X$ and a $z \in Z - \sigma(Y)$ with $g(z) = x$ would contradict the surjectivity of σ_x.

Therefore we have $\sigma(Y) = Z$ and for all $z \in Z$ we must have $\#\sigma^{-1}(z) \geq 1$. Now for $x' \in X$ we get $\deg f = \sum_{z \in g^{-1}(x')} \#\sigma^{-1}(z) \geq \#g^{-1}(x') = \deg g = \deg f$, this means we must have $\forall z \in Z \#\sigma^{-1}(z) = 1$.

Lemma 3.2. *Let X be connected, $f : Y \to X$ a finite covering.*

Then we have $Y = Z_1 \dot{\bigcup} \cdots \dot{\bigcup} Z_r$ where Z_i are the non-empty connected components of Y, and $f_i : Z_i \to X, f_i = f \mid Z_i$, are surjective finite coverings.

Proof. Without restriction assume $Y \neq \varnothing$ (otherwise $r = 0$). Consider the open and closed subsets $\varnothing \neq Z \subset Y$. $f(Z) = X$ as X is connected and $Z \to X$ is a finite covering If $Z' \subset Z$ and $Z' \bigcap f^{-1}(x) = Z \bigcap f^{-1}(x)$ then $Z' = Z$ by the previous Lemma. There are minimal $Z = \varnothing$ and these must be connected. This signifies the finite many minimal $Z's$ are the connected components of Y -and all is done.

4. Experiment and result

Three processes are included in out experiments: feature extraction, samples training, and samples recognition .We choose ten classes' 242 face images in the ORL database .To reduce computational complexity, each face image is downsampled to 64*64 pixels for experiments, and then normalize them. Figure 4 shows images of a few subjects. These images include facial contours, and variations in pose.

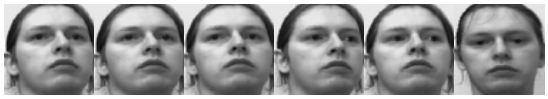

Fig 4. Face images in the ORL database

We can observe that these face images change continuously. A face image can be regarded as a point in the feature space, well then these face samples should be distributed continuously in the feature space. So the principle of PHC is satisfied.

4.1 Feature extraction (BRP mapping)

160 face images are selected as training samples. Dealt with the method of principle component analysis, the dimensions of all samples are reduced to140.

4.2 Samples training (Constructing covering sets)

It is a complex problem that how the samples are distributed in the feature space. Due to the computational and memory constraints, we use 3-degree-of-freedom to cover these face samples. In our experiments, See Fig 1, we selected arbitrary 4 images each raw to construct one neuron. Deal with the samples of all classes by this method and store theses neurons.

4.3Samples testing

Only 242 images are used in practical experiments, so we take $\sigma = 0$. Calculate the distance from an image sample waiting for recognized to neurons networks of each class. Use the method presented in 3.2 to recognize.

4.4 Experiment data and result

The experiment data are shown in Table1. a,b,……j denote ten classes of face images. The correct recognition rate is shown in Table2. The tested samples are divided into two parts- trained and untrained.

Table 1 Experiment data

Class	Quantity of Trained samples	Quantity of tested samples		Error recognition
		Trained	Untrained	
a	24	4	12	0
b	16	4	8	0
c	16	4	8	0
d	16	4	8	1
e	16	4	8	0
f	16	4	8	0
g	12	4	8	1
h	12	4	6	0
i	12	4	6	0
j	20	4	10	0
Total	160	40	82	2

Table 2 Recognition rate

Tested samples	Total	Quantity of correct recognition	Correct rate	
Trained samples	40	40	100%	
Untrained samples	82	80	97.6%	
Total	122	120	98.4%	

5. Conclusion

From the experiment result, we can draw the conclusions as follows:

1) How to select the trained samples is very important. The experiment result shows that our method is reasonable.
2) This experimental system can't recognize every untrained sample, which is close to the cognitive character of human being.
3) The number of trained samples affects the recognition rate. The more trained samples are, the higher correct recognition rate is.

From the analysis above, we see that, cognition algorithm based on multi-degree of freedom neurons can be efficiently applied to face recognition. With the improvement of the Algorithm, the correct recognition rate will be increased. And we hope that the Algorithm can be used in more practical problems.

Acknowledgements:

This work is supported by the Natural science Funds of Shenzhen University No.21.

References

[1] Jean Giraud, Surfaces de Riemann compactes, Cours de 3eme cycle, 1969/70.

[2] Roger Godement, Theorie des faisceaux, Actualites scientifiques et industrielles, no.1252, Hermann, Paris, 1964

[3] Wenming Cao, Hao Feng, Shoujue Wang: The application of DBF neural networks for object recognition. Inf. Sci. 160(1-4): 153-160 (2004)

[4] W Shoujue, Z Xingtao,Biomimetic pattern recognition theory and its applications, Chinese Journal of Electronics, 2004,Vol.13,No.3,373-377

[5] Shoujue Wang, Jiangliang Lai: Geometrical learning, descriptive geometry, and biomimetic pattern recognition. Neurocomputing 67: 9-28 (2005)

[6] Wenming Cao, Xiaoxia Pan, Shoujue Wang, Jing Hu: Digits Speech Recognition Based on Geometrical Learning. ADMA 2005: 415-422

Advanced Materials Research Vols. 204-210 (2011) pp 79-82

doi:10.4028/www.scientific.net/AMR.204-210.79

The Research of Chaos Mapping Method with Infinite Collapses to Mechanism Synthesis

Qiyuan LIU [1,a] ,Youxin LUO[1,b] ,Bin ZENG [1,c]

[1]College of Mechanical Engineering, Hunan University of Arts and Science, Changde, 415000, P.R.China

[a]lqy670@163.com, [b]LLYX123@126.com , [c]zengbin780923@sina.com

Keywords: s mapping; te collapses; Linkage mechanism; Nonlinear equations

Abstract: Many questions in natural science and engineering are transformed into nonlinear equations to be found, Newton iterative method is an important technique to one dimensional and multidimensional variables and iterative process exhibits sensitive dependence on initial guess point. The property of chaos sequences produced by one dimensional simple chaos mapping method with infinite collapses in finite interval was analyzed. For the first time, a new method based on utilizing one dimensional chaos mapping method with infinite collapses to obtain locate initial points to find all solutions of the nonlinear questions was proposed. The numerical examples in linkage synthesis and approximate synthesis show that the new method is correct and effective.

Introduction

Many questions in natural science and engineering are transformed into nonlinear equations to be found. How to find quickly and effectively all solutions in nonlinear equations are very important problem to mathematicians and engineers. There are many methods solving nonlinear equations, i.e., Newton iteration method and its improvement one, homology analysis method, mathematics mechanical method, Groebner basis method, resultant method, interval analysis method, Grey solution method and optimization method. Newton iterative technology is a common method solving nonlinear equation and equations. It has many features, i.e., 2-order convergence rate, fast convergence, intelligible iterative function, easier understanding kinetics feature, but more sensitive to the initial value, a large quantity of calculation, only a solution obtained. The chaos method proposed in [1-2] provided a new approach to solve nonlinear equations, and the method using rough iteration and precision iteration improves computational efficiency [3-4]. In this paper, the sensitive initial points were produced using simple chaos mapping method with infinite collapses in finite interval and then the chaos sequence set constructed was solved by Newton iteration method. For the first time, a new method to find all solutions based on chaos mapping method with infinite collapses in finite interval was proposed. The numerical examples in linkage kinetics synthesis show that the new method is correct and effective.

Simple Chaos Mapping with Infinite Collapses in Finite Interval

Chaos is formed under the effects of stretching and collapsing. A new chaos mapping method with infinite collapses in finite interval was proposed [5]. It is great value to research the applications of this chaos system in the mechanical engineering. The mapping is one-dimensional whose mathematical model is described by the equation as:

$$x_{k+1} = \mathrm{mod}(a / x_k, b) \tag{1}$$

where, $x_k \in (0,b)$, $a \in [1,\infty)$, $b \in (0,1), k = 0,1,2,\cdots$, $\mathrm{mod}(\cdot,b)$ is a mode function.

The iteration system defined by Eq. 1 is chaos and ergodic and it has a unique absolutely continuous invariant measure. When a is close to infinite or b to zero, the invariant distribution tends to be uniform distribution which has the probability density function $p(x) = 1/b, x \in (0,b)$. Taken $a = 1000, b = 1$, the probability distribution function shown in Fig. 1 is approximately

uniform distribution and the phase diagram is shown in Fig. 2. This mapping with the unlimited collapsing nature has the simple structure and more complex dynamics than the limited collapsing mappings such as Logistic mapping [5].

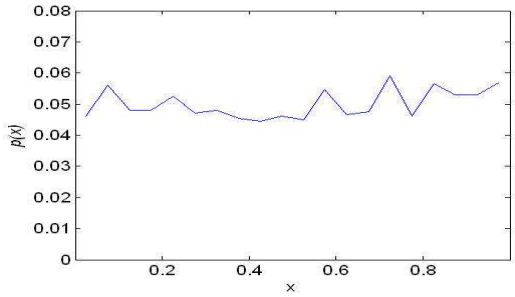

Fig. 1. The probability distribution of chaos sequences with $a = 1000$ and $b = 1$

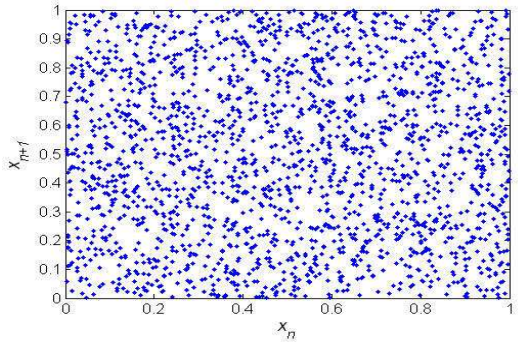

Fig. 2. The phase portrait of chaos mapping with $a = 1000$ and $b = 1$

Newton Iteration Function

The nonlinear equation is expressed as

$$f(\mathbf{x}) = 0 \tag{2}$$

Newton iteration method can be summarized as follows:

(1) Simply selecting $\mathbf{x}_0$;

(2) Iteration according to Eq. 3 as

$$x_{k+1} = x_k - \frac{f(x_k)}{f'(x_k)} \qquad k = 0,1,2,\cdots \tag{3}$$

where, $f(x_k)$ is the function value of $f(x)$ in x_k, $f'(x_k)$ is the first derivative value of $f(x)$ in x_k, that is the Jacobian matrix of $f(x)$ usually expressed as J. $f(x)$ is the function value of Newton iteration. Newton iterative method is originally used for single variable real equations, but it can be directly extended to the Banach space in order to multivariable nonlinear equations. When the initial value of iteration selected satisfies certain conditions, it is 2-order convergent in Newton iterative method. If $f'(x_k) = 0$ using Newton iterative method the singular would appear, so this phenomenon should be avoided. To improve the performance of Newton iterative method, there are some improved algorithms, but they are improved from the algorithm rather than from the mechanism.

Newton Iteration Method Based on Chaos Mapping with Infinite Collapses

Using Newton iteration method based on chaos mapping with infinite collapses, all solutions of nonlinear equations can be obtained. The calculation steps are as follows:

(1) Randomly selecting the initial points according to Eq. 1, we can construct hyperchaos sets $x_0(i,j)$ $(i = 1,2,\cdots,n$,where n is the number of variables. $j = 1,2,\cdots,N$, where N, the length of hyperchaos sets, is adjusted according to test circumstances).

(2) $x_0(i,j)$ is mapped to the variable interval $[a(i),b(i)]$ in order to generate the jth initial value $x(:,j)$.

(3) $x(:,j)$ regarded as the initial value of Newton iterative method, Eq. 3 has been iterated N times, then all the solutions $\mathbf{x}^*$ are obtained.

Applications in the Mechanism Synthesis

Fig.3 shows that the input angle θ_{1j} is generally required to maintain a certain function relationship with the output angle φ_{1j} in the planar four-link mechanism for function synthesis. The Cartesian coordinate system is established as s 3 C (1 0) A, B t to A_x, A_y, B_x, B_y as the design variables that are expressed as x_1, x_2, x_3, x_4 respectively.

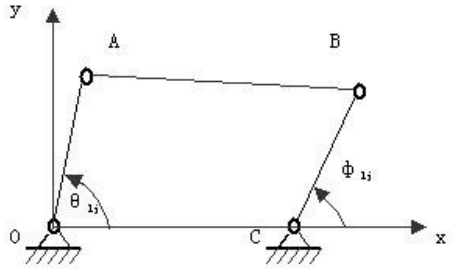

Fig. 3. The diagram of linkage mechanism

According to the constraint conditions that the link length is constant in the motion and displacement matrix, the following synthesis equation can be derived:

$$f_j(x) = P_{1j}x_1x_3 + P_{2j}x_1x_4 + P_{3j}x_2x_3 + P_{4j}x_2x_4 + P_{5j}x_1 + P_{6j}x_2 + P_{7j}x_3P_{8j}x_4 + P_{9j} \tag{4}$$

where, $j = 2、3、\cdots、m$, m is the number of the achieving point. If using the accurate points, we can achieve up to five locations.

$$P_{1j} = 1 - \cos(\theta_{1j} - \phi_{1j}); P_{2j} = -\sin(\theta_{1j} - \phi_{1j}); P_{3j} = \sin(\theta_{1j} - \phi_{1j});$$
$$P_{4j} = 1 - \cos(\theta_{1j} - \phi_{1j}); P_{5j} = \cos(\theta_{1j} - \phi_{1j}) - \cos(\theta_{1j});$$
$$P_{6j} = \sin(\theta_{1j} - \phi_{1j}) + \sin(\theta_{1j}); P_{7j} = \cos(\phi_{1j}) - 1; P_{8j} = -\sin(\phi_{1j});$$
$$P_{9j} = 1 - \cos(\phi_{1j})$$

B Eq. 4 $m-1$ design equations, the biggest accurate number of the problems is five.

In many cases, the problem of the linkage synthesis and approximate kinetics synthesis finally comes down to an unconstrained optimization problem, that is,

$$\min F(x) = \sum_{j=1}^{m} (f_j(x))^2 \tag{5}$$

The minimum necessary condition of the objective function is that $\frac{\partial F(x)}{\partial x} = 0$, that is,

$$\begin{cases} \sum_{j=2}^{m-1} f_{j-1}(P_{1j}x_3 + P_{2j}x_4 + P_{5j}) = 0 \\ \sum_{j=2}^{m-1} f_{j-1}(P_{3j}x_3 + P_{4j}x_4 + P_{6j}) = 0 \\ \sum_{j=2}^{m-1} f_{j-1}(P_{1j}x_1 + P_{3j}x_2 + P_{7j}) = 0 \\ \sum_{j=2}^{m} f_{j-1}(P_{2j}x_1 + P_{4j}x_2 + P_{8j}) = 0 \end{cases}$$

where, m is the number of the synthesis point.

That synthesizing planar four-link mechanism makes the relationship between the output angle φ_{1j} and the input angle θ_{1j} to meet the requirement as Tab. 1. Using the method in this paper and selecting $a=1000, b=1$ in Eq. 1 and the variable interval [0, 1], it took 0.104831s to synthesize accurately for all solutions: (The solutions in No. 1-4 of Tab. 2 [6]). I approximate synthesis, it took 16.218s and the solutions were obtained as shown in Tab. 2 (Some approximate solutions were also increased except for the solutions of No. 1-4 and they varied with the initial value, the length of chaos sequence and the variable interval of the mapping).

Tab. 1. Five groups of corresponding value of input angle θ_{1j} and output angle φ_{1j}

j	1	2	3	4	5
θ_{1j}	0	60	130	200	280
φ_{1j}	0	17	44	61	50

Tab. 2. The results of synthesis

No.	x_1	x_2	x_3	x_4	Notes
1.	0.34688351864093	0.15532289223008	2.37621431901423	1.07108276520215	to meet the requirements
2.	0.33802375122182	0.35284403147775	1.52301342502732	1.46008672456456	
3.	0.00876050327329	0.19878954898663	0.24358820102367	0.42972805218513	
4.	0.00000000000000	0.00000000000000	1.00000000000000	0.00000000000000	Degradation
5.	0.24810590331448	0.09742519788478	0.62411520956186	0.49721188127604	approximate solution
6.	-0.05656808459818	0.10789498343339	0.45524276496406	0.22173945773667	
7.	0.26879875742049	0.34866142549433	0.37945885805080	0.74548350193159	
8.	0.36143253460429	0.26070352447913	2.00210092194291	1.36915944896681	

Conclusions

In this paper, chaos sequence generated by simple one-dimensional chaos mapping with infinite collapses in finite interval was researched. For the first time, a new method based on simple chaos mapping with infinite collapses to find all solutions of nonlinear equations was proposed and the calculation steps were given. The numerical examples in linkage synthesis and approximate synthesis show that the new method is correct and effective. This new method lays the foundation for engineering applications and also proposes useful ideas for the chaos features of other iteration methods.

Acknowledgement

This research is supported by the grant of the 11th Five-Year Plan for the construct program of the (Mechanical D) in Hunan province (XJT2006180) and The National Natural Science Foundation of P.R. China (51075144).

References

[1] J. Xie and Y. Chen: China Mechanical Engineering, Vol. 13, No. 7 (2002), p. 608.

[2] L.T. Zhang and X.H. Dong: Machine Tool & Hydraulics, No. 1 (2003), p. 165.

[3] Y.X. Luo: Machine D Vol. 20, No.7 (2003), p. 27.

[4] Y.X. Luo and D.X. Li: Journal of C Engineering D 2003, Vol. 10, No. 2 (2003) 95.

[5] Y.H. Qiu, C. He and H.W. Zhu: High Technology Letters, No. 9 (2002), p. 13.

[6] A.X. Liu and T.L. Yang: *Dynamic Design of Mechanical System* (China Petrochemical Press, Beijing, 1999).

Advanced Materials Research Vols. 204-210 (2011) pp 83-87

doi:10.4028/www.scientific.net/AMR.204-210.83

Domain-based Level Trust Manage Model

Xiaoxue Ma[1], Zixian Wang[2], Jing Bian[1], Fei Liu[1]

[1]Hebei University, Baoding Hebei China

[2] The Central Institute for Correctional Police, Baoding, Hebei, China

bd_wzx@126.com

Keywords: Trust evaluation model, Trust degree, Trust domain, QoS

Abstract: Draw on the trust relationship of human society, domain model and domain trust are introduced to build domain-based level trust manage model (DLTMM). In various domains, according to physical services characteristics of their own, entities abstract representative attribution. According to their preferences the service requester preferences comprehensive evaluate the service attributions, and to determines whether transaction; After trading, the service requester will calculate the difference degree of quality of service according to the actual quality of service and the claimed quality of service, and then judge the trust degree of service provider. The simulation results show that the model can more accurate assessment of the trust entity, to some extent effective against malicious attacks, which proves the validity and accuracy of the model.

Introduction

Due to a large number of fraud and unreliable service quality in a dynamic user-oriented open network, the customer faced with how to identify and select efficient and secure resources or service [1]. The current solution is an trust evaluation system [2-6].

In 1996, In order to solve the safe problem of the network service, M.Blaze etc. first proposed the concept of "Trust Management"[7]. With extensive application of a variety of large scale distributed application system, the dynamic trust management and evaluation has become the hotspot in the field of information security. Eigen Trust model puts forward the distributed computing method based on DHT[8], using the trust algorithm that calculates global trust value by direct trust value with trust transfer characteristics, but this model exists convergence problem, and have the higher communication cost and relative value of global reputation. Zhou etc. [9 improve the Eigen Trust model for the aspects of determination of credible peers and the speed of trust iteration convergence, and puts forward the Power Trust model. When the most trusted models evaluate level of trust about service entities at present, the credibility of the service attributes whether the two sides trading result is credible is rather ambiguous, which makes the evaluation model lack of persuasion, and not very good depict the complexity and uncertainty of trust relationship between the two sides. In view of the above questions, learning trust relationship from human society, according to the service of the node itself, abstracting representative multiple service attributes from the trusted relationship of the node service, service requester comprehensive evaluates multiple service attributes provided by service provider based on personal interest, and combines with the trust value, decide whether to trade finally; after the transaction, service request calculates QoS(quality of service) difference degree according to actual QoS and service provider' own QoS claimed to judge the credibility of service provider, then gives corresponding rewards and punishment and trust update.

Trust Manage Model

DLTMM Frame

In accordance with their respective goods, we put these entities in different areas (some entities may belong to multiple domains), as shown in Figure 1.

In the frame, manager-agent is a global trust relationship manager, who manages all domain-agent.

It is the root of trust, responsible for the collection and management of domain-agent of the credibility information, maintenance of global trust relationship. The information managed by MA is: ID of domain-agent, domain trust, calculation of global trust and domain model. Domain-Agent is the manager of trust relationship, responsible for the collection and management of all entities within the credibility of information, maintenance of local trust. DA is responsible for the information is: domain entity search, reliability calculations, reliability of storage. MD is the domain.

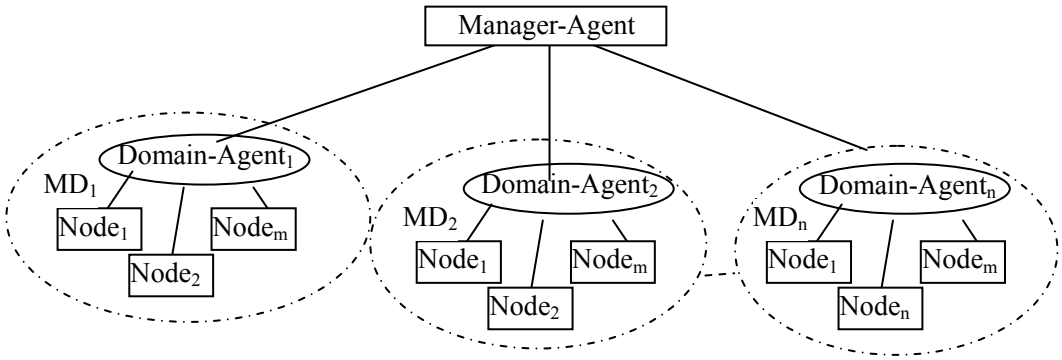

Figure1. Domain-based Level Trust Manage Model

Definitions

Definition 1 direct trust degree: the system entity x_i and entity x_j through direct interactive history and achieve the trust value of the entity x_i, shown by $DT(x_i, x_j)$

Definition 2 recommend trust degree: the system entity x_i achieves the trust value which is comprehensive calculated by direct trust degree of multiple entities acting on the entity x_j, shown by $RT(x_i, x_j)$.

Definition 3 domains of trust: it is a comprehensive trust in a domain which colculated of direct trust degree and recommended trust degree.

Definition 4 global trust degree: It is quantitative expression of trust, refer to comprehensive trust value which synthesizes the direct trust and recommend trust, shown by $T(x_i, x_j)$.

Definition 5 QoS attribute value oneself: the value of QoS which service provider claims according to their ability in t time, showed by $Q_{ATTR}^{x_j} = \{q_{attr_1}^{x_j}, q_{attr_2}^{x_j}, ..., q_{attr_M}^{x_j}\}$, and $0 \le q_{attr_m}^{x_j} \le 1$ represents QoS oneself of m-kind service attribute of the service provider x_j. In order to accurately depict QoS oneself, we suppose that service providers can update QoS attribute value themselves according to their immediate service performance and the feedback of the service requester.

Definition 6 trade QoS satisfaction evaluation: after every trade , for each service attribute, quality index is defined as $\{q_{attr_1}^{x_i,x_j}, q_{attr_2}^{x_i,x_j}, ..., q_{attr_M}^{x_i,x_j}\}$, which gets from service provider entity $x_j (x_j \in X)$ providing actual trade to service requester entity $x_i (x_i \in X)$, showed by $Q_{ATTR}^{x_i,x_j} = \{q_{attr_1}^{x_i,x_j}, q_{attr_2}^{x_i,x_j}, ..., q_{attr_M}^{x_i,x_j}\}$, and $0 \le q_{attr_m}^{x_i,x_j} \le 1 (m = 1, 2, ...M)$ represents evaluation value of m-kind service attribute from the service requester x_i to the service provider x_j.

Definition 7 Services Evaluation Factor (SEF): each entities have own preference for every service attribute in selecting the service object. Establishing that $\tilde{\omega}_m$ represents importance degree of m-kind service attribute relative to other service evaluate factor, and meets:

$$0 \le \tilde{\omega}_m \le 1, \ \sum_{m=1}^{M} \tilde{\omega}_m = 1 \tag{1}$$

then $\tilde{\omega}_m$ is called for the evaluate factor of m-kind attribute.

Definition 8 Transaction request vector: it is defined as the five-group $\mathrm{Re}q = (id, type, \lambda, \varepsilon, flag)$, in which id is the entity number; type is the domain for the requested goods; λ for the entity's self-confidence factor, ε is the minimum confidence threshold; flag is a flag, 0 or 1.

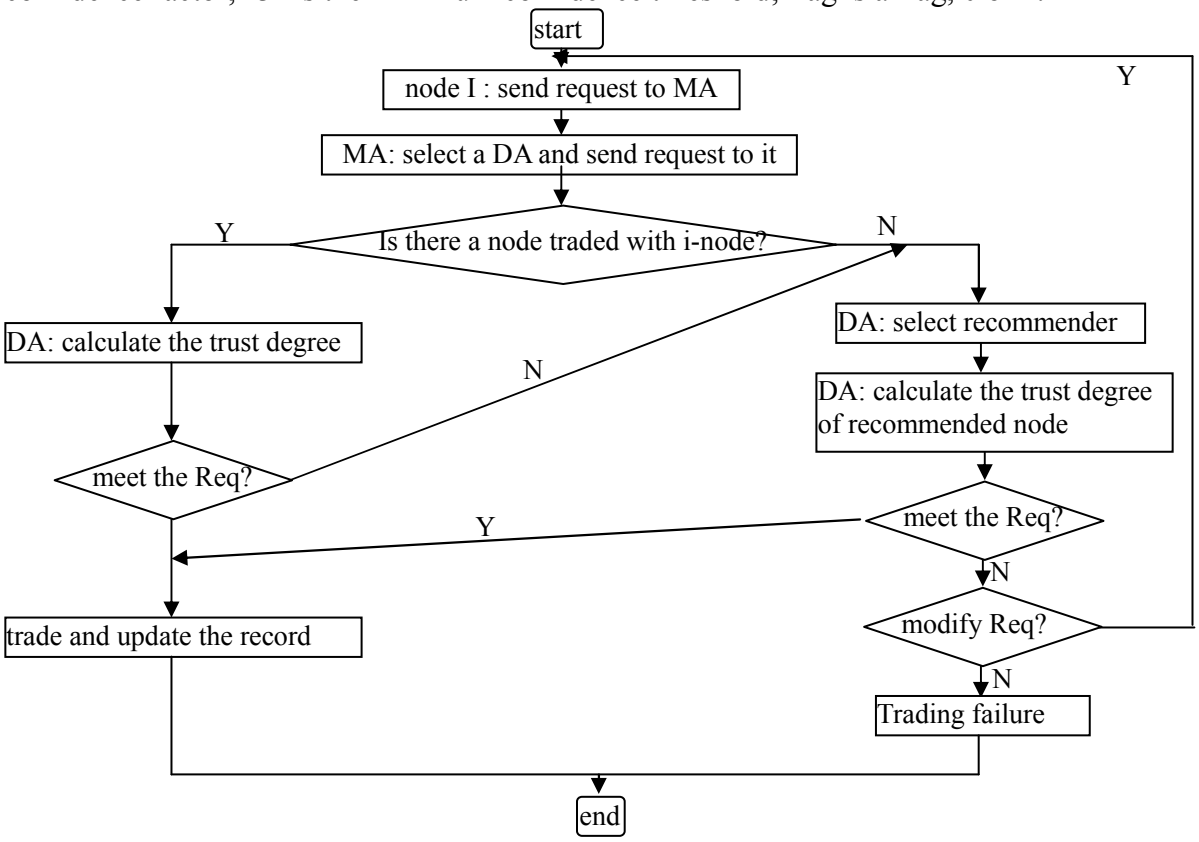

Trust evaluating of QoS

After the transactions between x_i and x_j, x_i will evaluate the QoS of x_j through the following expression, according to all attributes of service:

$$Q^t_{x_i,x_j} = Q(x_i, x_j, t) = \sum_{m=1}^{M} \tilde{\omega}_m q_m^{x_i,x_j} \tag{2}$$

After the end of a service, calculate the QoS evaluation Difference Degree according to the following equation:

$$D^{Q(xj)}_{Q(xi,xj)} = \frac{\left| Q^t_{x_i,x_j} - Q^{self,t}_{x_j} \right|}{Q^t_{x_i,x_j}} \tag{3}$$

$$V_k(x_i, x_j) = \begin{cases} 1, \ \text{when } D^{Q(xj)}_{Q(xi,xj)} \le \varepsilon \\ 0.5, \ \text{when } D^{Q(xj)}_{Q(xi,xj)} = null \\ 0, \ \text{when } D^{Q(xj)}_{Q(xi,xj)} > \varepsilon \end{cases} \tag{4}$$

The $V_k(x_i, x_j)$ expresses trust evaluation value which be got after the end of the transactions between service requester x_i and service provider x_j,according to the QoS.

Trust Calculation

The calculation of direct trust is following the equation (5):

$$DT(x_i,x_j)=\alpha\frac{\sum_{l=1}^{n}\Phi(t_l)\times\Phi(m_l)\times C_l}{n}(n>0) \quad (5)$$

where $\alpha=\sqrt{n/(n+1)}$ is the function of the number of transactions, $\Phi(t_l)=e^{-\lceil(t_0-t_l)/T\rceil}$ is the time decay quotient, t_0 is the time of this transaction, t_l is the time of the l times transaction, $\Phi(m_l)=e^{-1/m_l}(m_l>0)$ is used to adjust the amount of the transaction on the impact of direct trust.

And the calculation of the recommended trust is according to the following equation:

$$RT(x_i,x_j)=\sum_{k=1}^{N}DT(x_i,x_k)*DT(x_k,x_j)/N \quad (6)$$

Where N is the number recommended of entities.

The domain trust is calculated by equation (7):

$$T(X,x_i,x_j)=\lambda DT(x_i,x_j)+(1-\lambda)RT(x_i,x_j) \quad (0\le\lambda\le1) \quad (7)$$

It expresses the domain trust of entity in domain T

The global trust is:

$$T(x_i,x_j)=\frac{\sum_{j=1}^{n}T(Y,x_k,x_j)}{n}(T(Y,x_k,x_j)\neq0,n>0) \quad (8)$$

Simulation

In order to verify the validity of the model, we use the simulation software query cycle simulator[10] developed by the Stanford University. We make simulation experiments for the model based on P2P file sharing network environment with the JAVA development language.

Simulation environment: the entities are 1000, the number of files is 50,000, The simulation period is 100, Threshold value is 0.05, direct trust factor is 0.6, the historical factor is also 0.6.

In order to evaluate DLTMM model contain malicious attacks, in the simulation environment there is four types of nodes: Sincere Peer, Simply Malicious Peer, Strategic Malicious Peer, and Collusive Malicious Peer. Successful Transaction Rate, that is to say, in this system, the proportion of successful trades in all trades. In order to facilitate comparison, there is achieving the transactions of the Eigen Trust model and No trust model.

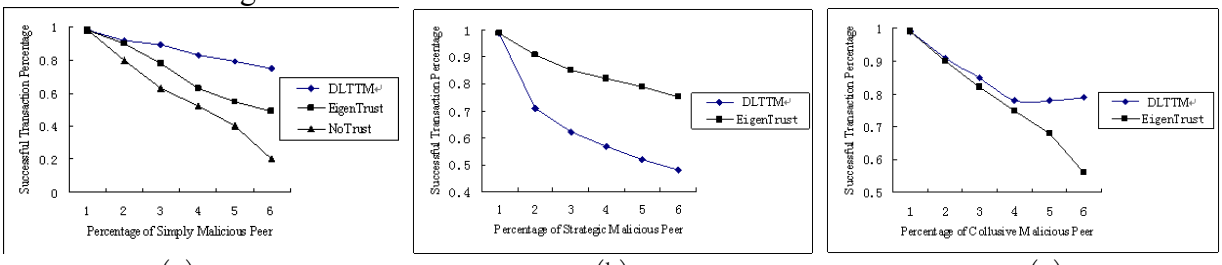

(a) (b) (c)

Figure 2. Change of Successful Transaction Rate with number of Malicious Peer

It can be seen from Figure 2, when there is no malicious entity in systems, the successful transaction rate can reach 100%. But with the increase of malicious entities, there is no trust model system successfully trading the fastest rate of decline. EigenTrust model because the lack of malicious peer punishment, the successful transaction rate of decline is relatively large. And DLTMM model increases with the number of transactions, because it can more effectively identify and suppress all kinds of malicious entities, a malicious entity reach the proportion of 50%, the rate of successful transaction still high, and the model shows robustness against malicious attacks.

Conclusion

Based on entities characteristics of their services, we abstract representative multi-service attributites from trust relationships to represent a trust evaluation model. The service requester based on their own preferences of service to evaluate the multi-service properties of service provider, combined with the trust value that determines whether the transaction doing; closing of the transaction, the service requester based on the actual quality of services received and service claimed by the provider to calculate the Quality of Service different degrees, to judge the credibility of service providers, and the corresponding rewards and punishments and trust updates. Simulation results show that the model can more accurately assess the entity's trust, can effectively curb the types of malicious attacks entities when a higher proportion of malicious entities can still maintain a relatively high rate of successful transactions.

Acknowledgment

This work is supported by National Natural Science Foundation of China (60873203), Natural Science Foundation of Hebei Province (F2010000319, F2010000331), Hebei Province Funds for Distinguished Young Scientists (F2010000317), Research Fund of Hebei Higher Education (Z2010122) .

Reference

[1] Zhang Qian, Sun Yu, Liu Zheng, Zhang Xia, Wen Xuezhi. Design of a distributed P2P-based grid content management architecture. Proceedings of the 3rd Annual Communication Networks and Services Research Conference, 2005:339-344

[2] LI Yong-Jun.DAI Ya-Fei. Research on Trust Mechanism for Peer-to-Peer Network. JOURNAL OF COMPUTERS [J],2010,33(3):390-405

[3] Song Shanshan, Hwang Kai, Kwok Yu-Kwork. Trusted Grid computing with security binding and trust integration. Journal of Grid computing[J], 2005,3(1):53-73

[4] Audun J, Roslan I, Colin B. A survey of trust and reputation systems for online service provision. Decision Support Systems, 2007.43(2):618-644

[5] Zhang Hong, Duan Haixin, Liu Wu. RRM:An incentive reputation model for promoting good behaviors in distributed systems [J]. Science in China.2008，38(10):1747-1759

[6] Xiaoyong Li, Xiaolin Gui. Research on Dynamic Trust Model for Large Scale Distributed Environment[J]. JOURNAL OF SOFTWARE, 2007,18(4):460-473

[7] M. Blaze, J. Feigenbaum and J. Lacy. Decentralized trust management. In Proceedings of the 17th Symposium on Security and Privacy, 1996: 164-173

[8] Kamvar SD, Schlosser MT. EigenRep: Reputation management in P2P networks. In: Lawrence S, ed. Proc. of the 12th Int'l World Wide Web Conf. Budapest: ACM Press, 2003,,123~134.

[9] ZHOU RUNFANG,KAI H.PowerTrust:A robust and scalable reputation system for trusted peer-to-peer computing[J].IEEE Transactions on Parallel and Distributed Systems,2007,18(4):460-473.

[10] Stanford P2P Sociology Project，http://p2p.stanford. edu /www/download.htm.

Advanced Materials Research Vols. 204-210 (2011) pp 88-94

doi:10.4028/www.scientific.net/AMR.204-210.88

Experimental study on the bio-drying characteristics and its influencing factors of paper mill sludge

XunAn Ning[1, a], QingLin Chen[1, b], JianBo Zhou[1, c], ZuoYi Yang[1, d], JingYong Liu[1, e]

[1]Faculty of Environmental Science and Engineering, Guangdong University of Technology, Guangzhou,Guangdong, 510006, China

[a]ningxunan666@126.com, [b]ivana2006@163.com,[c]langjian510@163.com, [d]Yangzy2003@126.com, [e]www053991@126.com

Keywords: Paper mill sludge (PMS), Bio-drying, Moisture content (MC)

Abstract. The bio-drying characteristics and its influencing factors of paper mill sludge (PMS) were investigated detailedly, by means of the heat generated by aerobic degradation of the organic substances in the PMS. In the orthogonal experiments, the good results were achieved with the followed optimization technics: starch (25.0g/500.0g), sawdust (40.0g/500.0g), inoculation (15.0mL/500.0g) and KH_2PO_4 (5.0g/500.0g). During bio-drying, the matrix temperature increased to 47.2° C within 12-24h rapidly under the given operation parameters, and the maximum was about 48.0° C. In the whole process the pH changed in the range of 6.11-7.87. The quantity of amylolytic bacteria reduced to the minimum in the first day, and the amylolytic bacteria grew well until the process of bio-drying finished. The ATP content was increased drastically in the first day and peaked in the fifth day, with the maximum ATP content was about 6.4×10^{-6}μmol/g. When bio-drying of PMS was finished, the VS content and moisture content (MC) reduced from 58.4% to 49.5% and 62.2% to 50.3% respectively.

Introduction

Paper mill sludge (PMS) is a kind of bio-solid waste and its large continuous production is becoming a worldwide environmental problem [1]. The reduction of volume and quantity reduction as well as stabilization are the principal methods for PMS treatment. The bio-drying, is an alternative pretreatments method targeting incineration developed in recent years, which is aiming at removing water from the high water content [2]. During the bio-drying, the main mechanism of bio-drying is using the heat generated during the aerobic degradation of organic substances to evaporate water derived from composting [3-5].

Nowadays, great attentions have been focused on the bio-drying process, which removes water mainly as vapour by adequate ventilation and high temperature resulting from organics degradation [6]. The microbial metabolism for the bio-drying process was similar to that for the composting process. However, the former aimed at the water removal, while the latter focused on the bio-stabilization and maturity of composted materials [2]. In this study, the performance of water removal and moisture content(MC) reduction were investigated, in order to optimize the parameters of the bio-drying in the whole process, including the temperature, pH, moisture content(MC), volatile solid(VS) content, Adenosine triphosphate (ATP) content and the quantity of bacteria, which was monitored to explain the performance of bio-drying.